Techno-Economic Assessment of Energy Transition toward High PV Penetration Grid: the Case of Kyushu, Japan

Samuel Matthew Girao Dumlao

Techno-Economic Assessment of Energy Transition toward High PV Penetration Grid: the Case of Kyushu, Japan

太陽光発電が大量導入された電力網へのエネルギー転換の技術経済的評価: 九州の場合

This dissertation is submitted in partial fulfillment of
the requirements for the degree of
Doctor of Philosophy in Energy Science

Samuel Matthew Girao Dumlao

Department of Socio-Environmental Energy Science
Graduate School of Energy Science
Kyoto University

February 2022

Samuel Matthew Girao Dumlao

Techno-Economic Assessment of Energy Transition toward High PV Penetration Grid: the Case of Kyushu, Japan

Ph.D. Dissertation, February 2022
Supervisor: Keiichi ISHIHARA
Reviewers: Yasuyuki SHIRAI and Seiichi OGATA

Kyoto University
Department of Socio-Environmental Energy Science
Graduate School of Energy Science
Yoshidahonmachi, Sakyo Ward
Kyoto 606-8501

Abstract

The energy transition towards renewable energy will be a challenging task, and there will be small factors that, when combined, could either hinder or push it forward. The Paris Agreement and the United Nations Sustainable Development Goals (UN-SDG) have helped promote renewable energy and contributed to the increase in renewable energy, particularly wind and solar. Solar photovoltaics (PV) is enticing for many countries due to the ease of deployment, and this has supported the increased installation globally. However, due to its problems on intermittency and non-dispatchability, solar PV will face potential issues such as unavailability, curtailment, and overproduction. Initially, the problem centered mainly on the intermittency of solar PV, but recently, due to the increase in solar PV in the grid, the issue of curtailment has emerged. In the future, solar PV capacity will reach a point where the installed capacity will be beyond the peak demand in the region; thus, there will be no demand for this energy production at peak generation days.

Japan has been increasing its solar PV capacity since the official launch of the Feed-in-Tariff (FiT) in July 2012. By 2019, it has already reached its 7% solar PV annual generation target, and the government has moved to increase the target further to 14%. However, as early as October 2018, curtailment has been observed in the Kyushu region. Located in the westernmost tip of the country, it is one of the regions leading the growth in solar PV installation in the country. In FY 2018, the annual solar penetration rate in the region was 9.46 %, and solar capacity is projected to grow further. Although other countries have encountered this phenomenon, the isolated nature of Japan's Electricity Grid presents a more challenging issue due to the inability to trade with neighboring countries. In this dissertation, Kyushu was used to represent Japan's future grid since it has diverse energy sources such as nuclear, coal, LNG, geothermal, biomass, wind, and a significantly large PV capacity.

Under this premise, this dissertation aims to understand the potential, limitations, and implications of incorporating other technology with solar PV to enable the region to transition to carbon-neutral energy sources, thereby decarbonizing the electricity grid. The study pursues this effort by first building an hourly Kyushu grid model that includes the generators and demand in the region. Then, with this model, mathematical, machine learning, and heuristic tools were used to explore future scenarios that involve high PV penetration. In all these scenarios, the study optimizes the utilization of the existing and new generators while ensuring the region's energy balance. Finally, the study further analyzes the operational cost of the whole grid to understand the financial impact of the changes.

In order to explore the potential pathways, the study first investigated the nature of curtailment by reproducing it using known periodicity and statistical data. The demand and

solar PV generation were modeled using Fourier transform, and it proved to be viable with around 3% error. The model was necessary for regions where hourly data is unavailable. The study also highlighted that curtailment would mainly be a problem during the spring and autumn. Furthermore, the results show that most curtailment will occur within a 6-hour window from 9:00 to 15:00. These insights are crucial in exploring efforts that could reduce curtailment, which energy planners must pursue to ensure the viability of additional solar capacity.

Since the goal is to reduce carbon dioxide emissions, the study pursued the idea of decommissioning coal power plants by further increasing the PV capacity. Weather-based synthetic energy demand and solar PV energy production were generated from historical data, which were used to analyze the capability of PV to reduce the coal's generation capacity. Results show that solar PV needed LNG to reduce coal's capacity. However, even with the support of LNG, solar PV can only reduce the coal power plants' generation capacity by 50%. It was also discovered that solar PV could not reduce coal capacity beyond 12 GW solar capacity (around 75% of daily peak demand), but it could still reduce the actual coal generation. In both cases, this is due to the generation capacity of coal, which is necessary during peak power consumption.

Following the idea that solar PV alone could not replace coal, the study then explored complementary diurnal electricity storage to reduce curtailment and ensure the continued viability of additional solar PV. Since electricity storage remains relatively expensive, the study also investigated the appropriate timing of investing storage based on projected PV growth rates. The study proposed a methodology that uses Monte Carlo random sampling and a financial evaluation focusing on a planning horizon to accomplish this goal. The results show the existence of a cost-optimal storage capacity growth trajectory that balances the cost penalty from curtailment and the additional investment cost from storage. This optimal trajectory reduces the impact of curtailment on the cost and utilizes more solar energy potential.

As a follow-up on the idea of using diurnal storage, the study then investigated the potential of using electric vehicles (EVs). EVs are appropriate in the case of Japan since previous researchers showed that the general population seldomly uses their vehicles. The analysis showed that 20 GWh was sufficient by 2031, which would require around 10% of Kyushu's passenger vehicles. Since additional capacity will only be beneficial during spring and autumn, a further increase in the target is inappropriate. The logistics growth model showed that the current adaption rate is insufficient. However, if the 20 GWh is achieved by 2031, EV as mobile storage could keep the curtailment to around 10%-15%. Initially, the impact of EVs on curtailment reduction is lower due to lower capacity. Thus, stalling the additional capacity until further volume increases might be necessary to keep the curtailment below 10%. Finally, given the need for long-term storage and additional power generation capacity to decommission coal and even LNG, the study pursued the idea of adding hydrogen power generation in the energy mix. Since this entails a significant change in the composition of the grid, the study used a Pareto Optimal Genetic Algorithm heuristic to evaluate various combinations of hydrogen infrastructure and importation schemes. The heuristic is necessary

to reduce the number of scenarios. The results show the combination that minimizes the capacity of hydrogen electrolyzers, tanks, and power generators and the necessary PV capacity to produce local hydrogen. The import scenarios show the impact of importation on the capacity of the hydrogen infrastructure. Through the additional hydrogen infrastructure, coal can be decommissioned totally. However, in order to decarbonize the Kyushu grid fully, it might be necessary to shift the dependence on LNG towards hydrogen.

From the viewpoint of the global discussion on energy transition, the Kyushu region can represent Japan as it encapsulates the country's characteristics, which have an isolated electricity grid, temperate climate, and highly industrialized sectors. Kyushu's isolated electricity grid case could be comparable to South Korea, Taiwan, the Philippines, and Hawaii since the connection to other electricity grids is limited. Therefore, the insights gained in this study could be used in these electricity grids, especially in regions with similar climates. Locally, the results could be a model for the Chugoku and Shikoku region since they might soon face the same issues based on the PV penetration in FY 2020. From the modeling perspective, the mathematical, machine learning, and heuristic tools used in this dissertation could easily be adapted to countries with hourly data. In addition, the heuristics used in this dissertation is crucial in discussing various changes in the grid if different priorities must be explored prior to the final decision.

Overall, the dissertation aimed at understanding the potential, limitations, and implications of various energy transition paths that are compatible with solar PV. The dissertation showed that PV could be a driver for the energy transition, but it will need the support of other technology to accomplish the decarbonization goals that will meet the Paris Agreement and UN Sustainable Development Goals.

Acknowledgement

First and foremost, I would like to express my gratitude to Ishihara-sensei for his wisdom, patience, and continued support on the topics and issues surrounding this dissertation. His insights have significantly molded the direction of this research. I am also grateful to Okumura-sensei and Ogawa-sensei for handling the laboratory activities; to Tsukamoto-san, Kaki-san, and Niitani-san for their administrative support; and to Takemoto-san for all my technical and reservation requests.

I thank my labmates in the Ishihara laboratory for the company, especially to Hsin-Tien Lin, Nilubon Luangchosiri, and Masataka Yamashita, for guiding me during my transition period in Japan. I am also thankful for the company I shared through classes and random meals with my classmates in my doctoral and Japanese language classes. I am also grateful to the Kyoto Association of Pinoy Scholars (KAPS) for the camaraderie and support throughout my doctoral studies.

I am grateful to the Ministry of Education, Culture, Sports, Science, and Technology (MEXT) of the Japanese Government for providing me with the opportunity to study in Japan. I am also thankful to Sonobe-sensei and the Kyoto University Research Administration (KURA) office staff for the Ambitious Intelligence Dynamic Acceleration (AIDA) program that helped collaborate with the developers of PyPSA in Germany. I would also like to acknowledge the developers of PyPSA for their kind responses to my inquiries.

I thank my family for their continued support in my goal of pursuing higher academic degrees.

I extend my gratitude to everyone who was not mentioned but was instrumental in writing this dissertation. Thank you very much! どうもありがとうございました! Maraming salamat po!

Publications

List of Publications

Dumlao, S. M. G., & Ishihara, K. N. (2020). Reproducing solar curtailment with Fourier analysis using Japan dataset. Energy Reports, 6 (Special Issue: CPESE 2019), pg 199–205. doi: https://doi.org/10.1016/j.egyr.2019.11.063. Peer-reviewed, cited as [1].

Dumlao, S. M. G., & Ishihara, K. N. (2021). Weather-Driven Scenario Analysis for Decommissioning Coal Power Plants in High PV Penetration Grids. Energies, 14(9), 2389. doi: https://doi.org/10.3390/en14092389. Peer-reviewed, cited as [2].

Dumlao, S. M. G., & Ishihara, K. N. (2021). Dynamic Cost-Optimal Assessment of Complementary Diurnal Electricity Storage Capacity in High PV Penetration Grid. Energies, 14(15), 4496. doi: https://doi.org/10.3390/en14154496. Peer-reviewed, cited as [3].

Dumlao, S. M. G., & Ishihara, K. N. (2022). Impact Assessment of Electric Vehicles as Curtailment Mitigating Mobile Storage in High PV Penetration Grid. Energy Reports, 8 (Special Issue: CPESE 2021), pg 736–744. doi: https://doi.org/10.1016/j.egyr.2021.11.223. Peer-reviewed, cited as [4].

Pending Publications

Dumlao, S. M. G., & Ishihara, K. N. Pareto-Optimal Genetic Algorithm for Hydrogen Technology Adoption in High PV Penetration Grid. Manuscript to be submitted to the International Journal of Hydrogen Energy.

Related Publications

Knüpfer, K., Dumlao, S. M. G., Esteban, M., Shibayama, T., & Ishihara, K. N. (2021). Analysis of PV Subsidy Schemes, Installed Capacity and Their Electricity Generation in Japan. Energies, 14(8), 2128. doi: https://doi.org/10.3390/en14082128. Peer-reviewed, cited as [5].

Contents

List of Tables

List of Figures

1 Introduction

1.1 Energy Transition

"Even sand could pile up and become a mountain" speaks a lot about small efforts or problems that could become bigger as it accumulates. The energy transition towards renewable energy will be a challenging task, and there will be small factors that, when combined, could either hinder or push it forward. In October 2016, the conditions for the entry into force of the Paris Agreement were met, and it entered into force on 4 November 2016. Signatories to this agreement agreed to submit a national climate plan to mitigate climate change by reducing greenhouse gas emissions. Similarly, one of the United Nations Sustainable Development Goals, established in 2015, is focused on affordable and clean energy. These two global initiatives helped promote renewable energy, such as wind, solar, and biomass, in the energy mix of several nations. As a result, several "green energy transition" initiatives are ongoing in countries such as Germany and Denmark, and subnational jurisdictions such as California, Scotland, and South Australia [6]. Besides these major players, more than 150 countries have national targets for renewable energy in the power sector [7]. The colossal task of the energy transition could be achieved when all these efforts are piled up together.

Change, although constant in human existence, is often challenging. This difficulty is exacerbated by unknown or vague things when the change is demanded. Sovacool [8] mentioned that there are several definitions for the energy transition, but it mainly surrounds around changes in the fuel source or the prime mover. He added that there is no magic formula for the energy transition since issues like scale, sociocultural, political, energy sources, and existing infrastructure will influence the approach in the transition. Building on previous energy transition, Gubler [9] said that persistence and continuity of policies will be crucial since the transition will take time, and new knowledge must be nurtured over time. He cautioned that balance in innovation portfolio and policies, as well as diversification, would help in hedging on uncertainties.

Globally, REN21 reported that hydropower, solar PV, and wind dominate the current renewable portfolio [7]. Although it ranks as the highest contributor, hydropower has barely increased recently while solar PV and wind increased by 139 GW and 93 GW in 2020, respectively. York and Bell caution that the world might not be transitioning, but rather, it is adding renewable energy into the energy mix [10]. They argued that during the transition from biomass to coal and then to petroleum, the previous energy sources remained; thus, an increase in the renewable energy capacity should be assessed carefully to ensure that it is reducing fossil fuel use.

Despite the recent victories in renewable energy installation, Sarrica et al. [11] raised the issue that the human dimension of energy should be addressed as well. Stephenson et al. created a conceptual framework focused on understanding the factors that influence energy consumption behavior and identifying opportunities for behavior change [12]. In this framework, the authors assumed that their energy behavior can be understood by understanding a community's cognitive norms, material culture, and energy practices. This insight might also hold true for people's receptiveness to changes in the energy sources as part of the energy transition.

1.2 High PV Penetration

All these initiatives have contributed to the increasing solar photovoltaics (PV) installation in the world, which grew from 138 GW to 760 GW from 2013 to 2020 [13]. In 2020, there is significant PV penetration in Germany (10.5%), Greece (10.4%), Australia (9.9%), Chile (9.8%), Italy (9.4%) and Japan (8.5%) [13]. Other countries might follow this trend, but these countries should consider the technical issues of solar PV. In this study, high PV penetration is framed relative to the impact of solar PV's capacity on the operation of the electricity grid. Therefore, this definition considers any electricity grid that could not operate without changes to the business-as-usual operation as a high PV penetration electricity grid. Such changes could involve the shutdown of existing generators or installing additional infrastructure to accommodate the solar capacity.

In incorporating solar PV into the grid, energy planners will encounter three main issues related to the capacity. First, solar is a variable energy source, and it is only available in the daytime, which requires other energy sources to handle days with no solar energy and provide energy during the evening. These characteristics are the main reason solar PV is less reliable and unsuitable in directly replacing baseloads such as coal or nuclear energy. Second, once a significant capacity is installed in the grid, the other generators have to adapt to solar energy generation. The International Energy Agency (IEA) classifies the impact of variable renewable energy (VRE) on the energy system's operation into four phases [14]. Within the 4 phases, in Phase 2, there is minor to moderate impact on system operation, but once a region or country reaches Phase 3, the renewable energy sources now determine the operation pattern of the system. These characteristics complicate the energy balance that the grid must meet at every instance of time. Finally, since solar capacity could be deployed in a larger capacity relative to traditional energy sources, solar capacity will go beyond the peak demand at some point in the adaption process. As a result, there will be no further demand to utilize its peak power. Despite the potential wasted solar energy, Perez et al. [15] argues that overbuilding is necessary to mitigate intermittency. These issues will be encountered at different stages in the solar PV deployment.

At the current penetration rates of some countries, solar curtailment has started to become a problem on top of the flexibility and variability issue of solar PV. Denholm et al. [16], researchers from the US National Renewable Energy Laboratory, noticed a peculiar impact

on the shape of the demand after subtracting solar generation and published this observation in February 2008. The California Independent System Operator later coined the term "duck curve" to describe this phenomenon, given that the shape of the net load resembles a duck as solar installation increases [17]. This curve highlights the necessary changes that the flexible generators have to perform. First, the flexible generators should be able to ramp up and down, and second, the minimum generation of these generators should be lower than the “belly” of the “duck curve.” Solar curtailment has to be implemented if either of these conditions is not satisfied. Curtailment generally happens when the flexible load is unable to reduce production to compensate for the high volume of solar energy.

Several countries with high variable renewable energy installation are already experiencing solar curtailment. The mismatch of PV supply and electricity demand and the limitation of other sources to respond to rapid changes limits the large-scale integration of solar PV [18], [19]. Possible solutions involve increasing the flexibility of other sources [6], [18], transmission [6], [20] and energy storage [18], [21]. Alternative solutions involve demand-side management [22]–[24] and installing PV to better match demand [21], [25].

Although the concept of flexibility has existed since the dawn of the electric power networks, it was primarily designed to respond to changes in demand and potential system faults [6]. In terms of flexibility, nuclear’s generation flexibility is limited by long ramp rate and minimal output changes, and despite coal’s slightly more flexible generation, it still has to maintain a certain minimum loading due to flame stability [18]. The intermittency of the renewable energy source has caused added complexity in the system.

Strengthening the transmission grid helps in providing the diversity of resources through a bigger geographical area, and it also provides the ability to send renewable energy from areas with high concentrations of renewable energy towards the demand [6]. In addition, power producers could also reduce the risk associated with their portfolios by distributing their assets throughout a large geographical area to offset variations associated with local weather changes [20].

Energy storage is seen to be the best solution to lessen the disadvantages of intermittent energy sources against baseload generators [18]. PV systems connected to energy storage can store excess production and discharge it as needed, thereby improving the match between supply and demand [21]. By adding 4 to 8 hours of storage capacity, wind and solar PV curtailment could be reduced significantly [26]. Despite it being the best option, energy storage remains an expensive solution. However, recent cost projection shows that the price might become cost-competitive soon [27].

In jurisdictions with high PV installation, such as Germany, California, and South Australia, there is minimal solar curtailment, but Japan and Hawaii face unique situations [6]. The electricity grid of the former is well-interconnected with neighboring countries and states [6]; thus, they are capable of trading excess energy to their neighbors. For instance, Germany can sell their excess solar or buy nuclear energy depending on the needs of their grid. On the other hand, Japan and Hawaii are isolated island nations and states with no trading options during peak solar production. According to O'Shaughnessy, Cruce, and Xu [28],

Chile and China reported 6% and 3% annual curtailment in 2018 due to geographical mismatch between supply and demand. The authors also compared the distributed nature of the German PV deployment in contrast to concentrated utility-scale deployment in US states like California, which has led to higher curtailment in California despite having relatively the same market size. Hawaii's case is on the extreme side since it is composed of several islands with no interconnection, and a single cloud could have a significant impact on power generation [29]. These specific scenarios show the distinctions of the problems faced by different regions or countries. As Sovacool stated, there is no magic formula that will solve all the problems in the energy transition [8]. Every scenario must be carefully studied prior to actual deployment to mitigate the risks associated with renewable energy.

1.3 Japan's case

1.3.1 National Case

In July 2018, the Government of Japan (GOJ) released Japan's 5th Strategic Energy Plan. GOJ reiterated its commitment to the projected energy mix for 2030, where fossil fuel-based generation will be reduced to 46%, and renewable energy will comprise 22–24%, of which solar energy will have a 7% contribution [30]. The Electric Power Companies, whose jurisdiction is shown in Figure 1.1, have supported the strategic plan, and this has driven the influx of solar PV installation in the grid through the FiT (Feed-in Tariff) scheme. The FiT scheme was officially launched in July 2012 following the promulgation of the "Act on special measures concerning procurement of electricity from renewable energy sources by electricity utilities" in August 2011 [31]. The scheme subsidized both residential and commercial energy producers [32] which ensured profitability of newly installed solar panels.

As seen in Figure 1.2, the PV capacity has drastically increased since 2012. As of March 2020, Japan has a total solar generation capacity of 54.4 GW. Tokyo has the most capacity at around 13.5 GW, followed by Chugoku and Kyushu at around 9.5 GW each [5]. In FY 2019, Japan generated almost 65 TWh through solar energy as seen in Figure 1.3. This generation capacity is 7.3% of the annual demand of 880 TWh in that particular year. By FY 2020, this penetration rate reached 8.3%, which shows that the target for solar was already achieved for two consecutive years.

In October 2021, GOJ released the 6th Strategic Energy Plan, which further increased the target share of renewable energy to 36-38%, of which solar now comprise 14-16%. The target for hydropower, wind, and biomass also increased to 11%, 5%, and 5%, respectively. Geothermal remains to be at 1%. This effectively brings down the thermal generators to 41%.

Figure 1.1: Jurisdiction of the Electric Power Companies in Japan rendered using GIS data from [33].

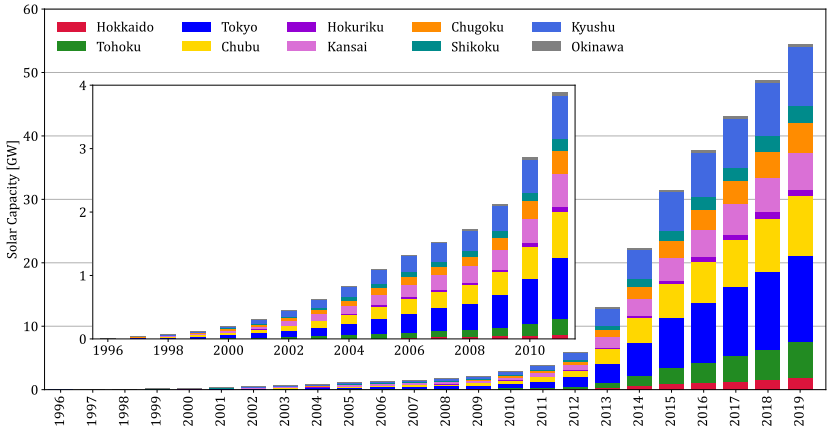

Figure 1.2: PV Capacity of Japan as of March 2020. Data was consolidated in [5].

1.3.2 Kyushu Region

The Kyushu region, located on the western tip of Japan, is one of the regions leading the country's solar PV generation. Although Tokyo and Chubu also have significant PV capacity, since these two regions have higher demand, the consequences of high PV penetration are

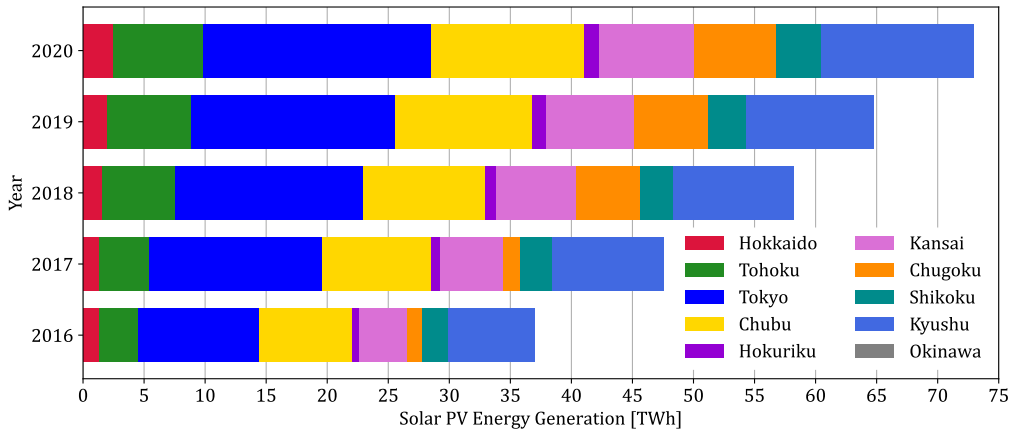

Figure 1.3: Electricity Generation of Japan from PV. Data was consolidated from various Electric Power Company listed by Organization for Cross-regional Coordination of Transmission Operators (OCCTO) in [34].

not yet felt. Tokyo and Chubu is also demand-driven, while Kyushu has relatively higher solar potential and cheaper land cost, which are the main drivers in increasing solar PV capacity in this region. As of early 2021, the Kyushu region has a total installed capacity of 10.1 GW, and the construction of additional plants that will increase this capacity further to roughly 16 GW [35] by around 2027 is already approved. As a result, the share of solar PV generation has been steadily increasing. Solar PV generation accounted for 7.0%, 8.6%, 9.5%, 10.1%, and 12.3% of the total yearly generation from FY 2016 to 2020 based on the data published by the Kyushu Electric Power Company (KyEPCO) in [36].

However, Kyushu remains heavily dependent on thermal generation despite the increased solar and nuclear, as seen in Figure 1.4. Thermal generation accounts for 72.6%, 69.8%, 53.8%, 51.2%, and 54.9% of the total yearly generation from FY 2016 to 2020 [36]. The decrease is mainly attributed to the increase in nuclear generation. As of June 2018, Kyushu restarted four of its six nuclear power plants (NPP) with a total capacity of 4.140 GW [37]. The other two power plants were permanently decommissioned. There is still an increasing need for additional solar investment to reduce the dependence on thermal power plants further. However, in October 2018, Kyushu was forced to curtail some solar production for the first time, which is also the first time for the whole country, to meet the energy balance. More curtailment occurred in March 2019, and it has been occurring seasonally.

In IEA's classification of renewable energy impact, Japan, as a country, is already in phase 2 where there is a minor to moderate impact on the system operation, whereas Kyushu, as a region, was categorized as phase 3, where VRE determines the operation pattern of the system [14]. This differentiation further shows that Kyushu is leading the country in terms of solar PV penetration and is already facing issues ahead of the country. Therefore, Kyushu's situation lends itself as a viable case study in exploring the potential impact of solar energy in reducing CO_2 emissions by replacing traditional energy sources with solar energy.

In this dissertation, Kyushu is used to represent Japan's future grid scenario since it has diverse energy sources such as nuclear, coal, LNG, geothermal, biomass, wind, and a

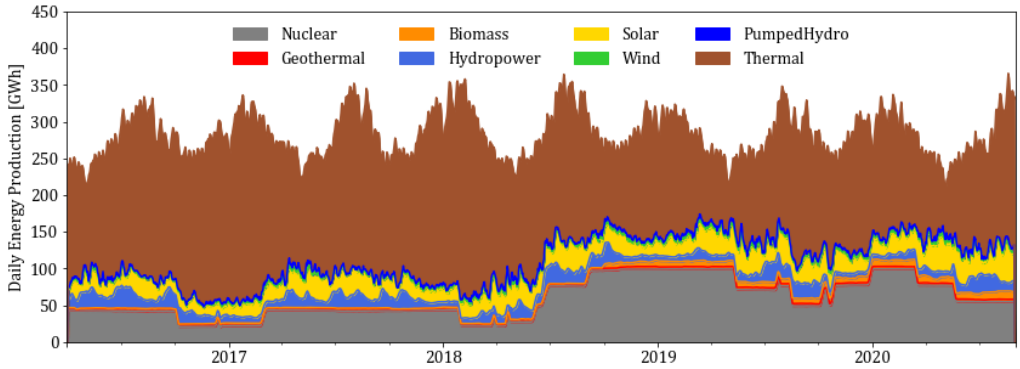

Figure 1.4: Energy Production of Kyushu (visualized from Kyushu Electric Power Company's data [36]).

significantly large PV capacity. The other regions will have similar generating capacity once they restart their nuclear plants and install more PV capacity. Japan also publishes publicly available data necessary to conduct an hourly energy balance simulation. Kyushu and the corresponding energy data and model is further discussed in Section 2.

1.4 Objective

Hedging on solar PV to be able to lead the energy transition will be technically challenging since this technology alone could not resolve the energy problems currently facing society. However, solar has proven itself a viable champion to serve as the foundation of the energy transition, especially in regions where wind and hydropower are either inadequate or already exhausted. Due to its problems on intermittency and nondispatchability, solar PV will have to rely on other technology to successfully decarbonize the grid. Such technology should be able to handle current and potential issues such as unavailability, curtailment, and overproduction. These complementary technologies must also be viable financially to ensure the competitiveness of the whole system. The Kyushu region in Japan is a viable candidate as a case study since it has already reached a penetration rate where the other technology is adjusted to accommodate the solar PV generation and there is are plans to continuously increase its solar PV capacity.

Under this premise, this dissertation aims to understand the potential, limitations, and implications of incorporating other technology with solar PV to transition toward carbon-neutral energy sources, thereby decarbonizing the electricity grid. The study pursues this effort by first building an hourly grid model that includes the generators and demand in the region. Then, with this model, mathematical, machine learning, and heuristic tools were used to explore future scenarios that involve high PV penetration. In all these scenarios, the study optimizes the utilization of the existing and new generators while ensuring the region's energy balance. Finally, the study further analyzes the operational cost of the whole grid to understand the financial impact of the changes.

1.5 Thesis Structure

The overview and objective of the study was presented in Chapter 1. Further background of the study is provided in Chapter 2, which provides additional information in relation to the design and assumptions in Chapters 3 to 7. These chapters, where several complementary technologies are analyzed, were structured to stand-alone.

Chapter 3 focuses on understanding the nature of curtailment by reproducing it using known periodicity and statistical data. In this chapter, the main focus is increasing the solar PV capacity and generating insights regarding the limitations of the current technology in adapting to large PV capacity in the grid. Fourier transform is used to generalize the weekly and daily fluctuations of the data.

Chapter 4 pursues the idea of decommissioning coal power plants by further increasing PV capacity and increasing flexible generation. The impact of weather on demand and solar PV generation is explored in this study to understand the risk of decommissioning coal power plants. K-Means clustering is used to generate synthetic demand profiles based on temperature and energy data, and this was used to generate the cases that the grid might face. This chapter aims to provide insights on the current technical potential of solar PV to reduce coal capacity in the grid and the corresponding increase in the cost of electricity generation.

Chapter 5 investigates the optimal amount of storage that could minimize curtailment to ensure the continued financial viability of solar PV. This study incorporates the gradual deployment of solar PV and the appropriate complementary storage that could minimize wasted solar generation. Monte Carlo random sampling and a financial evaluation focusing on a planning horizon are used to go through various storage capacity growth trajectories. This chapter mainly provides insights into the balance between the cost of wasted solar energy and additional storage infrastructure.

Chapter 6 extends Chapter 5 and explores the potential of electric vehicles as storage to reduce curtailment. This study looks into utilizing underutilized electric vehicles as storage during periods of high excess solar PV production. Similar to Chapter 5, this study also looks into the gradual increase in storage capacity by modeling the increase in the volume of electric vehicles using the logistics growth model.

Chapter 7 explores the potential of hydrogen as the complementary technology for solar that could potentially eliminate fossil-fuel-based power generation. This study navigates through several potential configurations of hydrogen technology and additional infrastructure to understand the technical limitations of these configurations. Since this configuration has several parameters, this study uses a Pareto optimal genetic algorithm-based optimization to identify and assess the configurations. This chapter provides insights into the additional investment that could eliminate fossil fuels in the electricity grid.

Based on the insights gained from Chapters 3 to 7, Chapter 8 concludes the study by summarizing the outcomes, generalizing the insights, and highlighting future works.

2 Background of the Study

This chapter discusses the common topics, ideas, assumptions, datasets, and tools discussed throughout the rest of the paper. Specific datasets, equations, and tools are discussed in the individual chapters to maintain the cohesiveness of the written material. Some of the information in this section is repeated in the specific sections to provide easier access to the information or add minor changes.

2.1 The Case of Kyushu

Kyushu Region, located in the western tip of Japan, has a total land area of 42,230 km^2 [38] and a total population of around 10.2 million as of 2019 [39]. It is comprised of 7 administratively independent prefectures as shown in Figure 2.1. The region has thriving tourism, construction, and manufacturing industries [39].

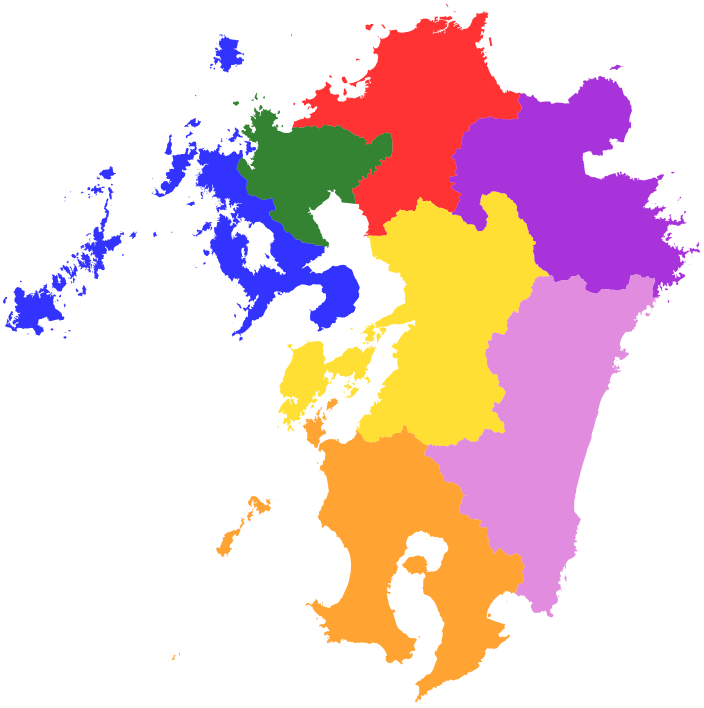

Figure 2.1: Map of Kyushu by Prefecture rendered using GIS data from [33].

Similar to the rest of the country, there was a spike in solar PV installation from 2012 to 2014, which peaked in 2014 where 2 GW solar capacity was installed, mainly driven by the FiT scheme. As seen in Figure 2.2, the region has continuously increased its PV capacity, which is already around 10.1 GW as of March 2020 [35]. Consequently, this has contributed to the increase in solar PV penetration in the region, as shown in Figure 2.3.

Along with the restart of the nuclear power plants in the region and the increase in solar PV capacity, Kyushu had to curtail some solar PV electricity in October 2018. It occurred again in March 2019 and has become a regular phenomenon during the spring and autumn. Figure 2.4 shows the curtailment profile of Kyushu in March 2019. The area graph shows the region's total generation from various energy sources. Curtailment is necessary when the overall demand (red line) is below the region's generation capacity (area graph). The overall demand includes the local Kyushu demand, the transmission, and the charging of the

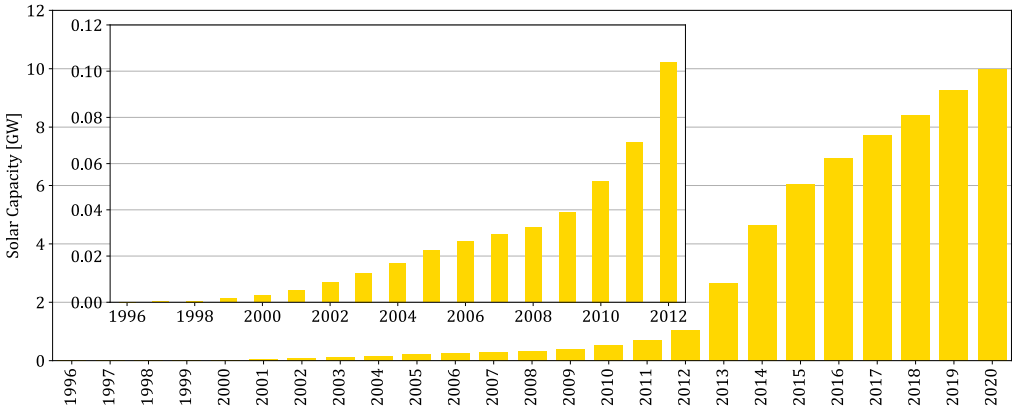

Figure 2.2: PV Capacity of Kyushu as of March 2020. Data was consolidated from [5] and [35].

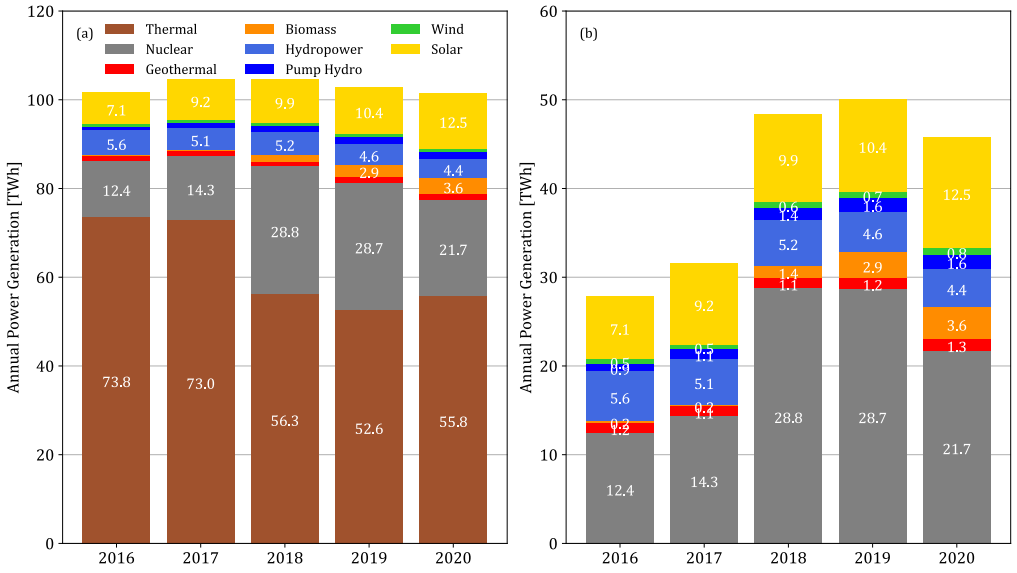

Figure 2.3: Annual Electricity Generation in Kyushu from FY 2016 to FY 2019. (a) shows the total electricty generation and (b) highlights the share of non-carbon sources. Data from [36].

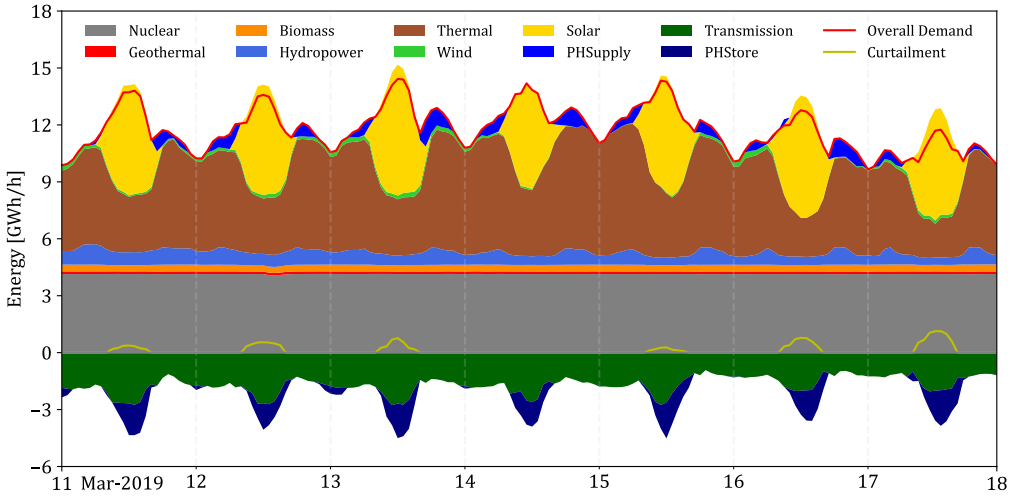

Figure 2.4: Curtailment Profile in Kyushu in March 2019 (visualized from Kyushu Electric Power Company's data [36]). PHSupply refers to the period when the Pump Hydro storage is supply energy to the grid while PHStore is when it is charging.

pump hydro. The curtailment's magnitude (yellow line) reached 1 GW at peak curtailment during the weekend. Moreover, the figure shows that the pump hydro storage (dark blue) was charged, the transmission (dark green) was increased, and the thermal production (brown) was reduced, but these efforts were insufficient to meet the energy balance. Recent data from October 2019 and March 2020 also show curtailment. Curtailment will eventually increase in frequency and magnitude since the installed solar capacity will continually grow based on the approved solar power plant plans.

As observed in Figure 2.4, Kyushu has several mechanisms to reduce solar curtailment. It mainly utilizes its transmission lines and pumped hydroelectric energy storage (PHES) to use the excess energy whenever the other generators cannot reduce their production. The Kanmon interconnection line connects the Kyushu region to the rest of the country via a 500 kV, 2.38 GW transmission line [40]. The region also has three hydroelectric power plants (pure pump-storage) with a total generation capacity of 2.3 GW and 6 hours of storage [41]. This storage was initially designed to store excess energy from the nuclear power plant but is now used to store energy during peak solar production and generate energy to support the ramp rate of the thermal plants.

Kyushu can generate as much as 20 GW at peak generation; thus, its 2.38 GW transmission capability to other regions is limited. Kyushu can then represents island nations with geographically isolated electrical grids like the Philippines, Indonesia, and Hawaii, or technologically isolated grids like South Korea. In this study, the transmission to the rest of Japan is treated as local demand to simplify the analysis.

2.2 Energy Data

From April 2016, the Electric Power Companies (EPCOs) in Japan were required to publish their hourly data publicly, and the individual websites are listed by the Organization for Cross-regional Coordination of Transmission Operators (OCCTO) in [34]. Focusing mainly on the data relevant to Kyushu, the hourly information about generation, transmission, and demand were collected from the website of Kyushu Electric Company [36]. In this report, curtailment information is also available. Transmission is technically bi-directional, but in practice, Kyushu mainly sends electricity to the rest of Japan; thus, transmission is considered part of the total load. Pumped hydro storage is seen as both generator and load depending on its operation. The published data does not include the specific distribution of the power generated from coal, LNG, or oil.

The properties of the generators in Kyushu are listed in Table 2.1 were consolidated based on various sources [42]–[44]. The Ministry for Economy, Trade, and Industry (METI) through Agency for Natural Resources and Energy (ANRE) publishes the number of power plants and the corresponding capacity per prefecture since 2019 [42]. Although the data was last updated in 2007, the Ministry of Land, Infrastructure, Transport, and Tourism has a detailed database of the power plant that includes information such as location, capacity, and fuel type [43]. Japan Beyond Coal [44] is a campaign that aims to decommission coal-fired power in Japan by 2030, and as part of its efforts, it regularly updates a database of all the coal-fired power plants in Japan with information such as capacity, scale, year of operation, company, and current status.

The study assumed that oil is no longer part of the energy mix, but coal remains a significant baseload power source. LNG, hydropower, and pump hydro are the flexible load in the region, while nuclear, biomass, and geothermal run as baseload generators. Wind capacity does not significantly impact the hourly balance in the grid due to its relatively low capacity. The minimum operating output power and the ramp limit were specifically gathered for each generator since this is necessary for the hourly balance. Aside from coal, which was assigned a ramp limit of 1%, the baseload were set to have a ramp limit of 0 since it was assumed that it should constantly run. For the simulation, the study assumed that there is no maintenance throughout the year. The flexible load were given a ramp limit of 40%. The information regarding the other infrastructure is added in the specific section where they are used.

Using the published resource utilization data from KyEPCO in [45], it was determined that the company generated 8 TWh from LNG in 2019 through their 4.625 GW LNG plants. This generation represents 20% LF for the company. An independent power producer owns the other 0.625 GW LNG power plants in the region, which are composed of mixed gas power generators. Assuming these IPP plants are running at a higher LF of 40%, it was determined that the LNG plants generated around 10 TWh in 2019. This limit was considered as the business-as-usual throughout the study.

Table 2.1: Generators in Kyushu as of FY 2019 (consolidated from [42]–[44])

Generator	Power [MW]	Carrier	$\mathrm{Output}_{\mathrm{min}}$ [%]	Ramp Limit [%]
Coal	7037	Coal	30	1
LNG	5250	Gas	15	40
Geothermal	160	Renewable	100	0
Biomass	450	Renewable	100	0
Solar	9000	Renewable	0	100
Nuclear	4140	Non-GHG	100	0
Wind	355	Renewable	15	40
Hydro	4000	Renewable	15	40

2.3 Energy Modeling

2.3.1 Energy Modeling Tools

The necessary changes in the electricity grid to meet the decarbonization efforts will require significant time and money. Therefore, it is crucial to model these changes to convince energy planners and policymakers to pursue these efforts. Pfenninger, Hawkes, and Keirstead [46] claimed that energy system models for the twenty-first century should take the issue on (1) time and space resolution, (2) balance of uncertainty and transparency, (3) complexity of the energy system, and (4) impact of the human behavior and social risks and opportunities.

Ringkjob, Haugan, and Solbrekke [47] reviewed 75 modeling tools used for energy and electricity systems with large shares of variable renewables. The authors only reviewed models that were published after 2012, and they validated the information by contacting the authors, of which 71 responded. Their review mainly focused on the purpose, spatiotemporal resolution, and techno-economic parameters of the models. They concluded that the existing models and modeling tools have sufficient capabilities, but issues such as variability, consumer participation, validation, transparency, and forecasting must still be addressed.

Morrison [48] wrote that as of July 2017, 28 energy system modeling projects made their source code public driven by the desire for improved public transparency, the need for genuine scientific reproducibility, and the hope for improved academic productivity and trust. The 28 projects were further divided into energy system frameworks and electricity sector frameworks. Energy system frameworks such as Balmorel [49], Calliope [50], and OSeMOSYS [51] models all forms of energy while electricity sector frameworks such as pandapower [52] and PyPSA [53] mainly focuses on the energy sector. Open Energy Modelling Initiative (openmod) website and wiki page keep track of new open source projects [54].

Heard et al. [55] challenged the existing published literature about 100% renewable energy in 2017. Among many issues, the author challenges the hourly resolution's sufficiency for the simulations. The authors did recognize the common claim that sufficient storage technologies will resolve reliability issues within the hour. Still, they counter that this is a risky claim since there might not be enough storage capacity to handle the fluctuation of renewable energy. In response to this article, Brown et al. [53] countered that fluctuation

due to short-term weather changes balances out when considering sizeable geographic areas such as region or country. The response further stated that one-hour resolution is sufficient for solar PV to capture the change in the evening and emphasized that this will be countered by the ramp rate of open cycle gas turbines and hydroelectric power plants.

Both the developers of pandapower and PyPSA saw the benefit of using Python programming language due to its open-source ecosystem that includes powerful computational library like `numpy` and the flexible `matplotlib` plotting library. This study also believes in the importance of the open-source ecosystem, especially since there will be instances when additional functionality must be implemented to account for specific details in the simulation. Since the source code of these modeling frameworks is available, such changes are possible. Although pandapower has more modeling components, it does not model storage units while PyPSA provides this functionality [52]. PyPSA was chosen for the modeling since it was foreseen that storage would be critical in modeling future energy systems in this study. Following the logic behind the sufficiency of the hourly resolution by Brown et al. [53], the study also deemed that hourly resolution will be sufficient for the simulations.

2.3.2 Python for Power System Analysis (PyPSA)

The hourly simulation used Python for the Power System Analysis (PyPSA) Modeling Framework [53]. The PyPSA environment provides a framework for the buses, lines, loads, generators, storage, and units, among many other parameters. Using these components, the network configuration show in Figure 2.5 was used to model the nodal balance in Kyushu. This configuration was modified as needed in the subsequent sections. The coal generator, the Kyushu demand, and the transmission demand were directly connected to a single bus. The rest of the generators was then connected to a sub-bus, which was then connected to the main bus. Creating the sub-bus ensured that the PHES could not charge from the coal generator, which prevented the optimizer from generating and storing more power from coal. Since there are still instances when the existing PHES capacity is charged by the other generators, albeit minimal, a connection was provided to facilitate this power flow.

For the optimization, the `pypsa.linopf` was mainly used by calling the `network.lopf` after building the `pypsa.network`. The Linear Optimal Power Flow (`pypsa.linopf` or LOPF) can optimize the dispatch of generation and storage, and the capacities of generation, storage, and transmission [56]. The optimization aims to minimize the total system cost for the duration of the simulation, which includes the additional investment for generator, storage,

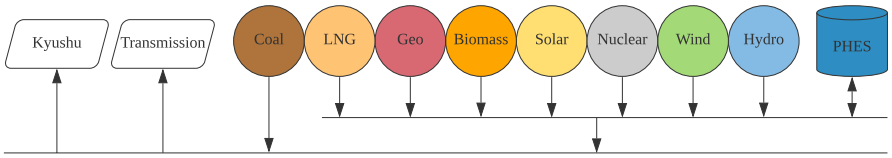

Figure 2.5: Configuration of the base design of the single-bus network used in the study. Modification were made as needed in the subsequent scenarios.

and transmission lines (if enabled in the optimization) and the unit cost of the power generation. Throughout the optimization, the maximum capacity of the generators, storage, and transmission serves as the main constraint. The optimization constraints the ramp rate of the generators by checking the maximum power transfer from one timestamp to the next (PyPSA uses the term snapshot). As a final constraint, the optimization must meet the energy balance within the set constraints to optimize the system in each timestamp. Therefore, the optimization will fail even if only one timestamp fails any of the constraints.

2.3.3 Optimizers

PyPSA supports various solvers such as the free solvers GLPK (GNU Linear Programming Kit) and CBC (Coin-or branch and cut) or the commercial solver Gurobi [56]. Written in ANSI C, GLPK is a cross-platform linear programming (LP) and mixed-integer programming (MIP) free and open-source software (FOSS) solver [57]. CBC is another FOSS solver written in C++ that mainly focuses on MIP, and it could easily be interfaced with GAMS, Python, and even Microsoft Excel [58]. Similar to GLPK and CBC, the commercial solver Gurobi is capable of solving LP and MIP problems, and it can utilize parallelism during its calculation [59].

Initially, the study used GLPK due to its straightforward installation process, but it is limited to a single-core processor. Since Gurobi provides academic license [60], this study opted to use it for its parallelization capability. Furthermore, since PyPSA abstracted the code formulation, all these optimizers could work directly with Python 3.

3 Reproducing Solar Curtailment with Fourier analysis

The contents of this chapter is based on Dumlao, S. M. G., & Ishihara, K. N. (2020). Reproducing solar curtailment with Fourier analysis using Japan dataset. Energy Reports, 6 (Special Issue: CPESE 2019), 199–205. doi: https://doi.org/10.1016/j.egyr.2019.11.063.

3.1 Introduction

Despite all efforts to reduce curtailment, it is inevitable; thus, it is essential to estimate the total energy production that can be effectively as this affects the Levelized Cost of Energy (LCOE) of solar PV. In the case of Japan, hourly data is available which makes the calculation easier. For some countries, data are not collected nor published; thus, calculating curtailment will be difficult. The case of Kyushu is a prime candidate in studying curtailment since it has the anticipated increase in solar installation and has more than sufficient data to extract essential information.

This study proposes a methodology to reproduce curtailment information using known periodicity and statistical data. An analysis of the future curtailment scenario is presented where curtailment is characterized. Fourier approximation of the significant segments of demand and solar production is approximated to reproduce the curtailment. Finally, an evaluation of the reproduction is presented where significant data are identified to an acceptable level of reproduction. Possible applications are also presented.

3.2 Data and Methods

The data were collected from the website of Kyushu Electric Company, where the hourly information about demand, generation, transmission, and curtailment are published [36]. Transmission is considered as part of the total load. Pumped hydro storage is seen as both

generator and load depending on its operation. Although the baseload could change within the year, the baseload was fixed to its maximum capacity.

In the simulation, all the other data were considered as fixed except for solar and thermal production. The simulation for the whole study focused on the 2018 hourly data. The solar installation was treated as the controlled variable, and the thermal generators produce the remaining demand. Solar energy is preferred unless the lower limit of the thermal plant is reached. The simulation used 15% minimum production for the thermal plant. If the limit is reached, the excess solar generation will be curtailed. The energy balance calculations were done using Python for Power System Analysis (PyPSA) [53].

Initially, the installed capacity was increased until 30 GW to visualize the impact of increasing installed capacity to the curtailment. The analysis then focused on 2 GW increments from the current installation of 8 GW to the scheduled installation of 16 GW. Monthly, weekly, and daily data were analyzed to extract information crucial to curtailment.

Taking into consideration the identified factors that affected the amount of curtailment, the demand and solar generation were first approximated using Fourier approximation and statistical data. Once all the essential data were approximated, the curtailment was recomputed using the same set of data and assumption used in the initial simulation. Finally, the results of the simulation using the actual data and reproduced data were compared and analyzed.

It can be seen in Figure 3.1 that initially, as PV installation increases, the production and consumption are aligned. After a certain point, there is an increasing gap between the PV production and consumption which represents increasing curtailment. At the anticipated installed capacity of 16 GW, it is expected that around 23% of the annual PV production will be curtailed. It is essential to understand the source of the curtailment to determine the estimation compromises.

PV production in Japan peaks in summer and gradually decreases until winter as seen in Figure 3.2. Generation reduces late spring due to rainy weather. The demand of Kyushu also

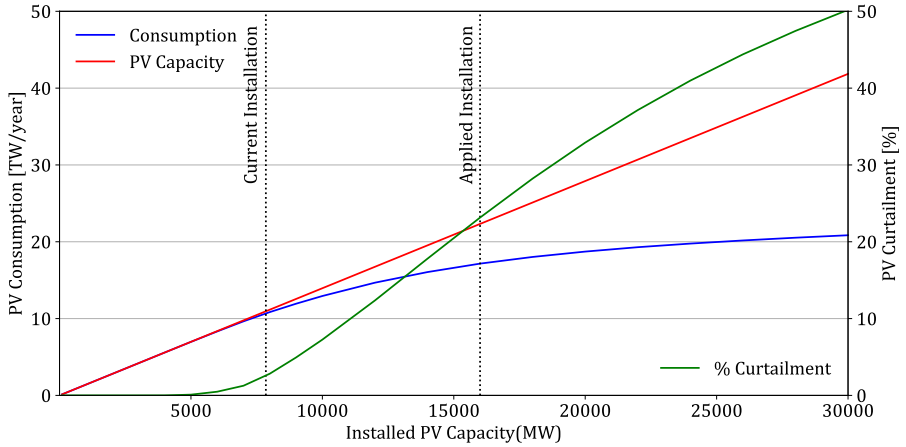

Figure 3.1: Simulated amount of curtailment using 2018.

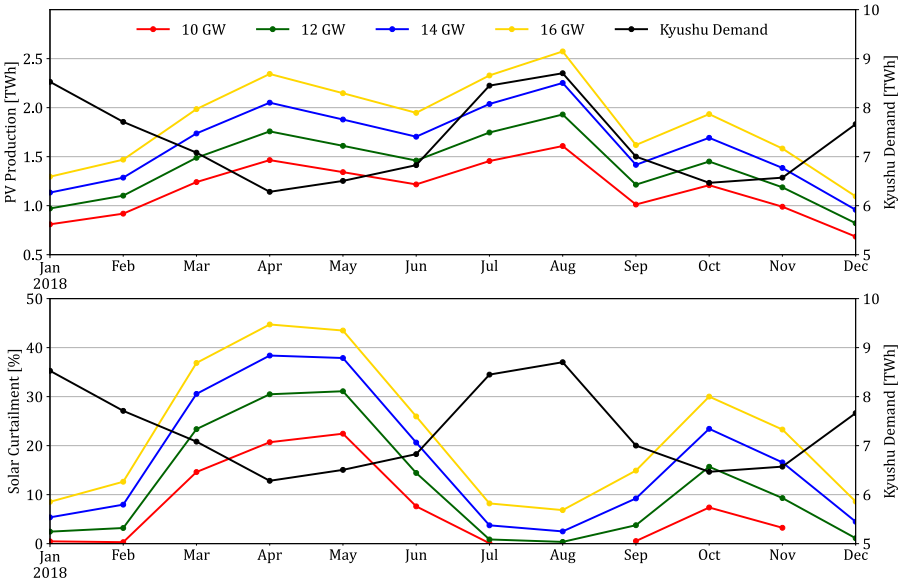

Figure 3.2: Kyushu demand, PV production, and % curtailment.

peaks in the summer and winter, but in contrast to the supply, there is less demand in spring and autumn. Based on the data seen in Figure 3.2, the difference in supply and demand during fall and spring led to higher curtailment rate. This shows the importance of focusing on the period with the highest mismatch in estimating curtailment.

Less demand in the weekend often leads to more curtailment during this period. In terms of frequency, curtailment also starts to manifest in the weekend and then eventually in the weekdays. Weekly variations compound the seasonal changes in demand resulting for curtailment to initially occur on the weekends of spring and autumn. This eventually spreads to other seasons as solar installation increases. Weekend fluctuations should also be well represented.

The majority of solar production happens in the middle of the day. However, at higher solar installation, curtailment may begin even at the start of the day. Despite this, upon closer inspection, the majority of the curtailment still occurs between 9:00 and 15:00 at the projected 16 GW installation in Kyushu. The approximation should, therefore, put higher importance to this part of the day. The rest of the day is acceptable compromises when necessary.

3.3 Results and Discussion

3.3.1 Demand Approximation

Initially, it was assumed that human behavior affects the demand curve. Therefore, the periodicity of human behavior should be considered. To utilize this periodicity, Fourier approximation is proposed. However, looking into the data reveals that each season has a different daily demand curve, which makes it challenging to identify the periodicity. To solve this problem, a segmented Fourier approximation was tested. The weekly periodicity was initially explored to appropriately divide the year. A Fourier Transform was used to identify the frequency components of each week. Using the magnitude of each frequency, K-means clustering was used to cluster the weeks into six segments.

It was observed that each segment has similar daily fluctuations. Another Fourier Transform was done to identify the frequency components of each segment. For each segment, seven harmonics representing the weekly and daily variations were selected. The 7th weekly harmonic coincided with the 1st daily harmonic. The DC component was also selected. It can be seen in the simplified cosine Fourier equation in (3.1) that the demand curve, for each segment, can be approximated using a DC offset (A_0), 6 weekly components, and 7 daily components. W_n and D_n is the ratio of the magnitude of each Fourier term using W_1 and D_1 as reference. The ratio of the components creates the overall shape of each model. B_0 and C_0 serves as the scaling factor for the weekly and daily components, respectively. Each frequency component has a corresponding phase shifts w_n and d_n based on the model.

$$demand\,(t) = A_0 + \ B_0 \sum_{1}^{6} 2W_n \cos\left(\frac{2\pi}{168} nt + w_n\right) + C_0 \sum_{1}^{7} 2D_n \cos\left(\frac{2\pi}{24} nt + d_n\right) \quad (3.1)$$

Approximating demand using (3.1) requires three sets of data: the model that was initially developed, model assignment for each week, and available data where the model will be fitted. There are various ways to assign a model per week. For this implementation, prior knowledge was used. The models and model assignments provide the corresponding magnitude W_n and D_n and phase shifts w_n and d_n for each frequencies for each week.

The available data points were then used to identify the scaling components B_0 and C_0 of the model for each week. The current implementation requires four data points (9AM, 3PM, 6PM, and 9PM) per day due to periods with half-day cycle. This can further be reduced to twelve data points per week by sampling weekdays, Saturdays, and Sundays. Another option is to reconstruct the data points using statistical data like average consumption, the number of peaks, peak values, and valley values. Using the daily harmonics (second summation), the initial shape of the week was approximated by identifying A_0 and C_0 using Least Square Method. The average weekday data was initially used. The weekly harmonics (first summation), were then used to fine-tune the approximated signal by identifying B_0.

In order to maintain uniformity, the same methodology was used for all segments despite segment 1 having less accuracy as seen in Figure 3.3. This was acceptable since there is less curtailment early in the year to have a significant impact on the curtailment calculation. The critical months in segment 2 and 3 (April, May, and June) were reproduced well. The weekend variations were also well represented.

3.3.2 Solar Approximation

Solar production does not have a periodicity that could be exploited. However, the general shape of solar production is the same. The solar generation can be approximated using a three-step process. First, Fourier approximation can be used to determine the shape. Second, the peaks can then be determined based on probability. Finally, using the peaks as an envelope, the peak of each curve can be used to approximate the actual solar production.

Results in Figure 3.4 (a) shows that the general shape can be reconstructed using three daily harmonics. Since the goal is to reproduce the curtailment, minor shape difference due to varying time for sunrise and sunset are acceptable compromises. This is acceptable since curtailment mostly happen from 09:00 to 15:00. Since solar production is stochastic, past solar radiation or peak data can be used to generate a probability distribution per month to reproduce the peaks. In this study, a discrete probability distribution per month was generated using the actual data. The distribution was then used to randomly generate the peaks shown in Figure 3.4 (b). Using the peak as an envelope, as shown in Figure 3.4 (b), the solar generation was approximated with the Fourier approximation of the shape.

3.3.3 Curtailment Reproduction

Using the baseload and flexible generator values used in the initial analysis of Kyushu and the approximated demand and solar production data, the curtailment was recalculated. Figure

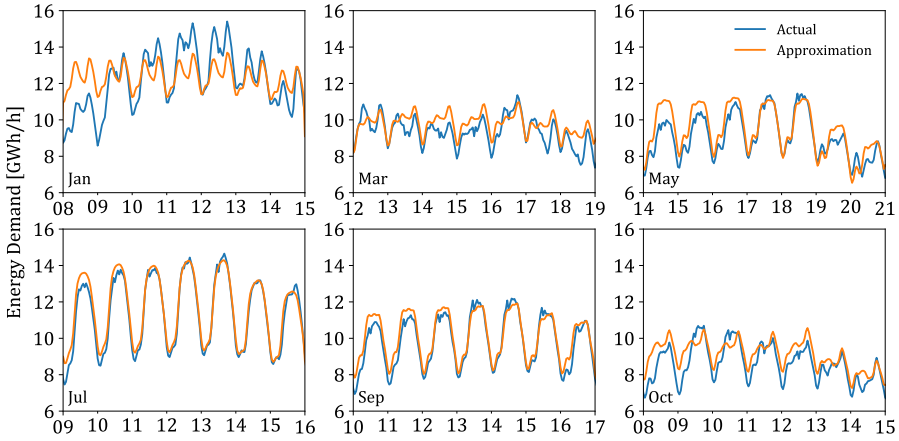

Figure 3.3: Demand approximation for each of the six segments.

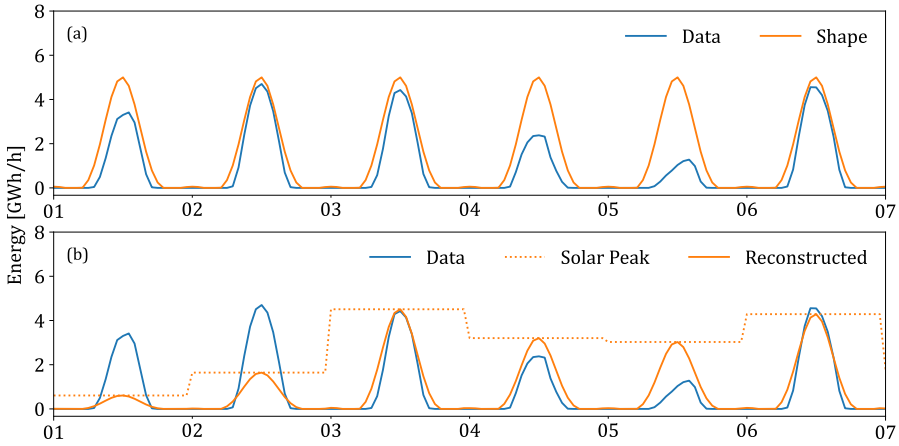

Figure 3.4: Solar approximation. The shape was reconstructed in (a), and the peaks were generated and the two information were combined in (b).

3.5 shows that the reproduced curtailment values closely resemble the initial simulation with different margins of error depending on the installed capacity. Figure 3.6 shows that the reproduced signal can also be used to analyze monthly curtailment.

3.4 Conclusion

A Fourier approximation methodology was presented to reproduce curtailment. The case of Kyushu was analyzed to extract factors that affect curtailment, and three major considerations were highlighted. First, curtailment occurs in the periods with the larger mismatch between supply and demand. Second, weekend fluctuations should be considered. Finally, focusing on the energy balance between 09:00 and 15:00, where the most of curtailment occurs, is sufficient.

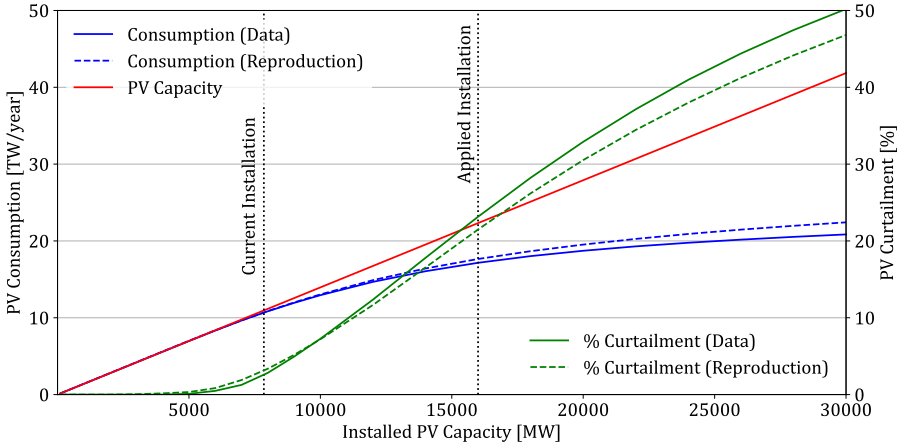

Figure 3.5: Comparison of the curtailment calculation.

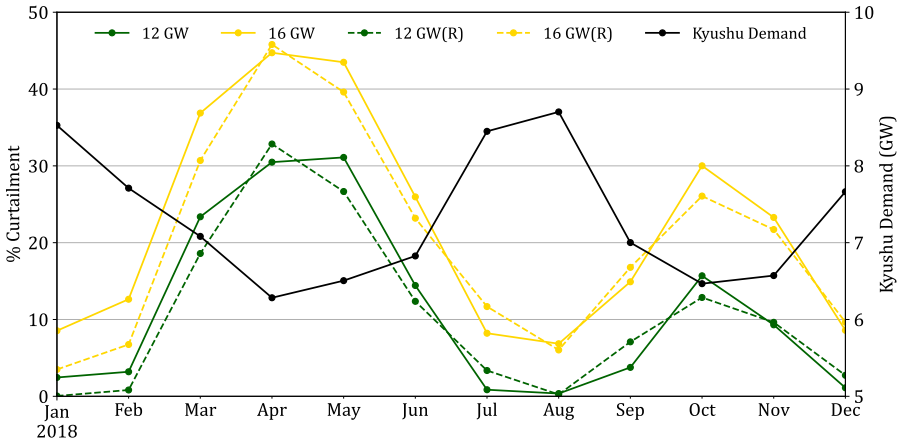

Figure 3.6: Comparison of the seasonal curtailment.

Following the three consideration, demand was modeled using Fourier approximation where 15 harmonics were sufficient to approximate the demand. The model can be used along with model assignment for each week, and existing data where the model will be fitted. The solar production was approximated using Fourier approximation for the shape and solar peak probability distribution for the peaks. Multiplying the two approximates the solar production.

Finally, the curtailment can be reproduced by calculating the energy balance for each hour using the approximated demand and solar curve, and known data about the flexible load and baseload. The current reproduction has up to 3% error depending on the installed capacity. This methodology can be used to reproduce curtailment for countries where the statistical or specific data can be collected without resorting to gathering hourly data.

4 Weather-Driven Scenario Analysis for Decommissioning Coal Power Plants

The contents of this chapter is based on Dumlao, S. M. G., & Ishihara, K. N. (2021). Weather-Driven Scenario Analysis for Decommissioning Coal Power Plants in High PV Penetration Grids. Energies, 14(9), 2389. doi: https://doi.org/10.3390/en14092389.

4.1 Introduction

4.1.1 Decommisioning Coal

Coal remains to be the cheapest and most economically stable source of electricity for many countries. However, it is also one of the major contributors of CO_2, which leads to global warming. Among the G7 countries, Germany (by 2038 [61]), France (by 2023 [62]), the United Kingdom (by 2024 [62]), Italy (by 2025 [62]), and Canada (by 2030 [63]) have presented their coal phase-out plans. Other European Union member countries have also developed their phase-out plans within the next two decades, and Austria and Belgium have already phased-out their coal plants [62]. Nonetheless, removing coal is a significant roadblock to the green energy transition in many countries, and as countries install increasing amounts of renewable energy, it might be time to consider reducing coal in the energy mix. Solar photovoltaics (PV) can be a green alternative to coal. However, the generation profile of solar energy is different from that of coal, which complicates the process of replacing coal with solar energy. Simultaneously, the variability of solar power requires another flexible source. Liquefied petroleum gas (LNG), given its flexibility, is often used to balance the VRE. Given these intertwined variables, it is necessary to understand the potential, limitations, and implications of using solar energy to replace coal, which are currently unclear.

Many countries see LNG as a bridge to a clean energy future that will pave the way for less coal in the energy mix [64]. It is still a fossil fuel, but it produces less CO_2, which is acceptable for now until a superior technology is available. Due to many countries' tendency to rely on LNG to reduce their CO_2 emissions, the demand for LNG has steadily been increasing, which threatens its supply and price. Shell reported in their LNG Outlook

2020 that global demand for LNG increased by 12.5% to 359 million tons in 2019, which they attributed mainly to the role of LNG in the low-carbon energy transition [65]. It has been reported that the price of LNG increased in October 2020 in anticipation of a colder winter in East Asia [66]. This shows the volatility of LNG's supply and price on the global market, which presents another factor for consideration in the analysis, since solar energy production needs LNG to a certain extent.

Aside from the potential CO_2 reduction benefits, reducing coal capacity could also reduce solar curtailment experienced by grids with high PV penetration. Kyushu started to suffer from curtailment in October 2018, which was initially explored in Chapter 3. Several studies have also explored this recent issue in Kyushu. Bunodiere and Lee [67] explored several scenarios to mitigate solar curtailment in Kyushu using a logic-based forecasting method and concluded that reducing the region's nuclear capacity will reduce curtailment. However, in their approach, they considered coal and LNG as thermal generators as a whole due to data limitations. A coal station behaves like a nuclear plant, since these two technologies are considered baseload generators. By treating coal as separate from LNG and as a baseload generator, it could also be said that coal could reduce curtailment. Although Japan initially used their pump hydro energy storage (PHES) to improve the flexibility of nuclear power plants [68], it is now used to store excess solar electricity generation. Li et al. [69] conducted a techno-economic assessment of large-scale PV integration with PHES and concluded that the PHES could effectively absorb some of the surplus PV production and could maintain low generation cost by using the surplus production. Since the available data regarding power generation in the region aggregate coal and LNG together, the understanding of coal generation in the energy balance is limited.

In order to fully understand the optimal conditions for coal, solar, and LNG production, it is necessary to conduct a power flow analysis to evaluate the impact of investing in more solar PV for driving coal decommissioning. This analysis will provide additional information about the energy balance, including information about solar power generation and curtailment, which are difficult to estimate. By gathering the generators' capacity and generation profiles and the demand profiles, the optimization can calculate the hourly energy balance and minimize the necessary coal capacity and generation. This insight provides the necessary understanding of the potential and limitations of solar energy in regard to replacing coal. However, to ensure the robustness of the analysis and the recommendation, the demand and solar power generation's stochasticity must be considered. It will be challenging to recommission a decommissioned plant due to an unforeseen circumstance; thus, careful analysis is necessary to account for potential variations.

Replacing part of coal's electricity production with solar electricity production, coupled with LNG electricity production, is a subset of the generation expansion planning (GEP) problem. Koltsaklis and Dagoumas [70] wrote a review article exploring the state-of-the-art generation expansion planning where they listed seven challenges to the GEP problem. One of the mentioned challenges is rooted in the risks involved in GEP. They enumerated several potential sources of risks and categorized them according to economic, political, regulatory, environmental, technical, social, and climate categories. Ioannou et al. [71]

reviewed the risk-based methods for sustainable energy system planning and categorized the risks in the same manner. They identified seven risk-based methods: mean-variance portfolio theory, real option analysis, Monte Carlo simulation, stochastic optimization technique, multi-criteria decision analysis, and scenario analysis.

4.1.2 Uncertainty due to Weather Variations

Santos et al. [72] conducted a study to identify uncertainties in the electricity system and demonstrated the corresponding impacts on the energy mix through scenario analysis. Their results highlighted that climate uncertainty represents primary risk sources for VRE, since it dictates the system's power generation. A review on the energy sector vulnerability to climate change [73] summarizes the authors' contributions on climate and energy, and they noted that climate change could affect variables that influence electricity generation from photovoltaics and concentrated solar power. The review highlighted that global solar radiation has increased in southeastern Europe [74] and decreased in Canada [75]. They also highlighted that power output calculations should account for air temperature, since it impacts the solar cell's efficiency [73].

Ioannou et al. [71] noted that energy planning has extensively used stochastic optimization techniques, and the stakeholder's motivation mainly drives the constraints. They also mentioned that the Monte Carlo simulation has many advantages, but it requires considerable data inputs to create probability density functions. Alternatively, scenario analysis evaluates the risks by creating potential future developments that range from the worst-case to the best-case scenario, which could then cover all the possible risks in the analysis. As highlighted by several authors [72]–[75], climate, and by extension weather, must be considered in modeling solar energy generation. Factors such as the changing solar irradiance and ambient temperature could influence solar panels' variability and efficiency.

4.1.3 Objective

By carefully identifying the test cases, scenario analysis is sufficient for ensuring the robustness of the analysis. The initial problem is then rooted in creating the scenarios representing the worst case, the best case, and the cases in between. The weather data analysis can provide the representative years that fit the scenario targets, such as warm summers, colder winters, extreme summers, and extreme winters. Although such data are limited, datasets could be synthesized based on the historical relationship between temperature and demand. Solar generation could be calculated from the irradiance and ambient temperature data. The robustness of the analysis and recommendation can be addressed by combining scenario analysis and past weather data.

Therefore, in this study, an hourly power flow analysis was conducted to understand the potential, limitations, and implications of using solar energy as a driver for decommissioning coal power plants. Understanding these factors can provide the necessary recommendations

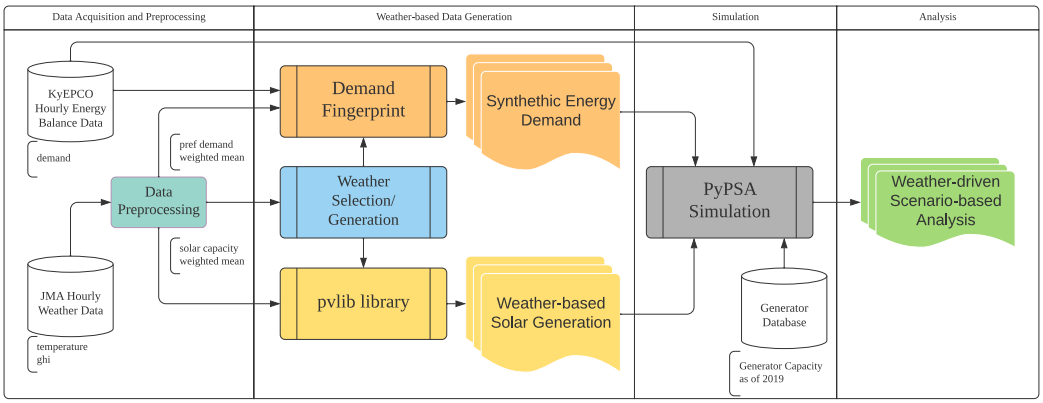

Figure 4.1: The proposed weather-driven scenario-based analysis approach capable of handling weather-related variations in electricity demand and solar energy production.

and precautions for energy planners. Since LNG scarcity is anticipated, LNG quota is one of the primary constraints. In order to ensure the robustness of the results, this study presents a straightforward weather-driven scenario generation that utilizes historical weather and electricity demand data processed through machine learning algorithms to generate scenarios that account for weather variations. Through the weather-driven approach, the study aims to reveal the impact of yearly variations in the factors that must be considered for long-term planning that reduce CO_2 emissions while ensuring grid reliability. The Kyushu region in Japan was used as a case study since (a) it is continuously increasing its solar capacity, (b) it has a fleet of coal power plants older than 40 years old ready for decommissioning, and (c) it has enough LNG power plant capacity to support the initial transition.

4.2 Methodology

The overview of the proposed weather-driven approach can be seen in Figure 4.1, where it is divided into four stages. First, data were collected from Kyushu Electric Power Company (KyEPCO) [36] and Japan Meteorological Agency (JMA) [76] and were pre-processed to fit the intended applications. The weather-based data generation has three components. A weather selection metric was designed based on comfort-levels to identify the years that could represent the scenarios in the region. The pvlib Python library [77] was used to calculate the photovoltaic systems' generation under various weather conditions. A demand fingerprint was developed to generate synthetic demand for the selected years. These synthetic data were then used as input to the hourly power flow optimization done in Python for Power System Analysis (PyPSA) [53]. Finally, the simulation results were analyzed.

Table 4.1: Weather Stations in Kyushu

Prefecture	Pref No.	Precinct	Block
Fukuoka	40	82	47807
Nagasaki	42	84	47817
Kumamoto	43	86	47819
Oita	44	83	47815
Miyazaki	45	87	47830
Kagoshima	46	88	47827

4.2.1 Data and Data Pre-Processing

Energy Demand

The energy data were collected from Kyushu Electric Company [36], where the hourly information about generation, transmission, and demand is published since April 2016. The data also include curtailment information for both solar and wind power. Transmission and pump hydro energy storage (PHES) could be positive or negative. For transmission, negative values represent energy export while positive values indicate electricity import. For PHES, negative and positive values represent the charging and generation phases, respectively. Although the data until December 2020 are already published, only data until March 2019 were used in the study since this represents four full fiscal years.

As seen in Figure 4.1, the energy data are used in both the demand fingerprint and simulation phase. Only the demand data were necessary for the demand fingerprint, while the other hourly data were used as parameters for the other generations and PHES.

Temperature and Irradiance

The temperature and irradiance data were collected from the Japan Meteorological Agency (JMA) [76], where the hourly weather data are published since 1946. For this study, 30 years of data were collected from 1990 to 2019 to serve as reference weather scenarios. A representative temperature was collected from each of the major cities' weather stations, as shown in Table 4.1.

In order to represent the mean temperature and mean irradiance in the region, solar-capacity-weighted mean and monthly-demand-weighted mean were used for the solar generation calculation and demand generation, respectively. Using the consolidated data from [5], Table 4.2 shows the shares of the solar PV installation in Kyushu since 2012 and the shares in 2019 were used as the reference for the solar-capacity-weighted mean temperature and irradiance. The Ministry of Economy, Trade, and Industry (METI) publishes each prefecture's monthly energy demand since April 2016 [42]. Table 4.3 shows the mean of each prefecture's shares from 2016 until 2019. These values were used to calculate the monthly-demand-weighted temperature mean used in the demand fingerprint.

The solar capacity ratio was used for the solar power generation calculation because the power generation's distribution is influenced by the distribution of the capacity. It is necessary

Table 4.2: Share of Solar Installations [%] in the Prefectures

Prefecture	2012	2013	2014	2015	2016	2017	2018	2019
Fukuoka	34.83	24.98	25.16	25.14	24.62	23.86	23.06	22.26
Saga	8.48	8.04	7.22	6.96	6.98	6.78	6.85	6.50
Nagasaki	8.98	9.67	9.11	9.82	10.02	9.66	9.46	9.48
Kumamoto	15.87	13.31	14.52	14.26	14.50	14.46	14.75	14.63
Oita	11.40	15.07	13.26	13.08	12.54	12.00	12.51	12.34
Miyazaki	8.66	11.59	11.94	11.78	11.66	12.53	12.82	13.03
Kagoshima	11.77	17.34	18.79	18.96	19.68	20.72	20.55	21.76

Table 4.3: Average monthly demand share [%] in Kyushu from 2016 to 2019

Prefecture	JAN	FEB	MAR	APR	MAY	JUN	JUL	AUG	SEP	OCT	NOV	DEC
Fukuoka	38.25	38.28	38.13	37.66	37.32	37.26	37.47	37.60	37.21	36.85	37.20	37.79
Saga	7.83	7.99	8.10	8.02	8.02	8.20	8.12	7.79	7.86	7.90	8.04	7.94
Nagasaki	9.55	9.51	9.35	9.42	9.40	9.25	9.28	9.60	9.48	9.23	9.22	9.39
Kumamoto	13.76	13.82	13.73	13.42	13.37	13.64	13.78	13.83	13.91	13.81	13.72	13.76
Oita	10.61	10.64	10.72	10.97	11.18	10.92	10.58	10.27	10.38	10.81	10.93	10.94
Miyazaki	8.49	8.27	8.45	8.75	8.77	8.72	8.63	8.54	8.54	8.81	8.73	8.55
Kagoshima	11.50	11.49	11.52	11.77	11.94	12.00	12.13	12.37	12.62	12.60	12.16	11.63

to use this weighted mean because the temperature where more solar panels are installed should have a more significant representation in the temperature used in the solar generation calculation. However, the temperature where there is greater demand should have more influence on the temperature used for demand calculations.

4.2.2 Weather-Based Data Generation

Representative Weather Selection

Since the scenarios are weather-driven, it is necessary to identify the years representing the various scenarios in the region. With this in mind, a metric system was created based on the notion that comfortable temperature levels are between 18 and 22 °C. Under 18 °C, people will start using their heaters, and above 22 °C, they will start using their air-conditioners.

Therefore, the metric system considers the mean and peak deviations per month from these values. Since the focus is to cover extreme cases, the years were ranked based on the summer-warmness and winter-coldness. Based on the rankings, six years were selected, as seen in Table 4.4. The frequency of occurrence was calculated based on the highest R^2 compared to the representative year from 1990 to 2019. The legends are used mainly in the figures in the results section.

It can be seen in Figure 4.2 that around August, 2013 has the highest peak and mean positive temperature deviation, while around February, 2012 has the highest peak and mean negative temperature deviation as intended by the sampling. 2014 has the lowest deviation overall since it is the lowest in summer and in the winter. The other representative years fall between these extreme cases.

Table 4.4: Kyushu weather scenario representative years

Summer	Winter	Representative	Legend	Frequency*	Comment
Mild	Mild	2014	14MM	2	Low variability
Mild	Severe	1991	91MS	6	Colder year
Severe	Mild	2016	16SM	8	Warmer year
Severe	Severe	2018	18SS	5	High variability
Extreme	-	2013	13E-	5	Extreme Summer
-	Extreme	2012	12-E	4	Extreme Winter

*Occurrence in the past 30 years from 1990 to 2019

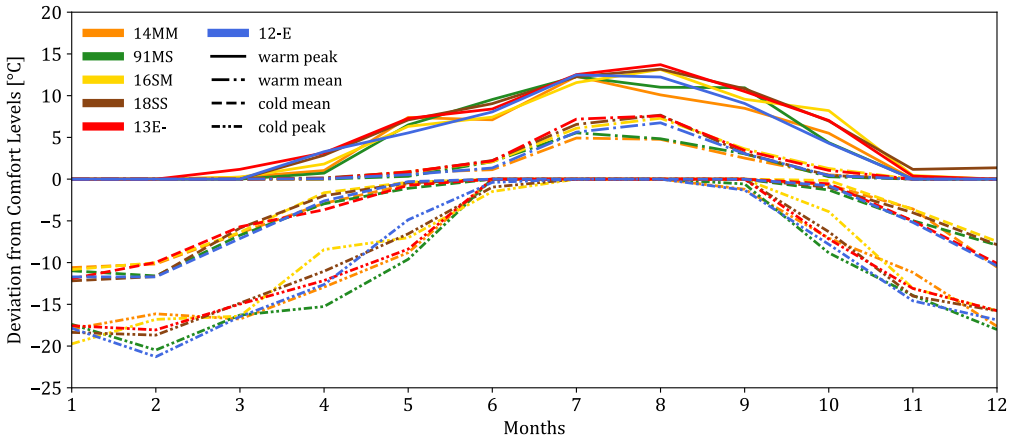

Figure 4.2: Temperature deviation of the representative year from the comfortable temperature of 18 °C to 22 °C.

Weather-Based Solar Generation

The weather-based solar power generation calculation was mainly based on the TMY to power tutorial written by the developers of *pvlib* [78]. Since the approach requires both the direct-normal irradiance (DNI) and diffuse horizontal irradiance (DHI), and JMA only provides the global horizontal irradiance (GHI), the built-in function *pvlib.irradiance.erbs* was used to estimate the DNI and DHI. The Erbs model [79] estimates the diffused fraction of GHI to calculate DHI and uses the solar zenith to calculate DNI. By providing the timezone, longitude, latitude, and altitude data along with the hourly GHI data from JMA, the DNI and DHI were calculated using *pvlib*'s built-in functions. Besides the irradiance data, the power generation calculation also requires temperature data to account for the impact of temperature on solar cells' efficiency. The solar-capacity-weighted mean was used for both the GHI and temperature since the solar power generation distribution is proportional to the generation capacity of each prefecture. Subsequently, the power generation values of a 208 W Kyocera Solar Panel and an ABB Micro 250 W micro-inverter were calculated using *pvlib.pvsystem.sapm* and *pvlib.inverter.sandia*. The resulting hourly annual generation was scaled by 208 Watts to represent the maximum power output for $PyPSA$.

Demand Fingerprint and Synthetic Demand Generation

Figure 4.3 shows the creation of the four parameters necessary to generate energy demand. The first two swim lanes in the flowchart show the identification of the cluster. Initially, the goal was to extract a demand shape or *fingerprint* from the data. Since human behavior through weekly routines greatly influences the demand, the energy demand data were split into weekly samples. The peaks and troughs of the demand patterns were identified to emphasize the demand's fingerprint. This process entailed moving the peaks and troughs to the following hourly locations: 0, 3, 6, 15, 18, 21, and 24, since it was discovered that the peaks and troughs occur at these times depending on the season. Actual values were selected for 9, 11, 12, and 13, since these values represent the midday demand dip that occurs due to the Japanese lunch hour, which is noticeable yearlong. After the alignment, since the goal was to extract the fingerprint, the demand's magnitude was scaled using z-transform. The resulting scaled value was then used as input to an FFT transform to extract the frequency components that comprise the fingerprint. Only the daily variations (multiples of 7 Hz) were selected as features for the clustering algorithm to reduce the noise. These feature values were scaled using z-transform to reduce the magnitude in the distance calculation.

These features were then clustered using the Kmeans algorithm through the $Kmeans$ method of the $sklearn.cluster$ Python library. Several values of K were explored, and through experimentation K = 5 was identified as the number of clusters that could explain the data. The clusters' fingerprints are shown in the inset of Figure 4.4. Once these clusters were identified, the weekday datasets were combined for each cluster, and another FFT transform was done to extract the

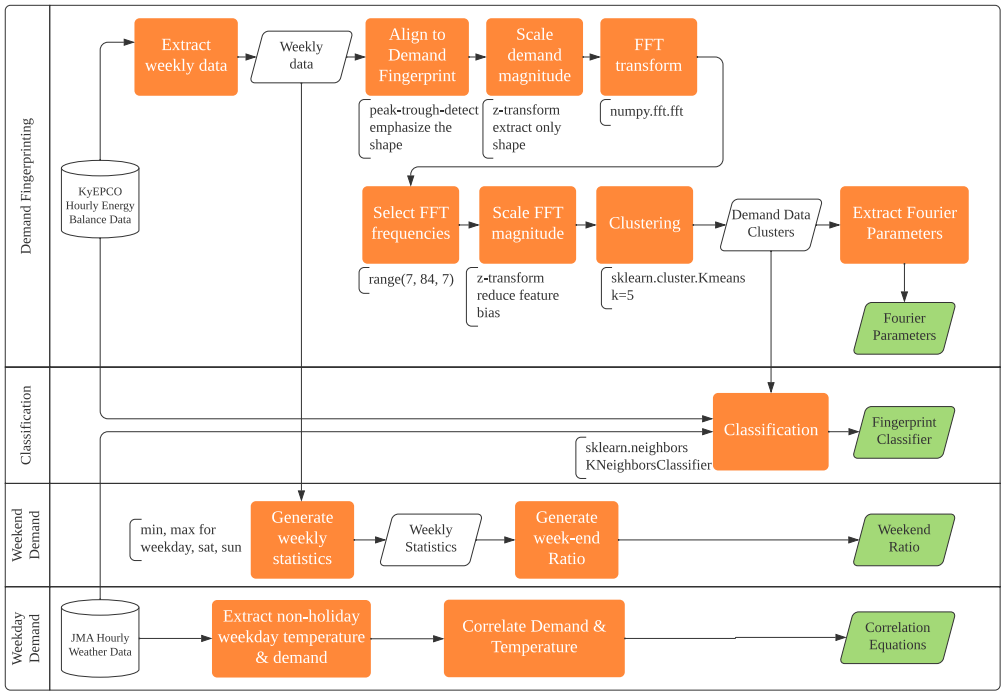

Figure 4.3: Generating the demand fingerprint based on the demand and temperature data.

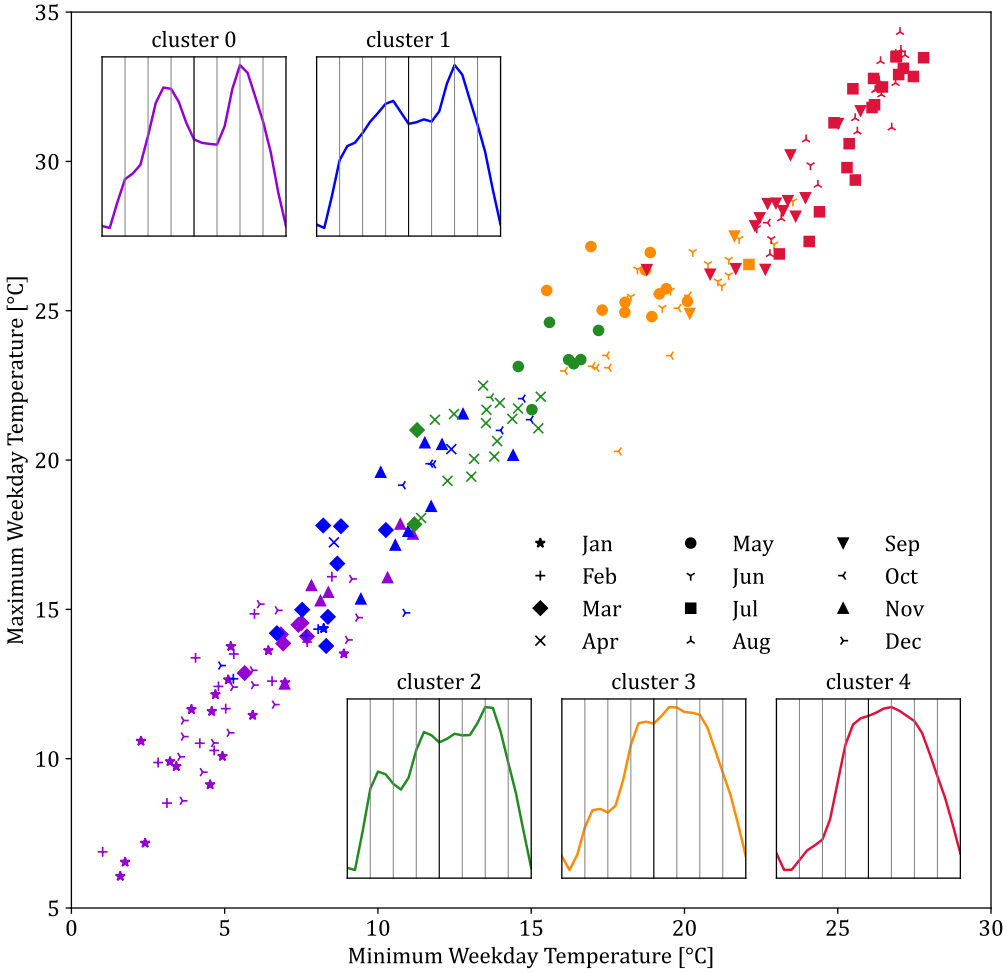

Figure 4.4: The weekly demand clusters of Kyushu from FY2016-2019.

Fourier parameters necessary to represent the waveform. Combining the datasets, after clustering, emphasized the pattern for each cluster and removed the noise. As with the pre-clustering data, only the daily variations (different frequencies depending on the sample sizes) were selected.

A classifier must be developed to identify the appropriate fingerprint for each week during the energy demand generation. Through data exploration, the maximum weekly temperature, minimum weekly temperature, and the month of the week were identified as the features that could be used to classify each week. The $KneighborsClassifier$ method of $sklearn.neighbors$ Python library was used with k = 5 to classify the weekly data. By running 80–20 training-test split 1000 times, the classification got an average accuracy score of 83%, with 66% and 95% as the minimum and maximum scores, respectively. This average accuracy score was deemed acceptable and this was used as the fingerprint classifier.

While the first two swim lanes in Figure 4.3 provided the demand's fingerprint, the last two provide the minimum and maximum values that stretch or compress the fingerprint. Through data exploration, it was observed that non-holiday weekday temperature and

demand have a strong correlation; thus, it was extracted and fitted into known functions. Using $scipy.optimize.curve\_fit$ method of the $scipy$ Python library, as seen in Figure 4.5, the minimum temperature and minimum demand were fitted to a quadratic curve with an R^2 of 0.80. The curve fitting for the maximum temperature and maximum demand required a piece-wise linear equation and was similarly fitted with an R^2 of 0.88. The weekend and holiday fitting were explored, but no meaningful functions were derived; thus, a simple weekday-to-weekend ratio was extracted by averaging all the known values. Seasonal variations in the ratio were initially explored, but no meaningful trend was seen; thus, the concept was dropped.

Generating yearly demand based on temperature is shown in Figure 4.6 where the green input blocks represent the models, values, and functions generated from Figure 4.3, and the red input block represents the weekly temperature statistics from the selected year. Using these inputs, a fingerprint assignment and the minimum and maximum demand per day were identified. The fingerprint is then fitted to the daily min-max demand using $scipy.optimize.curve\_fit$ method and provides the A_0 and B_0 coefficient for the Fourier representation. This is done for all weeks of the year to generate the entire year. Testing this approach with the known values for 2017, 2018, and 2019, the synthetic demand approach could get R^2 of 0.8675, 0.8714, and 0.8177, respectively. A sample of the demand curve can be seen in Figure 4.7, where the demand were closely synthesized. The problem with holidays (e.g., new year) is noticeable and some weekends are not reproduced accurately. However, the general shape or $fingerprint$ of the demand fits well with the actual values.

4.2.3 Hourly Simulation and Scenario Analysis

The hourly simulation used Python for the Power System Analysis ($PyPSA$) Modeling Framework [53]. The PyPSA environment provides a framework for the buses, lines, loads, generators, and storage, units among many other parameters. In this simulation, since Kyushu was modeled as a single point, only one bus was used, and all the loads, generators, and storage units were connected directly to this bus. The single-bus network was constructed based on Figure 4.8, where the coal generator, the Kyushu demand, and the transmission demand were directly connected to a single bus. The rest of the generators was then connected to a sub-bus, which was then connected to the main bus. Creating the

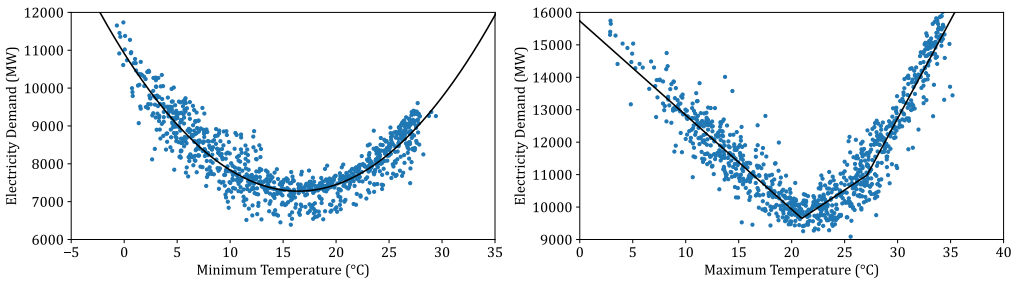

Figure 4.5: Correlation of Temperature and Demand in Kyushu

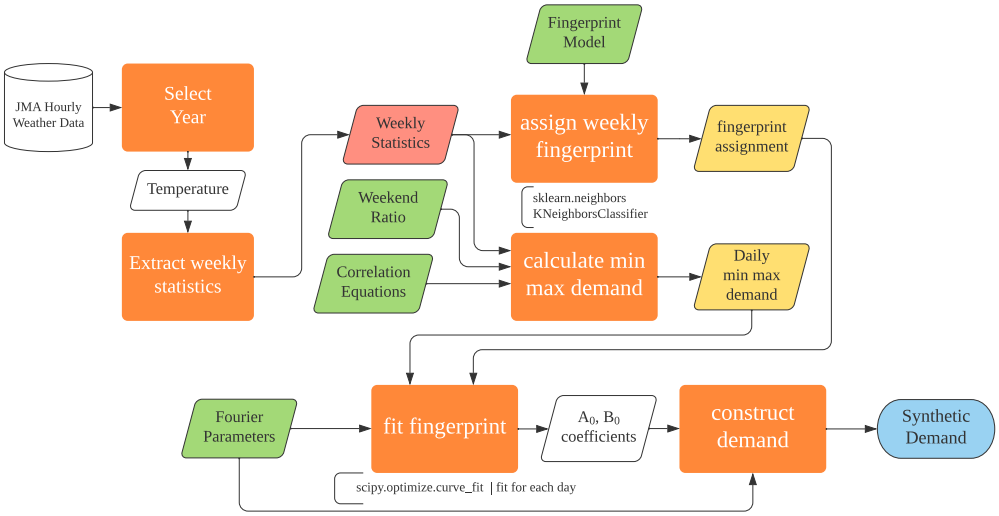

Figure 4.6: Temperature-dependent demand generation.

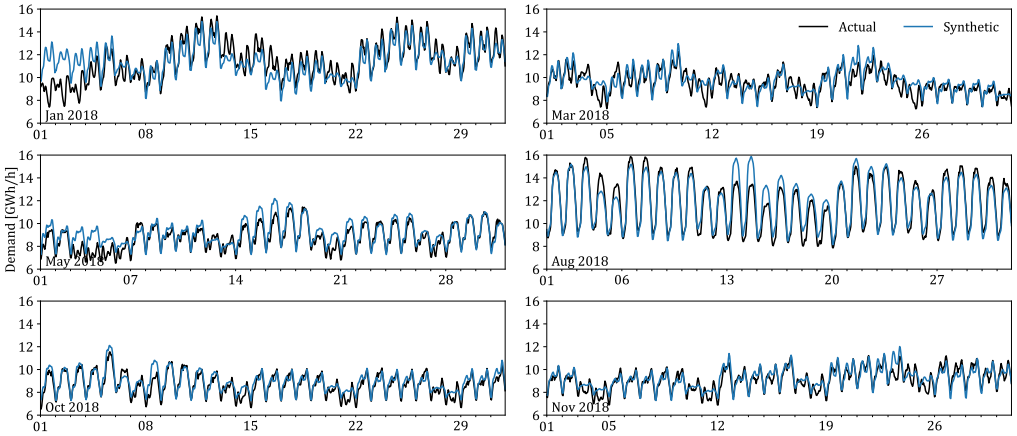

Figure 4.7: Sample demand synthesis for 2018.

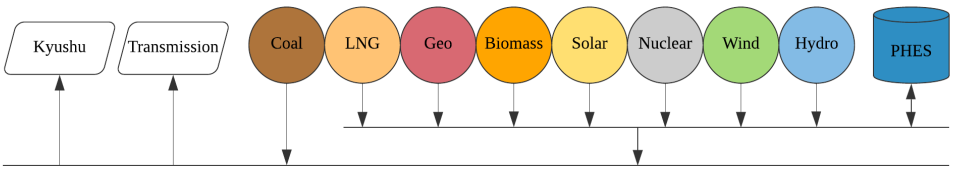

Figure 4.8: Configuration of the single-bus network used in the optimization.

sub-bus ensured that the PHES could not charge from the coal generator, which prevented the optimizer from generating and storing more power from coal for later use. For this study, the synthetic load and solar power generation profile for the representative years (Table 4.4) were used iteratively during the optimization.

Table 4.5: Generators in Kyushu (FY 2019)

Generator	Power [MW]	Carrier	$Output_{min}$ [%]	Ramp Limit [%]
Coal	7037	Coal	30	1
LNG	5250	Gas	15	40
Geothermal	160	Renewable	100	0
Biomass	450	Renewable	100	0
Solar	9000	Renewable	0	100
Nuclear	4140	Non-GHG	100	0
Wind	355	Renewable	15	40
Hydro	4000	Renewable	15	40

The installed solar capacity was increased by 1 GW increments from 0 GW until 20 GW. The latest known capacities for the other generators as of FY2019 are shown in Table 4.5, which was consolidated based on various sources [42]–[44]. Although the nuclear, geothermal, and biomass could change within the year, as a baseload, they were fixed to their respective maximum capacities to provide consistency throughout the years under simulation. Hydropower generation was based on the daily dispatch capacity calculated using the total daily dispatch in the 2019 data. The simulator allocated the hourly dispatch based on the optimization. However, minimum and maximum dispatch were still considered based on the actual data. The PHES was treated as both a generator and a load with a maximum transfer capacity of 2.3 GW, a total capacity of 13.8 GWh, and round trip efficiency of 0.70% (0.84% one way).

The optimization aims to minimize the coal capacity while ensuring energy balance. The hourly resolution was used due to the limitation of the available data. Solar energy is preferred as long as the minimum operating output or ramp limit seen in Table **??** for coal and LNG are satisfied. Since LNG might become a future bottleneck, LNG quota (in TWh) is used as a constraint in the simulation. LNG quota (LNG^{TWh}_{quota}) is defined as the maximum total annual electricity generation used in the optimization with the maximum generation capacity of 5.25 GW.

Using the recently published resource utilization data from KyEPCO [45], it was determined that the company generated 8 TWh from LNG in 2019 through their 4.625 GW LNG plants. This generation represents 20% LF for the company. An independent power producer owns the other 0.625 GW LNG power plants in the region, which are composed of mixed gas power generators. Assuming these IPP plants are running at a higher LF of 40%, it was determined that the LNG plants generated around 10 TWh in 2019. Using 10 TWh as the base case, the simulation gradually incremented the LNG quota by 20%, 60%, and 100%, yielding 12, 16, 20 TWh LNG quota. A report from Japan's Ministry of Economy, Trade, and Industry (METI) [80] showed that LNG is more economical than coal at LF < 60%; thus, the scenario analysis also explored 28 TWh (60% LF). Preliminary exploration also showed that increasing the quota further has a minor impact on the emission and cost unless more LNG capacity is installed; thus, this was not explored any further. Additional LNG quota could also increase energy security risk given the LNG market situation.

A summary of the LNG quota scenarios is shown in Table 4.6. The scenarios (LNG^{TWh}_{quota2} - LNG^{TWh}_{quota4}) reflects one way to reach each of the identified quota from the base case

Table 4.6: LNG Quota Scenarios

LNG Power Plant		LNG^{TWh}_{quota1}		LNG^{TWh}_{quota2}		LNG^{TWh}_{quota3}		LNG^{TWh}_{quota4}		LNG^{TWh}_{quota5}	
Category	Cap	LF	Gen	LF	Gen	LF	Gen	LF	Gen	LF	Gen
KyEPCO Steam	1800	20	3.15	20	3.15	20	3.15	20	3.15	60	9.46
KyEPCO CC	2825	20	4.95	27	6.68	44	10.89	60	14.85	62	15.34
IPP	625	40	2.19	40	2.19	40	2.19	40	2.19	60	3.29
Total	5250		10.29		12.03		16.23		20.19		28.09

* Capacity (Cap) in MW; Load factor (LF) in %; Generation (Gen) in TWh

Table 4.7: Cost of Electricity Generation [Yen/kWh]

Technology	METI 2014	METI 2030	MOFA 2018*	Applied**
Nuclear	10.1	10.1	-	10.1
Coal	12.3	12.9	6	12.3
LNG	13.7	13.4	10	13.7
Wind	21.9	13.9	10-22 (15)	17.9
Geothermal	19.2	19.2	-	19.2
Hydro	11.0	11.0	-	11
Biomass	12.6	13.3	-	12.6
Solar (Comm)	24.3	12.7	8-36 (17)	18.5
Solar (Home)	29.4	12.5	-	-

*Values in parentheses are the average values
**used in the calculation

(LNG^{TWh}_{quota1}). For the 12, 16, and 20 TWh scenarios, KyEPCO could increase their efficient power plants' LF. Increasing it further would require KyEPCO to increase their steam LNG plants' LF plants and coordinate with the IPP to increase their production.

4.2.4 Annual Generation Cost and CO_2 Emission Analysis

In 2015, Japan's Ministry of Economy, Trade, and Industry (METI) [81] reported and modeled the cost of electricity generation for 2014 and 2030. An Advisory Panel to the Foreign Minister on Climate Change (MOFA) [82] citing BloombergNEF presented their estimates on the cost of generation in 2018. Table 4.7 consolidates these reports along with the values used for the annual cost calculations. Generally, the cost in 2014 was used in the calculations except for wind and solar power, where it was averaged between the 2014 report and the 2030 model. Except for coal, the values are near the estimated values of BloombergNEF.

For the CO_2 emission analysis, the study mainly focuses on the CO_2 emission from fuel consumption, which does not cover the CO_2 emission during construction, maintenance, and disposal of the system. Therefore, the calculation assumes that, during generation, nuclear, geothermal, hydro, solar, and wind power do not generate CO_2 and biomass has net-zero CO_2 emissions. According to Japan's Ministry of Environment [83], depending on the technology, coal and LNG has a CO_2 emission of 0.95 kgCO2/kWh to 0.83 kgCO2/kWh and 0.51 kgCO2/kWh to 0.36 kgCO2/kWh, respectively. The average emission for coal (0.89 kgCO2/kWh) and LNG (0.44 kgCO2/kWh) were used in the analysis.

Since temperature leads to higher or lower demands, by calculating the levelized cost of generation and levelized CO_2 emissions, the relationship between cost and CO_2 becomes clearer. Although weather variations still have an impact, this impact is less when seen from a levelized perspective. The annual levelized cost of generation was calculated using (4.1). The hourly simulation provides the annual generation per technology ($Generation_{tech}^{kWh}$). By multiplying the generation per technology to the corresponding cost of electricity generation ($Cost_{tech}^{JPY/kWh}$), the total cost per year could be calculated. The levelized cost of generation on that particular year can then be calculated by dividing the total annual cost by the total annual generation. Similarly, the levelized CO_2 emission was calculated using (4.2) and the CO_2 emission per technology ($Emission_{tech}^{kG-CO2_2/kWh}$).

$$levelized\ cost\ of\ generation = \frac{\sum (\text{Generation}_{tech}^{kWh})(\text{Cost}_{tech}^{JPY/kWh})}{\sum \text{Generation}_{tech}^{kWh}} \tag{4.1}$$

$$levelized\ CO_2\ emissions = \frac{\sum (\text{Generation}_{tech}^{kWh})(\text{Emission}_{tech}^{kG-CO2_2/kWh})}{\sum \text{Generation}_{tech}^{kWh}} \tag{4.2}$$

4.3 Results

4.3.1 Demand and Solar Generation Profiles

Demand Duration Curve

The synthetic demands' duration curve can be seen in Figure 4.9, where the demands from 2013 and 2018 are noticeably higher than the rest of the representative years. It can also be seen that 2014 had a lower peak demand, as was intended by the selection of the representative years. Figure 4.10 focuses on the winter and summer months, and it is noticeable that winter still has a relatively lower demand compared to the peak summer demand in August. From this figure, it can be seen that the peak winter demand was represented well by 2012 in February. At the same time, 2013 represented the extreme case of summer demand in August. The demand barely reached 14 GW at peak for the other months, and most values were under 12 GW. This information is crucial in understanding the limitation of reducing the coal capacity since the generation capacity must be able to handle peak demands. For instance, although winter leads to higher demand, its impact is not as high as that of summer. Nonetheless, this does not translate to higher coal capacity since the generation profile of the other energy sources, in particular solar, also has seasonal variations.

Table 4.8: Monthly solar generation load factor [%] using the irradiance of the representative years

Year	JAN	FEB	MAR	APR	MAY	JUN	JUL	AUG	SEP	OCT	NOV	DEC
2014	13.28	11.47	14.89	14.59	17.03	9.94	11.45	9.05	11.38	13.80	11.61	10.15
1991	12.09	12.44	11.89	12.49	11.14	8.73	11.18	13.33	12.40	12.28	14.62	10.41
2016	7.94	12.40	15.34	11.84	13.59	10.67	13.75	15.90	10.52	9.18	12.64	11.93
2018	11.55	13.95	15.69	16.99	13.45	12.26	14.00	15.33	10.07	14.19	14.60	9.19
2013	11.03	13.77	14.84	16.34	16.09	9.53	14.70	14.70	14.73	13.29	12.01	10.67
2012	11.02	9.56	13.31	17.01	14.53	8.84	10.30	12.15	12.10	15.20	11.11	7.20
Mean	11.15	12.27	14.33	14.88	14.31	9.99	12.56	13.41	11.87	12.99	12.77	9.93

Solar Load Factor

The solar load factor for each month can be seen in Table 4.8. Since 2016 and 2018 have higher summer demand, August's higher load factor will be helpful, but the relatively lower load factor for 2013 will be an issue since this year has higher demand. The lower load factor in December could be a potential issue, but since the load factor increases by February, this could accommodate the increase in demand during this peak winter period.

4.3.2 Coal Decommissioning Potential

Figure 4.11 shows the minimum coal capacity that could satisfy the demand for each of the 30 scenarios. The impact of yearly variations can be observed through the range of minimum coal capacity for each LNG quota scenario. As the LNG quota increases, the coal capacity could gradually be decommissioned without adding additional LNG capacity.

About 3.5 GW of the 7 GW coal capacity is older than 40 years old and should be decommissioned in the near future. However, based on the simulation results, this will be challenging if the LNG quota is not met. In the near term, where 10 GW of solar energy is already

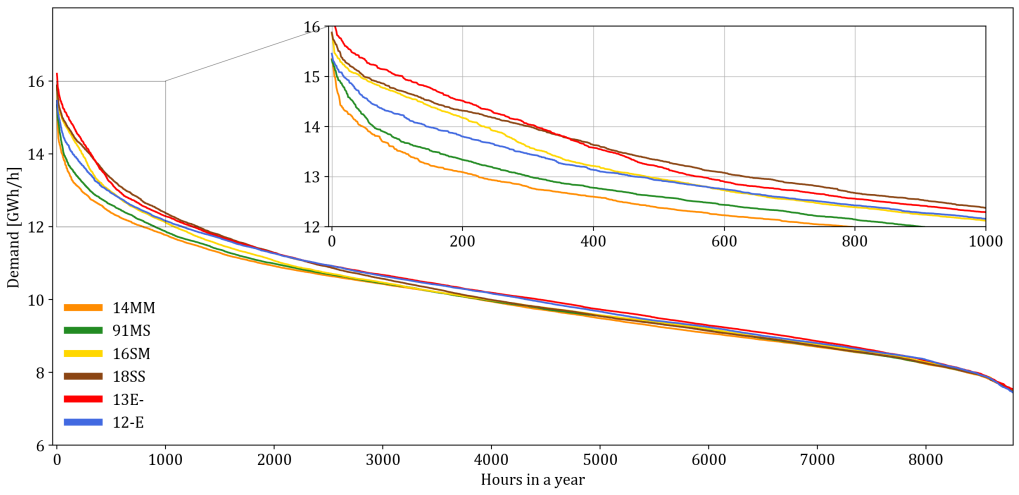

Figure 4.9: Duration curve of the synthetic demand.

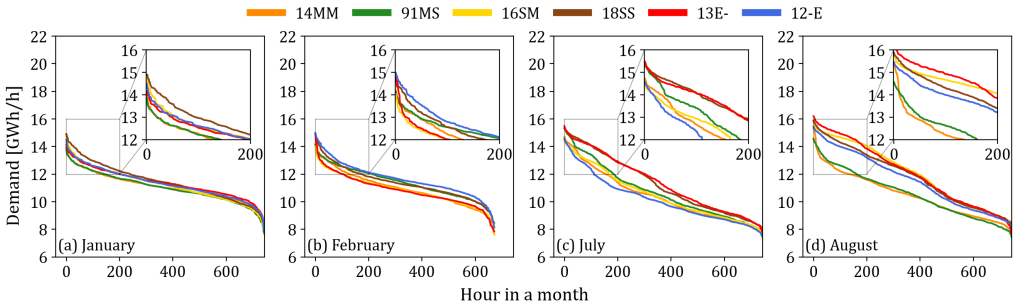

Figure 4.10: Monthly duration curve of the synthetic demand.

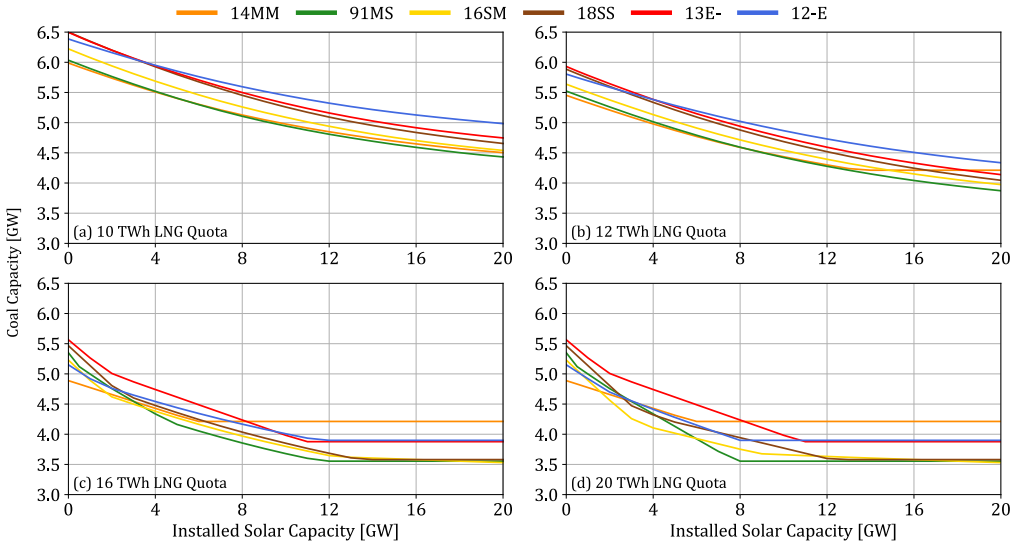

Figure 4.11: Minimum required coal capacity as installed solar capacity increases, and various LNG quotas.

installed, the LNG quota must be at least 16 TWh. In the long term, where 16 GW of solar energy is already installed, the LNG quota must be at least 12 TWh. In both cases, as highlighted in Figure 4.12, around 400 to 600 MW of standby coal capacity is necessary to account for the yearly variations. As noted in the analysis of the demand duration curve, this standby capacity will be needed during the winter and summer periods, particularly in January, February, August, and September (Figure 4.10). Nonetheless, Figure 4.12 clearly shows the limitation for solar power in regard to decommissioning coal power plants beyond 12 GW installed capacity, since the minimum coal capacity no longer decreases despite additional solar generation.

4.3.3 Coal Generation and Load Factor

Despite the floored impact of solar power on coal decommissioning, it can still reduce the coal generation and load factor. As seen in Figure 4.13, even beyond 12 GW, the coal generation is constantly decreasing in all LNG quota scenarios. Figure 4.14 further reveals

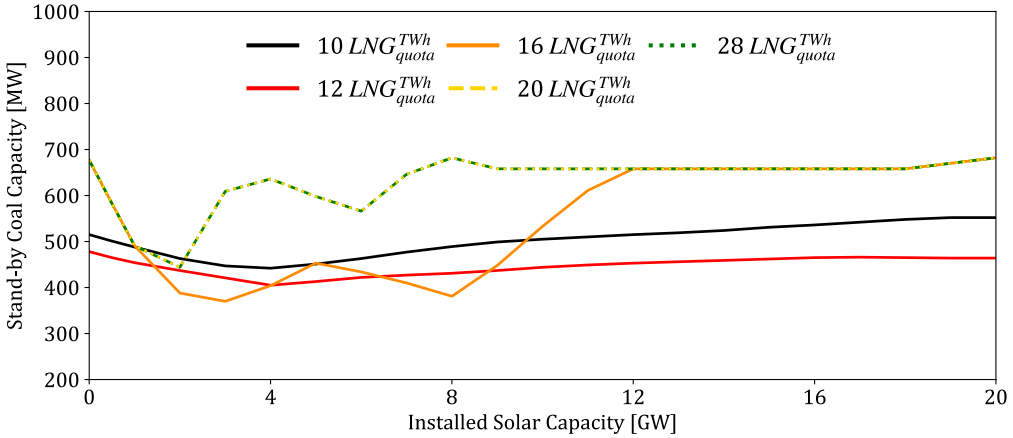

Figure 4.12: Standby coal capacity needed to ensure that the electricity grid can still handle weather-driven demand variations.

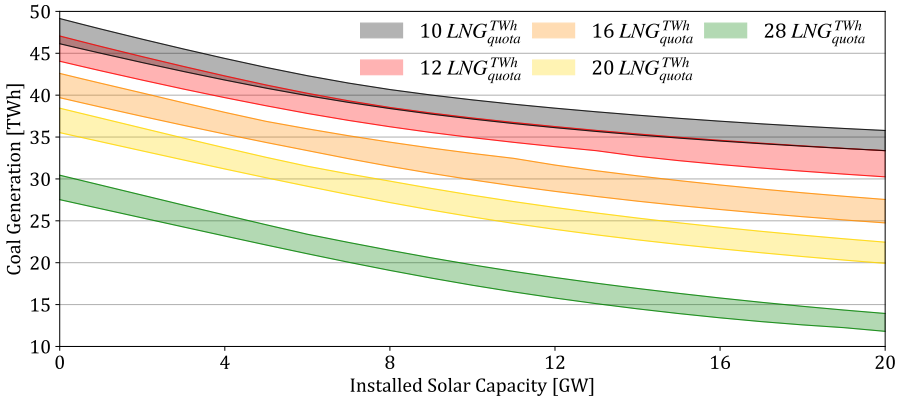

Figure 4.13: The coal generation in different LNG quota scenarios.

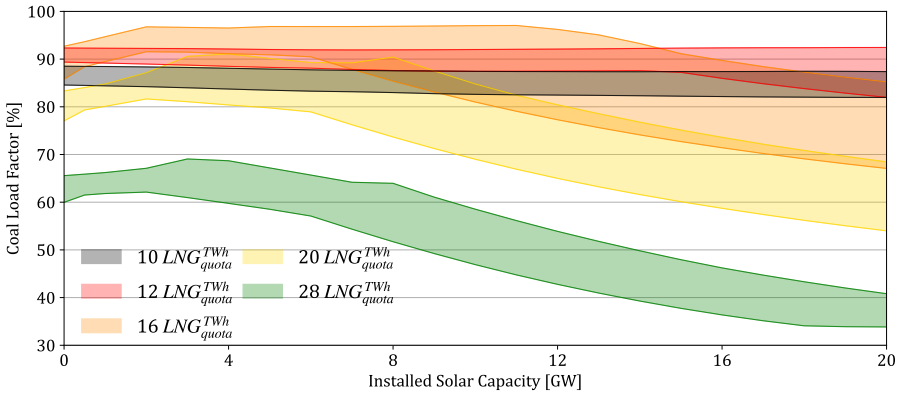

Figure 4.14: The coal load factor in different LNG quota scenarios.

that the load factor decreases as more solar capacity is installed into the grid. It should be noted that the load factors were computed using the minimum coal capacity as presented in Figure 4.11, which results in both a decrease in capacity and utilization rate.

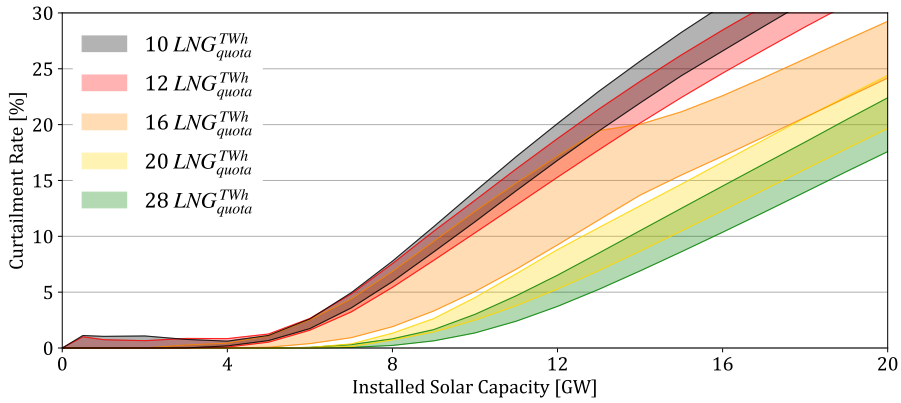

Figure 4.15: Projected curtailment rates assuming the optimal coal capacity was followed, with the corresponding annual LNG quotas.

4.3.4 Impact on Solar Curtailment Rate

As a consequence of the optimization that reduced the coal capacity and complementing solar power with a more flexible generator in the form of LNG, the curtailment was reduced to varying degrees. Figure 4.15 shows the range of curtailment rates based on the yearly variations and annual LNG quotas. Increasing the LNG quota from 12 TWh to 24 TWh, which in turn decreases the coal capacity, could reduce curtailment from 14% down to 3% in the worst-case scenario for the 10 GW installed solar capacity. Beyond the 28 TWh LNG quota, there are minor changes in the curtailment reduction. However, it could also be noted that the 20 TWh LNG quota can reduce the curtailment from 14% down to 3%. The curtailment reduction becomes more evident as the solar capacity increases. However, beyond 16 GW installed capacity, even with sufficient complementary LNG, solar curtailment will always be greater than 10% at best and 30% at worst.

4.3.5 Impact on Annual Cost and CO_2 Generation

Figure 4.16 shows the CO_2 emissions generated due to the fuel consumed by coal and LNG generators.The combination of solar and LNG electricity generation could cut the CO_2 emissions by half when comparing the "No solar + 10 TWh LNG" and "20 GW Solar + 28 TWh LNG" scenarios. The impact of solar power is also readily seen by comparing the values in each LNG quota scenario, which should be attributed to its capability to reduce coal generation even beyond 12 GW.

As seen in Figure 4.17, since solar power has a higher generation cost than using LNG, its impact on the annual generation cost is more significant. The weather conditions greatly influence the annual generation cost: 2014 and 2013 represented the lowest and highest costs, respectively. The variations in the cost attributed to the LNG scenarios were more evident in 2013 followed by 2018 and 2016 caused by higher coal production during the extreme and severe summers. In the least costly year, the cost ranged from 1.22 to 1.36

Table 4.9: Cost and CO_2 emission of the reference scenario

	14MM	91MS	16SM	18SS	13E-	12-E	Mean
Levelized Cost [Yen/kWh]	12.5464	12.5266	12.5331	12.5819	12.5820	12.5160	12.5477
Levelized CO_2 [kgCO_2/kWh]	0.3640	0.3683	0.3714	0.3679	0.3723	0.3764	0.3700

trillion JPY (11.48% increase), and in the most costly year, the cost ranged from 1.26 to 1.41 (12% increase) trillion JPY (April 2021: 100 JPY = 0.92 USD = 0.77 EUR).

Using 2016 as the representative, Figure 4.18 shows the impact of the installed solar capacity and the LNG quota on the levelized cost of generation and levelized CO_2 emissions. Currently, the Kyushu region already has 10 GW of installed solar capacity and generates around 10 TWh from LNG. This reference scenario is annotated as scenario 0 (S_0) in Figure 4.18 and values for the levelized cost and CO_2 emissions for the various weather conditions are shown in Table 4.9.

From this reference scenario, the company could further decrease their CO_2 emissions by having more LNG generation, adding more solar capacity, or both, but at the expense of increasing their generation cost. Five potential scenarios are annotated as S_1 to S_5 in Figure 4.18 and the impacts are tabulated in Tables 4.10 and 4.11. Initially, the LNG generation could be ramped up to 20 TWh to complement the solar capacity increase, as seen in S_1. This increased the generation cost by an average of 0.63% and decreased the CO_2 emissions by an average of 12.80% to 0.3226 kgCO_2/kWh. From S_1, solar capacity could continuously increase, as seen in S_2 and S_3, or LNG could increase further as seen in S_3. The impact of S_2 and S_4 in reducing CO_2 emissions was the same, but the increase in cost was lower for S_4. S_5 represents the greenest yet feasible scenario that reduces the CO_2 emissions by an average of 37.31% but increases the cost by 5.60%.

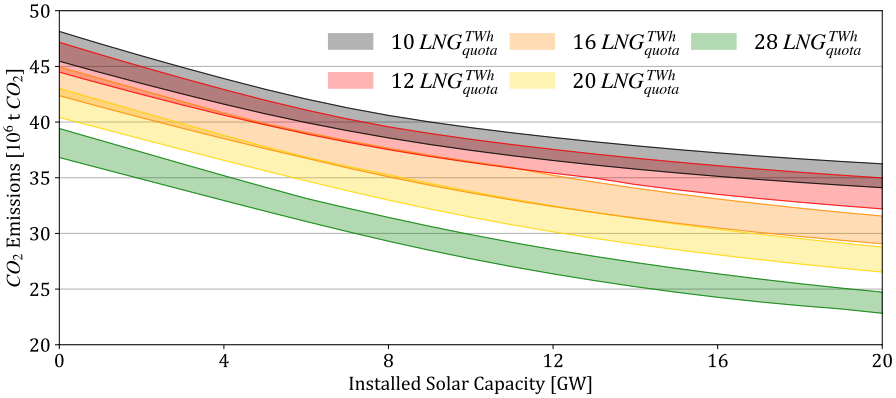

Figure 4.16: Range of CO_2 emissions for various scenarios in Kyushu.

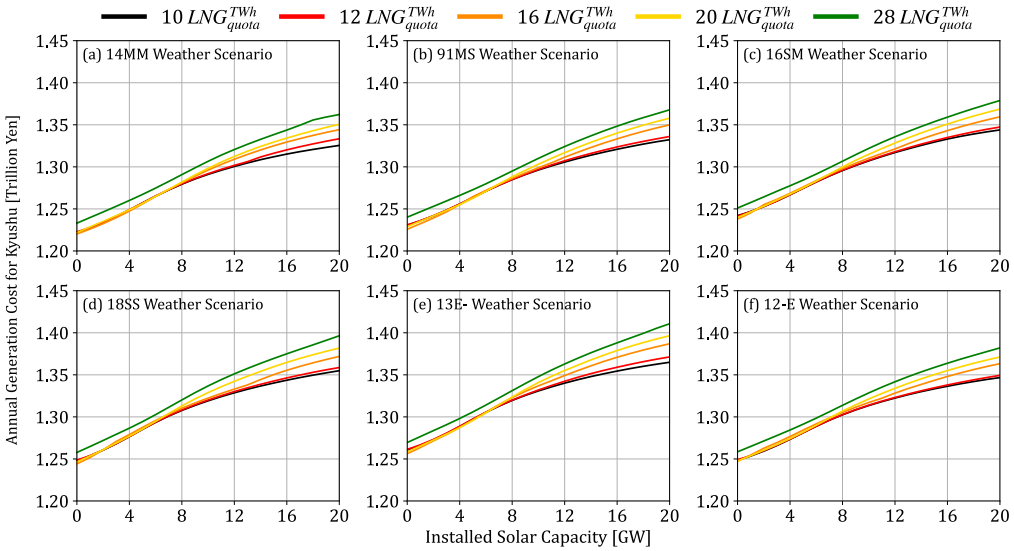

Figure 4.17: Annual generation costs for various scenarios in Kyushu.

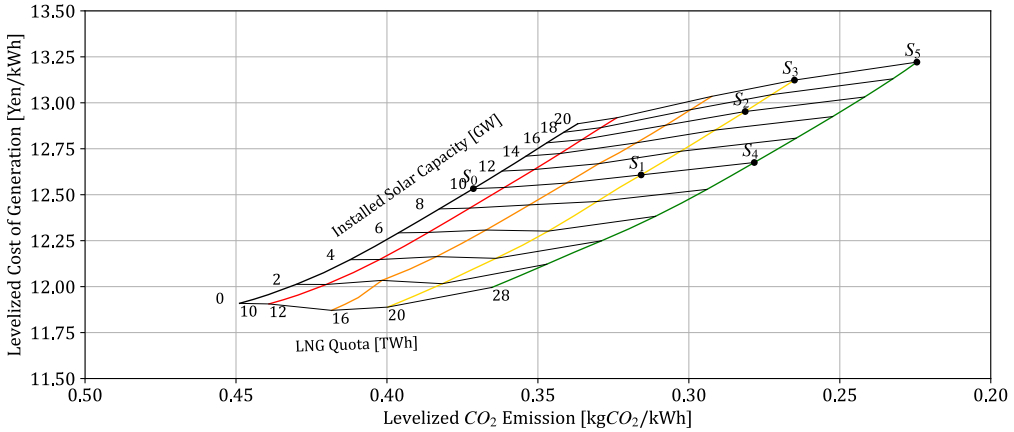

Figure 4.18: Levelized generation cost and CO_2 emissions for the warmer year (16SM) scenario. The CO_2 emissions (abscissa) are formatted in decreasing order to emphasize the trend. S_0 reflects the current situation, and S_1-S_5 are the potential future scenarios.

4.4 Discussion

4.4.1 Potential and Limitations of Solar PV in Coal Decommissioning

Although it cannot phase-out coal, the results show that solar energy has enough potential to be the driver for coal decommissioning with LNG's help. It has also been shown that the decommissioning potential is robust against yearly weather-driven demand, and standby-plants could be used for the colder and warmer periods of the year. Although solar power has

Table 4.10: Cost Increase from the reference scenario

Scenarios				Increase in Cost per kWh [%]						
No	Name	$Solar_{cap}^{GW}$	LNG_{quota}^{TWh}	14MM	91MS	16SM	18SS	13E-	12-E	Mean
S_1	Increase LNG_{quota}^{TWh} 1	10	20	0.56	0.53	0.60	0.74	0.75	0.59	0.63
S_2	Increase $Solar_{cap}^{GW}$ 1	16	20	3.34	3.38	3.35	3.46	3.61	3.17	3.39
S_3	Increase $Solar_{cap}^{GW}$ 2	20	20	4.61	4.75	4.71	4.75	4.93	4.40	4.69
S_4	Increase LNG_{quota}^{TWh} 2	10	28	1.20	1.07	1.13	1.34	1.28	1.14	1.19
S_5	Increase both	20	28	5.51	5.52	5.49	5.86	6.00	5.22	5.60

Table 4.11: CO_2 emission decrease from the reference scenario

Scenarios				Decrease in CO_2 emission per kWh [%]						
No	Name	$Solar_{cap}^{GW}$	LNG_{quota}^{TWh}	14MM	91MS	16SM	18SS	13E-	12-E	Mean
S_1	Increase LNG_{quota}^{TWh} 1	10	20	-13.50	-12.74	-12.55	-12.91	-12.94	-12.18	-12.80
S_2	Increase $Solar_{cap}^{GW}$ 1	16	20	-22.78	-22.53	-22.10	-22.66	-22.78	-21.02	-22.31
S_3	Increase $Solar_{cap}^{GW}$ 2	20	20	-27.05	-27.18	-26.62	-27.24	-27.29	-25.15	-26.75
S_4	Increase LNG_{quota}^{TWh} 2	10	28	-23.77	-23.24	-22.93	-23.37	-23.09	-22.27	-23.11
S_5	Increase both	20	28	-36.45	-38.32	-37.84	-37.97	-37.58	-35.70	-37.31

limitations in reducing coal capacity, it continually decreases the necessary coal generation, thereby reducing the load factor of coal plants and the corresponding CO_2 emissions.

In Kyushu's case, given the 10 GW solar capacity along with a 16 TWh complementary LNG quota, 3.5 GW of the 7 GW coal power plants could be decommissioned. This configuration is already achievable by increasing the LF of the combined-cycle plants of KyEPCO from 20% to 44%. Beyond 12 GW installed solar capacity, solar power alone has no impact on reducing the coal capacity, but it could still reduce coal generation. Compared to the reference scenario, it was shown that CO_2 emissions could be reduced by 27% through 20 GW of solar power and a 20 TWh annual LNG quota. The reduction could reach 37% if all the LNG plants in the region are utilized at 60% LF. As a related consequence, reducing coal and introducing more LNG reduced solar curtailment. This potential and limitations show that energy planners should take the necessary precautions in adding solar energy to the grid since there is an appropriate balance. Solar can reduce coal capacity, but it alone cannot phase-out coal. As was shown in Kyushu's case, a thorough analysis of the situation that includes complementary energy sources should be considered in evaluating the potential of solar power in coal decommissioning.

4.4.2 Implications of Solar PV in Coal Decommissioning

Solar has its drawbacks in the form of cost and dependence on complementary flexible generators. The results show that in countries like Japan, where solar power remains to be more expensive than conventional generators—solar power presents an additional cost. Its dependence on flexible generators, which LNG currently fills, poses a threat to its ability to stand-alone. As the demand for LNG steadily increases, this will threaten its supply and price. The cost of LNG could exacerbate the cost problems of solar.

In Kyushu's case, increasing the solar capacity from 10 GW to 16 GW and 20 GW increases the levelized cost of generation by 3.39% and 4.69%, respectively. Increasing the LNG quota has a minor impact at the moment since the current LNG price is only about 12% higher than coal. In contrast, solar is still almost twice as expensive as coal. Solar prices around the world have been decreasing, and it might decrease in Japan in the future. The impact on CO_2 and cost now becomes a policy decision, and the ratio between these two factors presents several potential combinations between LNG quota and installed solar capacity that could yield identical cost or the same CO_2 targets as seen in S_2 and S_4. More LNG is necessary when cost is prioritized, but it will lead to more dependence on LNG. Alternatively, by investing more in solar capacity, it could lead the CO_2 reduction efforts and local power generation. This scenario entails lower dependence on both coal and LNG, which are both imported fuels. As with the previous results, the impact of weather on these values is evident, as seen in the variations in the levelized cost and levelized CO_2 emissions.

4.4.3 Potential Solutions beyond Solar PV

The supply and demand mismatch in winter and summer is one of the major roadblocks in the total phase-out of coal power plants through solar energy. Diurnal storage will be enough to solve the mismatch during summer, but seasonal storage or seasonal generation will be necessary for winter. Since there is still enough excess energy during peak solar production in summer, storage is the straightforward solution once these options become economically feasible. However, since there is less solar energy in winter, there is not enough excess solar energy for diurnal storage to work, which opens an opportunity for seasonal technology. Seasonal storage in the form of power-to-gas (P2G) could store the excess solar in autumn for winter. Combined heat and power (CHP) plants could be operated at a higher capacity in winter if local water heating is established.

4.4.4 Impact of Weather on Energy Transition Plans

The stochastic nature of demand and renewable energy sources was the primary motivation for developing the weather-driven approach since energy transition recommendations should consider scenarios that will test the limits of the planned energy mix. The variations are significant at 400 MW to 600 MW coal capacity, as seen from the results. In Japan's case, this translates to 1–3 coal power plants, but for smaller nations with smaller plants, this could be composed of more than five plants that should be on standby in the event of an extreme weather condition. Coordinating smaller plants will require more dialogue and agreements between the government and plant operators. Consequently, the government could also run standby plants to ensure the reliability of the system. It has also been shown that weather influences the potential for CO_2 reduction and the system's overall annual generation cost. Beyond coal decommissioning, weather will remain a necessary variable in energy planning since it influences the demand, which is the primary source of stochasticity in the analysis. As more VREs are added to the green energy transition, weather becomes

a crucial variable for both wind and solar. Rainfall data could also influence hydropower generation, which was not explored in this study. It could also influence the viability of PHES since this requires sufficient water reservoirs affected by rain and water evaporation. Little is known about wave energy's potential, but the weather will also influence it since it depends on nature.

4.4.5 Importance and Limitation of the Proposed Approach

The proposed weather-driven scenario-based analysis revealed the importance of the LNG quota, demand variations, and solar generation through the annual hourly simulation. System reliability could be analyzed using the duration curve, but this does not show the hourly balance, which is greatly influenced by demand and solar generation's stochasticity. Through careful selection of representative years, the range of potential scenarios was identified and analyzed to ensure robust results. However, the approach is dependent on the yearly assignment and is limited by the probabilistic matching of weekends and holidays to high irradiance days. The former is influenced by human behavior, while the latter is non-deterministic. Thus, although the simulation considered the yearly variations, the probability of a low irradiance day being matched to a high-demand weekday was not covered by the approach. Nonetheless, the approach can be used to provide robust recommendations for green energy transition since it covers the stochastic nature of demand and variable renewable energy. In this study, the approach was used to determine the minimum coal capacity that can ensure the system's reliability, but it could also be used for energy storage assessments and capacity planning. This study only used a single-bus network, but it could be expanded to a national grid level by representing each region as a bus. The approach can then be used for grid expansion planning.

4.5 Conclusion

Driven by the idea of transitioning to a green electricity grid, an hourly power flow analysis was conducted to understand the potential, limitations, and implications of using solar energy as a driver for decommissioning coal power plants. The weather-driven scenario analysis ensured the robustness of the results and recommendations. The analysis revealed that solar power could reduce about half of Kyushu's coal capacity with the aid of LNG. Beyond 12 GW, solar power could not reduce the minimum coal capacity necessary to ensure the system's reliability, but it could still reduce the coal generation and the overall CO_2 emissions. The reduction in coal capacity comes at a cost, since solar power is still relatively more expensive in Japan. By installing 20 GW of solar PV systems and having 28 TWh of available LNG, the levelized CO_2 emissions could be reduced by 37%, but this would increase the levelized cost of generation by 5.6%. Most of the price increase is owed to the price of solar electricity generation, which remains high in Japan. In Kyushu's case, this change could be achieved without constructing additional power plants, since the LNG plants are operated

at a low LF. However, additional planning is necessary to acquire more LNG. Countries that use LNG plants as peak-load generators share the same potential, and the results show that a minor change in the system could have a significant impact on emission goals.

The results emphasized that solar power with the aid of LNG could partially replace coal capacity, but it alone could not phase-out coal. For energy planners who are only starting to increase their solar capacity, insights from this work could help with understanding the interactions between coal, solar, and LNG electricity generation. For planners in countries with a considerable amount of solar power (>8%), the results from this study could serve as a precaution by highlighting the risks of further increasing the solar power penetration. Although solar power helped solve midday peak power, the problem remains because it simply shifted to periods where there is no solar energy. Summer and winter are challenging periods due to the increase in peak demand. Although it is counterintuitive, solar energy is not enough during summer, or, to be more precise, misaligned since the problem occurs in the late afternoon. Diurnal storage can address the misalignment in summer, but winter presents a more intricate problem, since the solar energy is insufficient. Thus, exploring other technologies that could further complement solar energy is necessary.

The weather-driven approach revealed the importance of weather in the analysis, as it affected the results to varying degrees. In addition, 400–600 MW of standby coal capacity is necessary due to the yearly fluctuations. Coal generation, coal load factor, curtailment rate, and CO_2 emissions vary by 7–18%, 8–27%, 0–5%, and 6–8%, respectively. Identifying the representative year is crucial since it should cover the worst case, best case, and the cases in between. Energy planners and policymakers should consider the weather when analyzing energy plans, as it could provide a range of values that can guide them in making the correct decisions. Since the approach can generate scenarios based on weather data, it could also be used for storage assessment and capacity planning. The approach could also be used for grid expansion planning by increasing the number of buses and modeling multiple demands. These energy planning topics could also benefit from the range of insights generated through the weather-driven approach.

5 Dynamic Cost-Optimal Assessment of Complementary Diurnal Electricity Storage Capacity

The contents of this chapter is based on Dumlao, S. M. G., & Ishihara, K. N. (2021). Dynamic Cost-Optimal Assessment of Complementary Diurnal Electricity Storage Capacity in High PV Penetration Grid. Energies, 14(15), 4496. doi: https://doi.org/10.3390/en14154496.

5.1 Introduction

5.1.1 Electrical Energy Storage

There are several ways to categorize electrical energy storage (EES) such as stored energy type [84], energy conversion interface [85], [86], storage mechanism [85], [87], and energy storage purpose [88]. Figure 5.1 categorizes the electrical storage systems based on the conversion interface. Direct electrical storage mainly stores energy via electric fields in capacitors and magnetic fields in inductors without the need for conversion [84], [85]. Their use is well-known in electronic circuits, but their capacity to store energy is limited. Electrochemical energy storage utilizes electrochemical reactions to store and produce energy, and the capacity ranges from 100 W to MW [88]. Mechanical energy storage stores energy either through kinetic energy or potential energy [84]. This type of storage produces fewer contaminants throughout its life cycle [87], but its geographical location is its main limitation [88], [89].

Chemical energy storage covers technologies where electrical energy produces chemical compounds that could later generate electricity [88]. Electricity can be stored through the production of gas or liquid that could later be used for energy generation or direct utilization [90]. In contrast to the previous three types, the production plant for chemical energy storage is often separate from the generation plant. Thermal energy storage stores energy through temperature change, phase change, or chemical structure change in the

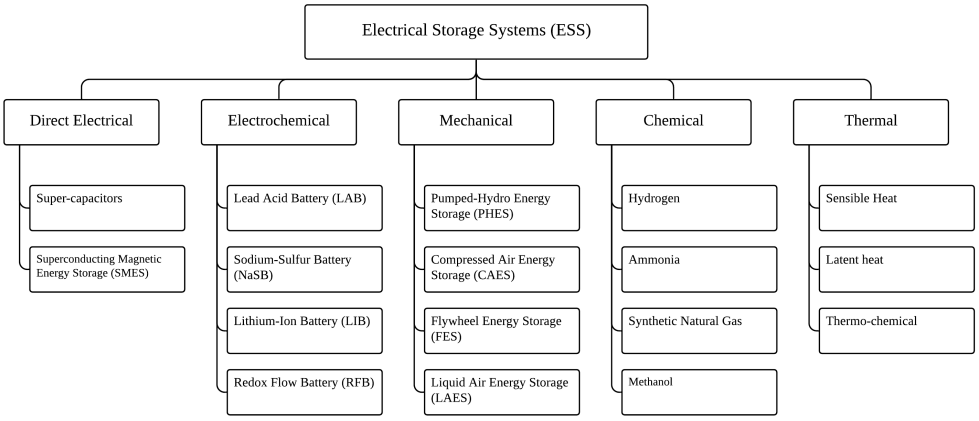

Figure 5.1: Types of Electrical Storage Systems based on the energy conversion interface. Adapted from [84]–[88], [90].

material [88]. This kind of energy storage is often used alongside concentrated solar power (CSP) plant for dispatchable generation [91]. Similar to chemical storage, the "charging" and "discharging" interfaces for thermal energy are separate facilities.

Since the theoretical maximum capacity of direct electrical storage is limited, it is infeasible for grid-level storage. The dynamics between the storage and generation of chemical electrical storage may prove to be useful for long-term storage, but since it requires two different facilities, for short-term storage the complexity of the system could hinder its operation; thus, it will not be explored further in this study. Similarly, thermal electrical storage will not be explored further since the current application is limited to CSP. Mechanical and electrochemical electrical storage provides a straightforward conversion between electricity and storage, which is appropriate for diurnal storage. These kinds of storage are essentially built and then cycle through charging and discharging. The capacities of such electrical storage systems are limited mainly by the area and the cost of the installation. The study will mainly focus on these two types of electrical storage.

Pumped hydroelectric energy storage (PHES) requires two reservoirs. It stores energy by pumping water uphill and generates electricity by releasing the water downhill like a typical hydropower plant [88]. It is the most mature and widely used large-scale energy storage technology, but it is limited by several natural geological features, including adequate elevation and sufficient water supply [88]. Compressed air energy storage (CAES) stores energy by compressing air to high pressures using electrically driven compressors [89]. It generates electricity by allowing the air to expand and mixing the air with fuel in a combustor to drive the turbines [89]. Usually, the compression cycle requires cooling, and the expanding cycle needs preheating [89]. Although it is already considered a developed technology, it suffers the same geographical restrictions of PHES since it requires access to large underground cavities, aquifers, and caverns [89]. Flywheel energy (FES) storage stores electrical energy in the form of rotational energy, but it is designed to deal with short-term voltage disturbance to improve power quality [88]. Liquid air energy storage (LAES) stores

Table 5.1: Electrical Storage System (ESS) Parameters

Parameters	unit	LAB	NaSB	LIB	VRB	PHES	CAES	FES	LAES
Round-trip Efficiency	%	75	80	90	80	75	60	88	50
Discharge Duration		m-h	m-h	m-h	m-h	m-h	m-h	s-m	m-h
Depth of Discharge	%	50	80	80	100	100	100	100	100
Cycle Life	cycle	2000-4500	2500-4500	1500-4500	10k-13k	20k-50k	> 13k	20k-100k	-
Calendary Life	years	5-15	10-15	5-15	5-15	40-60	20-60	15	30-40
Reference		[85], [86], [95], [96]	[85], [88], [95], [96]	[85], [88], [95], [96]	[85], [88], [95], [96]	[85], [86], [88], [95]	[85], [86], [88], [95]	[85], [88], [95], [97]	[92]

energy by storing liquefied cool air in tanks [92]. Electricity is generated by allowing the air to evaporate and drive the turbine [92]. Since it utilizes tanks designed for liquefied air, it does not have geographic restrictions, but its efficiency is low [92].

Lead-acid (PbO_2) battery, although considered to have lower efficiency and energy density, is still used because of its low cost, high reliability and technological maturity [88]. This technology also has a short lifetime at a high depth of discharge, and it requires periodic water maintenance [85]. Sodium sulfur (NaS) battery is one of the batteries used for commercial electrical energy storage in electric utility distribution due to its high energy density, energy efficiency and long cycle capability [88]. However, high capital cost, high operational temperature requirement and high operational hazard limit its application [88]. The increasing number of portable electronic devices has placed a spotlight on Lithium-ion (Li-ion) batteries. Li-ion's high power, energy density, and efficiency make it a potential solution for grid-level storage [86]. However, depending on lithium alone might lead to insufficient supply in the future [93]. Recently, there is an increasing interest in the redox flow battery (RFB) due to its low maintenance cost, overcharging tolerance, and deep charging capability [88], but this technology is still in the development phase [94].

Several studies have summarized the technical and economic properties of existing and potential ESS [85], [86], [88], [95]–[97]. A recent review by Borri et al. [92] summarizes recent trends in LAES. From these sources, Table 5.1 summarizes some of the parameters crucial in understanding mechanical and electrochemical storage. Each technology has a different round-trip efficiency, which has an impact on the discharge capacity of the system. To ensure a longer lifetime for some of the batteries (LAB, NaSB, and LIB), they are not completely discharged; thus, only a fraction of their actual capacity is usable. This drawback is not present in mechanical energy storage.

The cost of ESS is highly contentious. There are various ways to compute capital expenses and operational expenses. Some authors focus on both the power delivery cost and energy capacity cost [86], [88], [96], [97], while some authors mainly focus on the energy capacity cost and assume a particular duration for the power delivery [98]–[100]. The former allows more flexibility in the calculations, but the latter simplifies the assumptions in the calculations. Since the focus of this paper is on diurnal storage, the focus will be on the cost of the energy capacity. Schmidt et al. [98] concluded that the capital cost of ESS systems is on a trajectory towards 340 USD/kWh and 175 USD/kWh for stationary and battery pack storage, respectively, once the total installed capacity reached 1 TWh. They estimated that the storage cost by 2030 would be between 290 USD/kWh to 520 USD/kWh, where PHES and Li-Ion represent the lowest and highest costs, respectively. These conclusions

are relatively higher than the projections of Cole and Frazier [99]. After analyzing 25 publications, they concluded that the capital cost of a 4-h battery system would be between 124 USD/kWh and 301 USD/kWh. In Lazard's 2020 Levelized Cost of Storage Analysis [27], they mentioned in their assumption that they used 475 USD/kWh and 102 USD/kW as their ESS cost for utility-scale PV + storage system. These assumptions are closer to the cost projections of Cole and Frazier for 2020, albeit a pessimistic assumption.

5.1.2 Economic Assessment

Levelized Cost of Energy (LCOE), calculated by dividing the life cycle cost of the system by its lifetime energy production, is one of the most commonly used economic metrics in comparing energy generators [100]. Early literature stated that it allows the comparison of alternative technologies despite the difference in operational scale, investment, and operating periods [101]. It has become one of the standard economic metrics used in comparing technology, especially in comparing renewable energy with conventional energy (such as coal and Liquefied Natural Gas (LNG)) [102]–[104].

LCOE is not directly applicable in assessing storage cost since energy storage does not generate its energy. Adapting the basic idea behind LCOE, Jülch et al. [96], [105] defined Levelized Cost of Storage (LCOS) as the sum of all the annual expenses (such as operational cost and charging cost) and capital cost divided by the sum of delivered energy over the lifetime of the storage. The approach is relatively similar to LCOE, but instead of generating the energy, LCOS purchases electricity and the delivered energy incorporates the cycle lost (charge and discharge). After examining the LCOS for several ESS technologies, the author highlighted that LCOS is influenced by the design of the storage plant, cost of electricity, and operating hours [96].

Lai and McCulloch [100] focused on a mathematical approach to isolate the LCOS, where storage was seen as separate from the system, and introduced the idea of Levelized Cost of Delivery (LCOD) that provided the relationship between LCOE and LCOS. Schmidt et al. [97] provided a comprehensive analysis of nine storage technologies for several applications and concluded that Li-Ion batteries are the most competitive, and PHES, CEAS, and hydrogen are best for long discharge application.

Storage is starting to be financially viable, and several studies have explored the idea of identifying appropriate storage allocation. Li et al. [69] conducted a technical-economic assessment of large-scale PV integration with PHES in the Kyushu region. PHES was chosen in their study because they evaluated that the topography and geology in the area are favorable to the development of PHES. Their results showed that the additional income from the PV surplus was not enough to cover the additional investment in PHES, but it could offset the initial investment. Anagnostopoulos and Papantonis [106] investigated the performance of pumped storage to support large-scale variable renewable energy in Greece. The authors used the internal rate of return in their economic evaluation and concluded that the project's viability is significantly dependent on the curtailed energy's magnitude and

distribution. Liu et al. [107] wrote a review article on energy storage for the electric grid, and in their economic subsection, they mentioned that utility-owned storage provides an excellent opportunity to implement energy arbitrage. Their study highlighted the case of California, but the exact details of the costs and benefits were not disclosed. Nonetheless, the study mentioned that the utility-owned storage systems were making a profit.

5.1.3 Objective

Most studies consider storage as an additional cost that must be recovered by storing excess solar energy. However, as solar penetration increases further, the cost penalty to solar PV owners due to solar curtailment increases to a point where solar might no longer be economically competitive. At this point, storage is no longer an additional cost but a necessary infrastructure to maintain solar energy's competitiveness. Consequently, ESS planning should be considered in regions with imminent curtailment issues. There is a need for an optimization approach that provides a target value for the optimal complementary storage capacity in each year, which minimizes the generation cost of renewable energy. This optimization should consider the changes in the cost of ESS and PV and the continuous growth of solar PV. To date, most studies primarily focus on the optimal value for the project and not for the whole system nor for a specific planning horizon. LCOE, LCOS, and LCOD mainly focus on the project's profitability, making it challenging to analyze the impact of additional investments on the existing system. These approaches are well-suited for individual projects but inappropriate for analyzing the whole system, where the capacity of solar and ESS are dynamically changing over several years. Furthermore, these financial assessments are unsuitable for optimization that considers the impacts of early or delayed investments. To the best of the authors' knowledge, an ESS growth trajectory optimization has not previously been explored.

Therefore, this study conducts a techno-economic analysis to present the cost-optimal storage growth trajectory that could support the dynamic integration of solar PV through a particular planning horizon. The optimization aims to balance the cost penalty from curtailment and the additional investment cost of storage. The technical analysis focuses on the energy balance changes due to the increasing solar PV and storage capacity. The economic analysis looks into the changes in the energy generation cost due to solar panel price, storage price, and the utilization rate of the system. A methodology for the cost-optimal assessment is proposed to tackle the time-bound optimization of storage capacity that complements the increasing solar capacity. The proposed approach utilizes a two-step optimization process that performs (a) a technical optimization that maximizes the PV and ESS utilization while ensuring hourly energy balance and (b) an economic optimization that identifies the ESS growth trajectory with the lowest generation cost within the planning horizon. The Kyushu region in Japan was used as a case study since it continuously increases its solar capacity and is at the precipice of high PV curtailment.

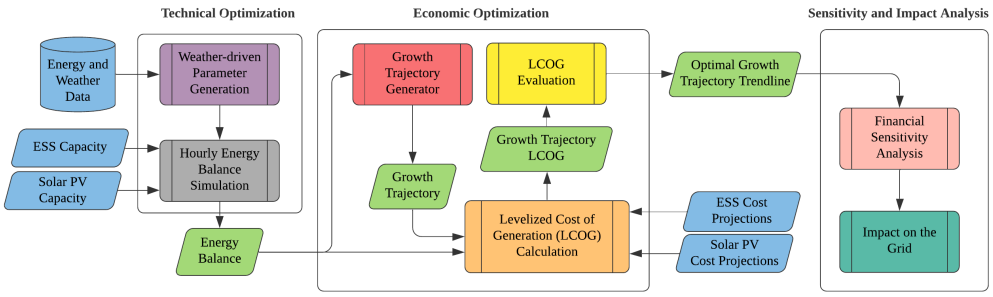

Figure 5.2: Proposed Cost-Optimal Storage Capacity Assessment using Hourly Simulation, Monte Carlo Sampling, and Levelized Cost of Generation. Blue parallelograms represent the input of the system such as the ESS and PV capacity for the scenarios and the ESS and PV cost projections for the financial calculation. Green parallelograms represent the intermediate output of the processes.

5.2 Methodology

Figure 5.2 shows the overview of the proposed cost-optimal storage capacity assessment, where three process clusters are highlighted. First, the technical optimization focused on maximizing the utilization of the additional ESS from a purely technical perspective. Python for Power System Analysis (PyPSA) Modeling Framework (v0.17.1) [53], which formulates and solves a linear programming problem for optimal power flow, was used to optimize the hourly energy balance. The optimization calculated the energy balance based on various ESS and solar PV capacity scenarios. This calculation was used in the economic optimization, which focused on calculating the optimal growth trajectory. Using the information about the maximum ESS that could support the specified scenarios, the growth trajectory candidates were generated manually and through a Monte Carlo random sampling. The proposed Levelized Cost of Generation (LCOG) was used to provide a financial index for each growth trajectory using financial data about ESS and solar PV and the pre-computed energy balance. The optimal ESS growth trajectory is the trajectory with the least LCOG within the planning horizon. Finally, a sensitivity analysis was conducted to assess the parameters that could affect the trajectory, and an impact analysis was carried out to understand the impact of following the trajectory on the electricity grid.

5.2.1 Technical Optimization

The hourly simulation used Python for the Power System Analysis (PyPSA) Modeling Framework (v0.17.1) [53]. The PyPSA environment provides a framework for the buses, lines, loads, generators, storage, and units, among many other parameters. In this simulation, Kyushu was modeled as a single point, but additional sub-buses were added to monitor the changes in the energy balance due to the additional ESS, as seen in Figure 5.3. The coal generator was connected directly to the main bus B0 to prevent it from charging the ESS. Since there are still instances when the existing ESS capacity is charged by the other generators, albeit minimal, sub-bus B1 was provisioned to monitor this power flow. B2 was

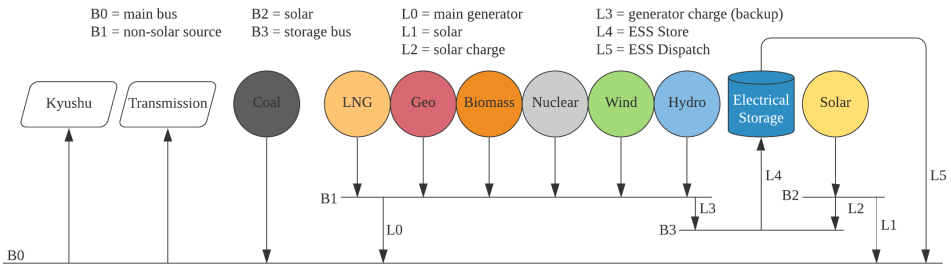

Figure 5.3: Configuration of the grid used in the optimization.

Table 5.2: Generators in Kyushu as of FY2019

Generator	Power [MW]	Carrier	$\mathrm{Output}_{\mathrm{min}}$ [%]	Ramp Limit [%]
Coal	7037	Coal	30	1
LNG	5250	Gas	15	40
Geothermal	160	Renewable	100	0
Biomass	450	Renewable	100	0
Solar	9000	Renewable	0	100
Nuclear	4140	Non-GHG	100	0
Wind	355	Renewable	15	40
Hydro	4000	Renewable	15	40

provisioned to monitor the interaction between the PV and ESS. Sub-bus B3 serves as the input for solar and the other generator for the ESS through lines L2 and L3, respectively. Solar has a direct connection to the main bus through line L1, while the delivered energy from ESS goes through L5.

For this study, the synthetic load and solar generation profile for the average year (2018) generated in Chapter 4 was used for the optimization since it was determined that this year represents the year with the highest variability. Similarly, the generator parameters seen in Table 5.2, which were used in the previous Chapter, were also used in this study. These generator properties were consolidated based on various sources [42]–[44]. This study's solar capacity followed the solar capacity growth in Kyushu from 2012 to 2020, which was detailed in [5]. From the latest published capacity of around 10 GW in 2021 [36], the simulation incremented the PV capacity by 600 MW, 800 MW, and 1 GW per year for the next ten years. The ESS capacity was incremented by 1 GWh from the current 13 GWh capacity until 80 GWh. A preliminary analysis determined 80 GWh as the terminal ESS capacity for the 20 GW solar capacity.

For the optimization, the system prioritizes solar while ensuring energy balance and satisfying the minimum operating output or ramp limit seen in Table **??**. Although the nuclear, geothermal and biomass could change within the year, as baseload, it was fixed to its respective maximum capacities to provide consistency throughout the years under simulation. Hydropower generation is based on the daily dispatch capacity calculated using the total daily dispatch in 2019. The simulator allocates the hourly dispatch based on the optimization. However, minimum and maximum dispatch is still considered based on the actual data. The LNG was capped at 10 TWh since this was determined as the current budget in the region in

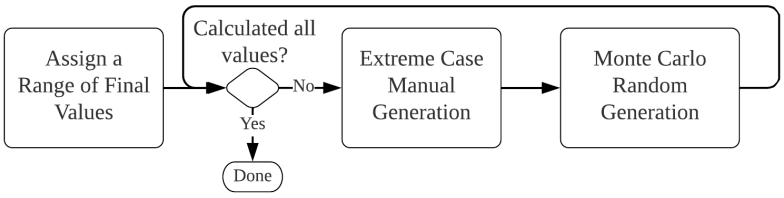

Figure 5.4: Overview of the growth trajectory generation.

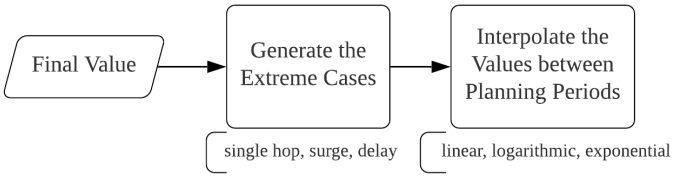

Figure 5.5: Manual Generation to handle the extreme cases.

Chapter 4. Since the analysis focuses on a period of one year, the resulting hourly simulation was consolidated into yearly statistics, which will be used in the economic optimization.

5.2.2 Economic Optimization

Growth Trajectory Generation

The optimal growth trajectory of ESS is difficult to ascertain due to the enormous amount of potential paths that it could reach. Testing all the paths, even at wide-ranging intervals, seems to be a daunting task. Therefore, this is where Monte Carlo random sampling can be applied. Essentially, this random sampling provides a statistical sample of the available solution space that can identify the optimal solution.

Figure 5.4 shows the overview of the growth trajectory generation. An initial range of final values was predefined. In this study, the evaluation started from 7 GWh until 67 GWh with intervals of 2 GWh. All these final values go through the manual and random case generation. As outlined in Figure 5.5, the manual generation, which covers the extreme cases, provides the growth trajectory for single hop, surge, and delay. Single hop focuses on the idea that the planning for the whole duration is conceived at the start, which will dictate the growth trajectory from beginning to end. The surge is similar to the single hop, but the final value is achieved early (e.g., 30 GWh by 2025) and will stay there. On the other hand, the delay scenario will delay the start of the planning (e.g., 0 GWh until 2025) and grow from there. The surge and delay cases were generated from 2021 until 2031 with a 2 year interval. Using these targets, the values in between were interpolated using linear, logarithmic, and exponential growth.

Figure 5.6 outlines the random sampling for the middle cases. The solution space in between the extreme cases is vast, and random sampling reduces the computational requirement of

Table 5.3: Planning Hops

hops	hops #	Sample [%]
2021, 2023, 2031	3	50
2021, 2025, 2031	3	50
2021, 2027, 2031	3	50
2021, 2029, 2031	3	50
2021, 2023, 2025, 2031	4	10
2021, 2023, 2027, 2031	4	10
2021, 2023, 2029, 2031	4	10
2021, 2025, 2027, 2031	4	10
2021, 2025, 2029, 2031	4	10
2021, 2027, 2029, 2031	4	10
2021, 2023, 2025, 2027, 2031	5	5
2021, 2023, 2025, 2029, 2031	5	5
2021, 2023, 2027, 2029, 2031	5	5
2021, 2025, 2027, 2029, 2031	5	5
2021, 2023, 2025, 2027, 2029, 2031	6	1

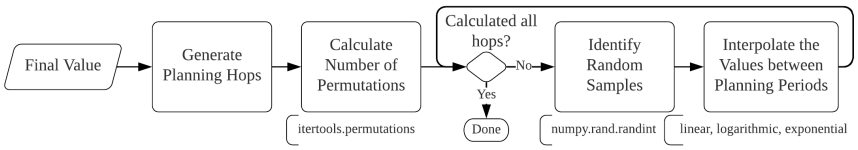

Figure 5.6: Monte Carlo random sampling for the middle cases.

the analysis. However, to ensure that the sampled values represent the whole solution space, it is necessary to approach the sampling methodologically. Similar to the manual generation, the random generation starts with the final value. From this value, planning hops were generated from 2021 until 2031 with a 2 year interval. Table 5.3 shows the combination of the hops. The sampling rate was identified for each hop length. The number of potential permutations are calculated using the final value and the length of each combination. The growth trajectories were then randomly selected using the target number of samples. Similar to the manual case, the values in between were interpolated using linear, logarithmic and exponential growth. Figure 5.7 shows a sample growth trajectory using manual generation and random sampling.

Using the specified intervals for the ESS capacity and planning hops, it was determined that there were around five million possible growth trajectories. Following the sampling rate in Table 5.3, around 430,000 were evaluated. Since there is a possibility of overlap during the generation, the sample size varies depending on the random seed.

Financial Evaluation

The proposed Levelized Cost of Generation (LCOG) shown in (5.1) is used in the financial evaluation of the optimal growth trajectory. The formula is a slight modification of the annuitized Levelized Cost of Energy (LCOE) formula discussed by Lai and McCulloch [100]. Although they did mention that the present value approach is more appropriate in calculating LCOE, to identify the optimal capacity for a particular planning horizon, as is the goal of

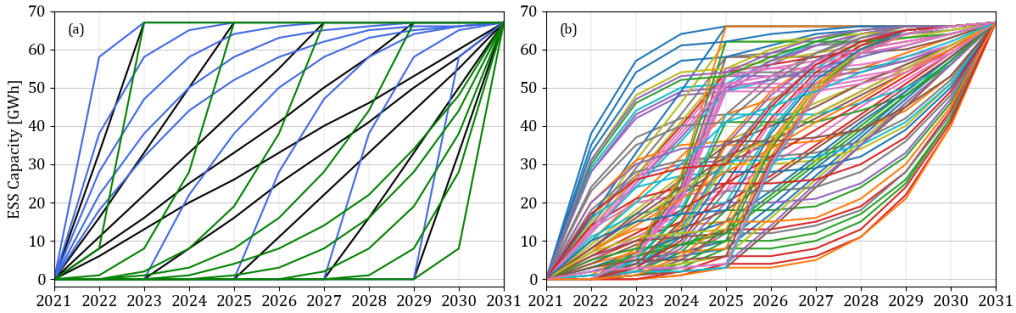

Figure 5.7: Sample growth trajectory generation using (a) manual generation to handle the extreme cases and (b) Monte Carlo random sampling to provide the random samples in the middle. (a) shows the filling process between planning years, where black, blue, and green represent linear, logarithmic, and exponential growth, respectively. (b) represents one of the planning hops (2021, 2025, 2031) and the filling process as shown in (a).

this work, the annuitizing method is more appropriate since it has to consider additional installation as time progresses. They also emphasized that the variability of solar makes the annuitized formula less appropriate. However, this particular issue is essential in this particular calculation because not only is the energy production variable, with curtailment it is also dependent on the total PV capacity for that particular year. Using LCOE as a foundation, LCOG was formulated by taking into consideration the time component. In contrast to LCOE, which focuses on a unit of energy's production cost for the whole lifetime of the energy generator, the LCOG focuses on a unit of energy's generation cost throughout the planning horizon. This notion facilitates the ability to assess the system as a whole at a certain point in time or a specific period.

$$\mathrm{LCOG}_{y_R}^{PV+ESS} = \frac{\sum_{y_r=y_{R_0}}^{y_{R_n}} \left(\sum_{y_i=y_0}^{y_n} \left(C_{y_i,y_r}^{PV} + C_{y_i,y_r}^{ESS} \right) \right)}{\sum_{y_r=y_{R_0}}^{y_{R_n}} E_{y_r}^{PV+ESS}}. \tag{5.1}$$

LCOG levelizes the cost of generation within the planning horizon by dividing the total annuitized cost by the total energy generated throughout that period, as seen in the outer summation of the numerator and the denominator. y_R refers to the period under evaluation that begins from y_{R_0} until y_{R_n}. In this study, y_R is 2022–2031, as shown by the bounded box in Figure 5.8. The inner summation in the numerator represents the cost per year, which is the summation of the annuitized cost of PV and ESS. Since the capital cost changes every year, the annuitized cost will depend on the capacity and annuity in that particular year. The cost is calculated using (5.2) and (5.3), where annuity is computed using (5.4). Japan's interest rate (r) of 3% was used in the calculation. The lifetime of PV and ESS was estimated to be 20 and 15 years, respectively, in this study. Each box in Figure 5.8 represents an annuity cost either from PV or ESS. The sum of the boxes with the bounding box represents the total cost for the duration of the planning horizon.

$$C_{y_i}^{PV} = Cap_{y_i}^{PV} A_{y_i}^{PV} \tag{5.2}$$

$$C_{y_i}^{ESS} = Cap_{y_i}^{ESS} A_{y_i}^{ESS} \tag{5.3}$$

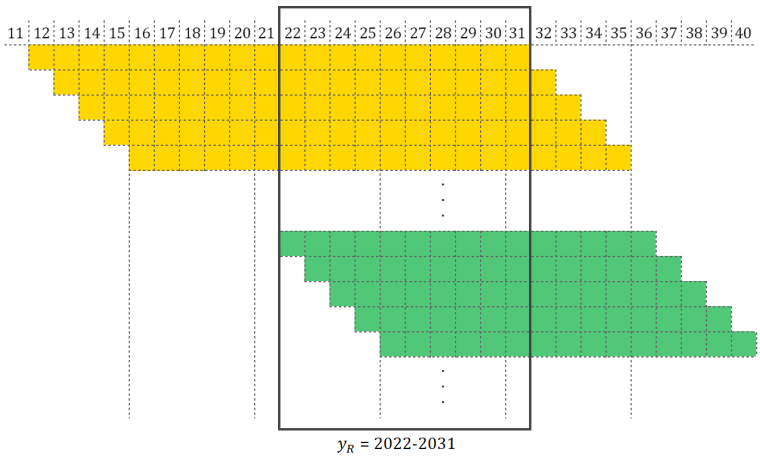

Figure 5.8: Visualization of the elements of the LCOG. Each box represents an annuity cost either from PV (yellow) or ESS (green). The bounded box represents the planning horizon in this study.

$$A_y = P_y \left[\frac{r\,(1+r)^n}{(1+r)^n - 1} \right] \text{ (used for both PV and ESS).} \tag{5.4}$$

The cost projections for PV and ESS can be seen in Figure 5.9. The unit cost of solar for each year was used to compute for the annuity ($A_{y_i}^{PV}$) from the principal cost ($P_{y_i}^{PV}$) using (5.4). In the case of Japan, aside from the panel, there are minimal cost changes; thus, the projection focused on the reduction in PV panel price. A 10% learning curve per year was used since this is the current cost reduction trend. The study assumed that this would continue until 2031. The unit price or principal cost of ESS ($P_{y_i}^{ESS}$) was taken from Cole and Frazier [99], since their projections already considered several publications and they provided the corresponding values for each year while other references only focused on specific years. For the initial calculation, the middle projection for the ESS unit cost ($\mathrm{ESS}_{\mathrm{mid}}$) was used. Since the computation used JPY, this was converted from USD to JPY using the current conversion of 1 USD = 110 JPY.

Levelized Cost of Generation (LCOG) Evaluation

At this stage, the LCOG of the candidate growth trajectories were evaluated to extract the optimal growth trajectory. Primarily, the goal was to identify the growth trajectory that yields the minimum LCOG. Secondarily, the variations against the other potential solutions were analyzed to assess the impact of not achieving the optimal target. Preliminary analysis showed that several growth trajectories have a relatively similar LCOG compared to the optimal growth trajectory. It was also observed that, for each ESS capacity by 2031 (ESS_{2031}^{cap}), there is a local optimal value. Looking into the 100 samples with the lowest LCOG, it was also observed that the candidates have relatively similar growth trajectories. These trajectories with the lowest LCOG per ESS_{2031}^{cap} were selected as representatives, and a trend line was created using these values. The final goal of the economic optimization is the identification of the trajectory with the minimum LCOG as shown in (5.5). This goal is achieved at this stage by selecting the candidate trajectory with the lowest LCOG. The ESS

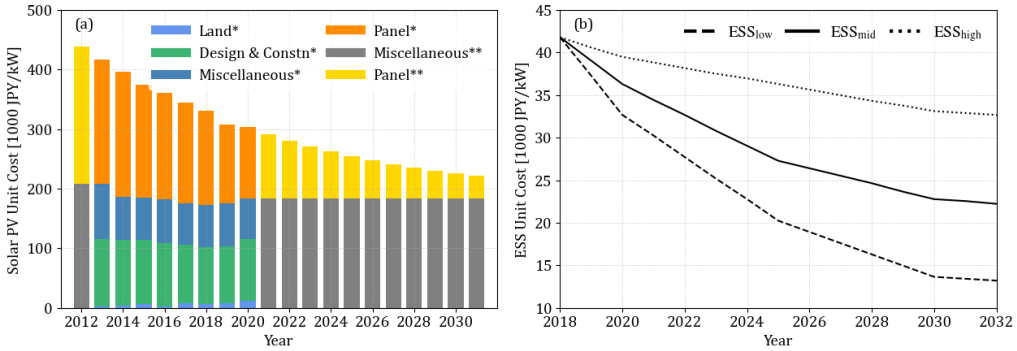

Figure 5.9: Cost projections for the unit cost of (a) solar PV and (b) ESS. In (a), * is the historical data from Japan's Ministry of Economy, Trade and Industry [108], where the unit cost is disaggregated into land, design and construction, miscellaneous, and panel price. For the projected values (labeled with **) from 2021 onwards, the land, design and construction, and miscellaneous fees (combined as miscellaneous **) were expected to have minor changes, while the solar panel would continuously decrease by 10% per year. The value for 2012 was also extrapolated since the available historical data started in 2013. (b) shows the cost projections of Cole and Frazier [99] for battery storage with three cost reduction scenarios.

capacity trajectory is considered the exogenous variable in this optimization since the model predetermines the other variables.

$$min\left(\mathrm{LCOG}_{y_R}^{PV+ESS}(Cap_{y_i,y_r}^{ESS})\right) \tag{5.5}$$

5.2.3 Analysis & Recommendation

Financial Sensitivity Analysis

A sensitivity analysis was conducted to assess the impact of the solar growth rate and ESS unit cost projection on the optimal growth trajectory. For PV, the growth rate was varied under the assumption that larger PV capacity leads to larger curtailment that will require more ESS. In the past three years, PV was increasing by around 1 GW, but it slowed down due to curtailment; thus, 800 MW/year was seen as the realistic case. However, it is ideal to reduce it further to 600 MW/year to slow down the curtailment rate. Consequently, maintaining the 1 GW/year growth is undesirable since it will have the reverse effect. For the ESS unit cost, the projections in Figure 5.9b were explored to test the robustness of the optimal growth trajectory against the unit cost of storage.

Impact on the Grid

The LCOG for the whole grid includes the other generators. These were treated as dispatchable generations, and the cost was calculated based on the generated amount and the estimated cost as seen in Table 5.4. It is assumed that there will be minor changes in the price of the other generators in the next decade.

Table 5.4: Cost of Electricity Generation [Yen/kWh]

Technology	METI 2014	METI 2030	MOFA 2018*	Applied**
Nuclear	10.1	10.1	-	10.1
Coal	12.3	12.9	6	12.3
LNG	13.7	13.4	10	13.7
Wind	21.9	13.9	10-22 (15)	17.9
Geothermal	19.2	19.2	-	19.2
Hydro	11.0	11.0	-	11
Biomass	12.6	13.3	-	12.6

* Values in parentheses are the average values
** Used in the calculation

For the CO_2 emission analysis, the study mainly focuses on the CO_2 emission from fuel consumption, which does not cover the CO_2 emission during the construction, maintenance, and disposal of the system. The calculation assumes that nuclear, geothermal, hydro, solar, and wind does not generate CO_2 and biomass has a net-zero CO_2 emission during electricity generation. According to Japan's Ministry of Environment [83], depending on the technology, coal and LNG has a CO_2 emission of 0.95 $kgCO_2$/kWh to 0.83 $kgCO_2$/kWh and 0.51 $kgCO_2$/kWh to 0.36 $kgCO_2$/kWh, respectively. The average emissions for coal (0.89 $kgCO_2$/kWh) and LNG (0.44 $kgCO_2$/kWh) were used in the analysis.

5.3 Results

5.3.1 Energy Change

Figure 5.10 shows the changes in the solar energy delivered to the grid. It can be seen that, aside from the stored solar, the delivered solar also increased because of the flexibility afforded by the storage. Similar to LNG, it is shown that storage can provide flexibility that could help reduce the ramp rate of the other energy sources. The figure also shows the energy loss due to the charging and discharging cycle (cycle loss), which increases as the amount of ESS capacity increases. The figure also served as a preliminary insight into the maximum ESS capacity for the simulation, since it shows that curtailment will become minimal once 80 GWh was reached.

5.3.2 Optimal Growth Trajectory

The initial exploration of the sampled growth trajectories showed that the first 100,000 samples have a marginal difference with the minimum LCOG. The calculation showed that, depending on the ESS capacity by 2031 (ESS^{cap}_{2031}), there is a growth trajectory that could yield a relatively similar LCOG, which shows that there is a range of acceptable growth trajectories. Figure 5.11a shows the 100 trajectories with the lowest LCOG for several ESS^{cap}_{2031} and it can be observed that, for ESS capacities greater than 15 GWh, the LCOG

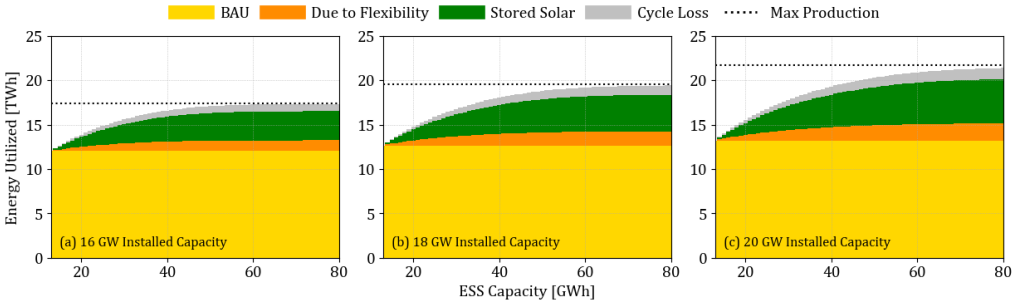

Figure 5.10: Changes in the total contribution of energy from the combined solar and ESS system.

of the trajectories are almost the same. The trajectories with the lowest LCOG for each ESS_{2031}^{cap} are also shown in the figure. Within this trend line, the optimal growth trajectory has the lowest LCOG and is marked as the minima.

Figure 5.11b shows the representative trajectories and the optimal growth trajectory, where it could be seen that the optimal growth trajectory follows an almost linear trend. The representative trajectories generally follow the optimal trajectory until the maximum ESS capacity for that trajectory is reached. The representative trajectories mainly follow the optimal path until it faces a restriction, which in this case is the maximum assigned capacity for that trajectory. The behavior signifies that the initial goal is to reach the optimal trajectory and retain that capacity until further funding is available. It also shows that investing higher than the optimal trajectory is counter-productive.

5.3.3 Sensitivity Analysis

The sensitivity of the LCOG and the optimal growth trajectory to the growth rate of solar and changes in ESS unit cost can be seen in Figure 5.12. As seen in Figure 5.12a, in all cases, the LCOG gradually decreases but the change for the $\mathrm{ESS}_{\mathrm{high}}$ is minimal. In contrast, the LCOG for the $\mathrm{ESS}_{\mathrm{low}}$ drops until it reaches 30 GWh. The minima for lower solar growth rate (e.g., PV_{600}) occurs earlier since there is less curtailment to store. On the other hand, since higher solar growth rates (e.g., PV_{1000}) lead to higher curtailment, the minima are higher since the utilization rate of the ESS remains high, even at these capacity ranges.

Cross-referencing with the corresponding growth trajectory of each minimum shown in Figure 5.12b, it can be seen that initially, the growth trajectory is the same, but it diverges around 2024. There are points of intersection for the growth rate, but the solar capacity and ESS cost significantly affect the slope of the growth trajectories. Figure 5.12b also shows that the trend flips around in 2023 and 2024. Initially, the optimal trend for $\mathrm{ESS}_{\mathrm{high}}$ is higher than the other cases, but its overall slope is less steep. In contrast, the other cases have lower initial values, but, given their higher slopes, these cases reached higher values by 2031. These trends show that, for instances where the cost reduction is minimal ($\mathrm{ESS}_{\mathrm{high}}$), it is best to invest early and immediately reduce the impact of curtailment. However, for instances where cost is seen to drastically reduce in the future ($\mathrm{ESS}_{\mathrm{low}}$), it is best to delay. It

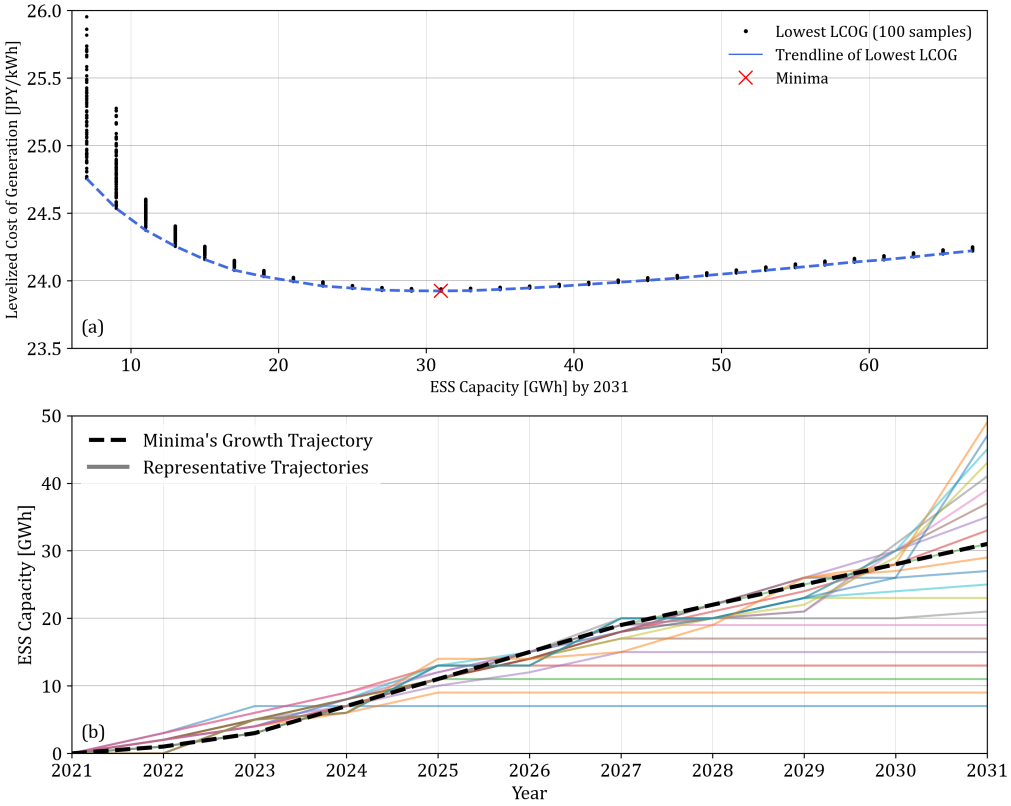

Figure 5.11: (a) Minimum LCOG per max ESS capacity in 2031. (b) Growth trajectory of the samples with the lowest LCOG sorted according to the ESS capacity by 2031 (ESS^{cap}_{2031}). In (**b**), the minima's (optimal) trajectory is shown as a dashed line and the representative trajectories are shown as faded solid lines.

can also be observed that higher solar capacity growth rates lead to higher required ESS since more curtailment should be recovered. This insight is already intuitive, but it is difficult to assess the capacity and duration of the delay. The optimal growth trajectory presents the capacity to be installed at the minimum to balance the loss and additional investment.

5.3.4 Impact on the Grid

The analysis of the impact on the grid focused on the average case using the optimal ESS capacity in Figure 5.12. Since the focus of the optimization is financial, there will still be some curtailment. However, as shown in Figure 5.13a, the curtailment rate, which is expected to increase continuously, could be kept at around 5–12% through the optimal growth trajectory. It can be observed that the curtailment rate immediately dropped to 12% for $\mathrm{ESS}_{\mathrm{high}}$ and remained there. In contrast, the curtailment rate gradually reduced to 5% in $\mathrm{ESS}_{\mathrm{low}}$ and settled there. This observation shows that (a) the lower the cost, the more curtailment can be absorbed and (b) the acceptable curtailment rate will depend on the cost of storage.

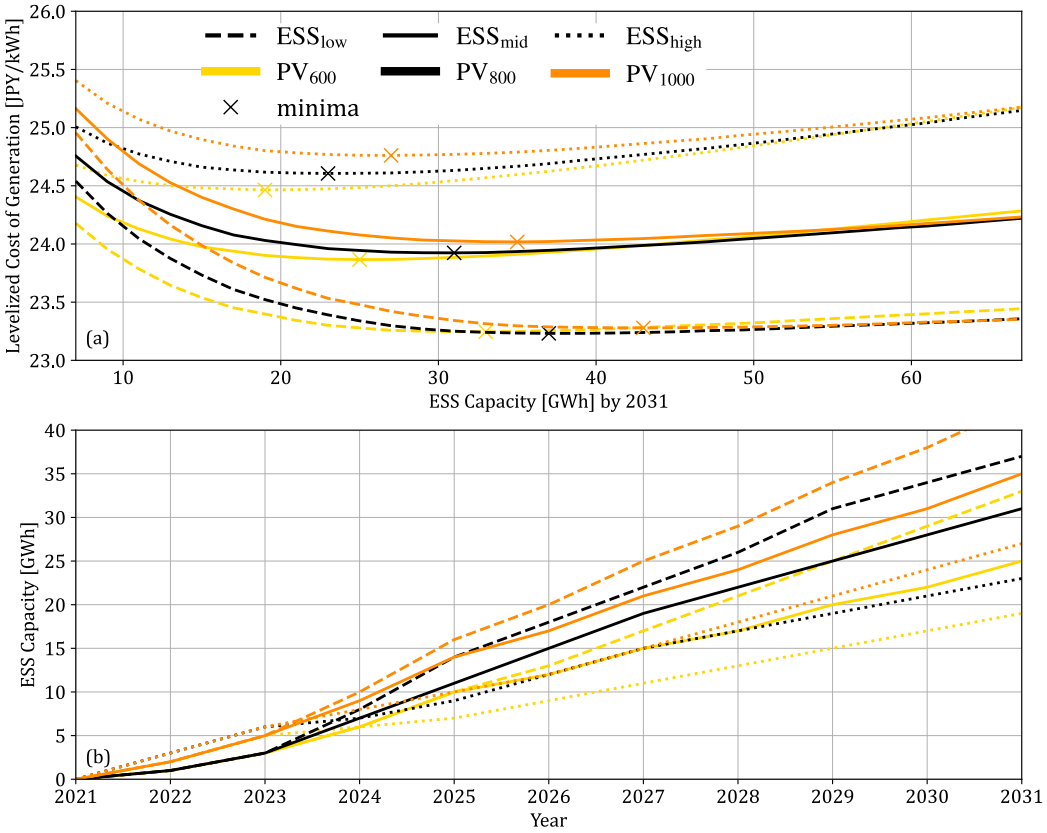

Figure 5.12: Impact of the solar capacity growth rate and ESS unit cost on (a) LCOG trend line and (b) the cost-optimal growth trajectory. Convention: the color of the line represents the solar capacity growth rate, while the line style represents the project ESS unit cost.

Figure 5.13b shows the annual LCOG using the optimal ESS growth trajectory. It can be seen that the ESS can reduce the curtailment penalty by up to 4–6 JPY/kWh by 2030. The annual LCOG trend follows the trend of the curtailment rate. The LCOG quickly dropped in $\mathrm{ESS}_{\mathrm{high}}$ and remained relatively high compared to the slower but continuous drop for $\mathrm{ESS}_{\mathrm{low}}$.

The total annual cost of electricity generation for the whole of Kyushu is shown in Figure 5.14a. Immediately, the impact of additional solar capacity on the annual generation cost is noticeable. It can be observed that, in all cost scenarios, additional storage was able to reduce the annual generation cost. Interestingly, the cost reduction for the three ESS cases is relatively similar. This observation shows that the optimization mainly focuses on the overall impact on the cost reduction. For $\mathrm{ESS}_{\mathrm{high}}$, the reduction to a 10% curtailment rate was sufficient to almost match the 5% reduction of $\mathrm{ESS}_{\mathrm{low}}$. However, it can be seen that the impact on the CO_2 emissions is more significant, as seen in Figure 5.14b. Intuitively, higher PV capacity will lead to lower emissions and, since the delivered solar could increase with the aid of ESS, the emissions decrease further. As previously highlighted in Figure 5.10, aside from the energy delivered through the ESS, the ESS also provides additional flexibility to the grid. These two benefits of ESS reduced the need to generate energy from coal, which leads to a

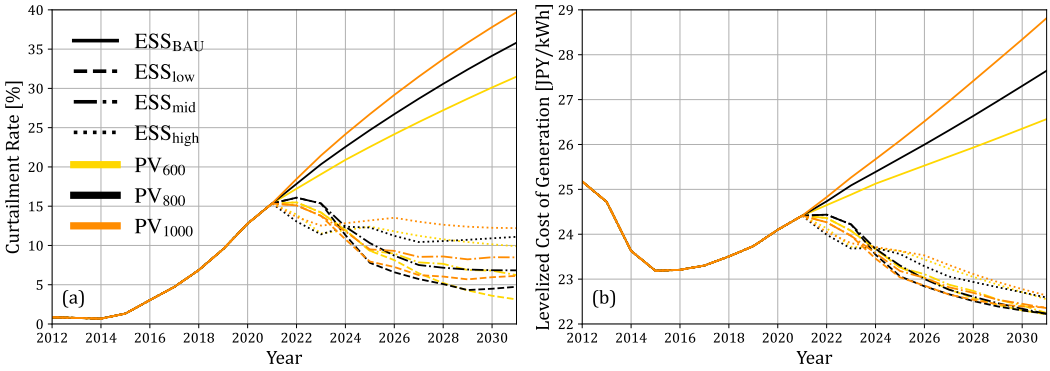

Figure 5.13: (a) Curtailment rate of solar and (b) Levelized Cost of Generation of the business as usual (BAU; no change in ESS capacity) and the optimal ESS scenario.

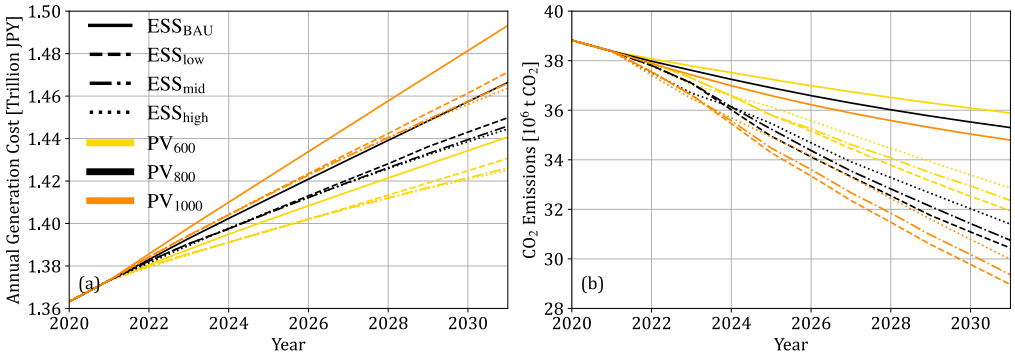

Figure 5.14: (a) Total annual cost and (b) CO_2 emissions of the electricity generation for the whole Kyushu grid of business as usual (BAU; no change in ESS capacity) and the optimal ESS scenario.

reduction of CO_2 emissions. With the help of ESS, 2–6 million tons of CO_2 could be avoided per year by 2030.

Finally, Figure 5.15 shows the relationship of the annual LCOG and the levelized CO_2 emissions. As previously highlighted, ESS could slightly reduce the LCOG, but it greatly helps in reducing the CO_2 emissions. By focusing only on solar, the levelized CO_2 emissions could go down to 0.3238–0.3342 kgCO_2/kWh, but with the aid of ESS, this could go down further to 0.2753–0.2825 kgCO_2/kWh. The figure also shows the complementary benefit for PV and ESS in reducing curtailment. A higher solar growth rate and lower ESS unit cost generally lead to lower CO_2 emissions, leading to higher costs. Therefore, a policy decision must be made to balance the power generation's economic and environmental impacts on the island.

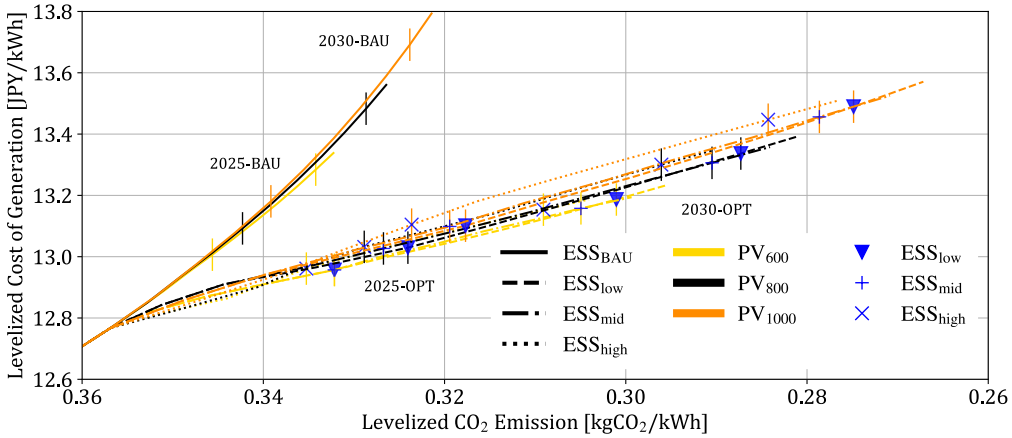

Figure 5.15: Ratio of the annual Levelized cost of generation and levelized CO_2 emissions for the various scenario. The CO_2 emissions (abscissa) are formatted in decreasing order to emphasize the trend. The additional blue markers show the values for 2025 and 2030 for the different scenarios.

5.4 Discussion

5.4.1 Ensuring Continuous Competitiveness of Solar

Curtailment is inevitable under high PV penetration; thus, additional precautions and planning are necessary to minimize its economic impact, which might hinder further deployment of PV. The results show a cost-optimal storage capacity that could reduce the curtailment rate to acceptable levels. Furthermore, results show that there is an optimal growth trajectory for reaching the optimal capacity. By following this growth trajectory, the curtailment rate, which grows larger and larger as the PV penetration rate increases, could be reduced to around 5–10%. Since the optimization focuses on the financial objective, the 5–10% curtailment rate seems acceptable and should be part of the initial cost calculation for new projects. Beyond this curtailment rate, it is financially sound to invest in ESS.

5.4.2 Solar Energy and Its Impact on CO_2 Emissions

The results also show that, although solar alone can reduce CO_2 emissions, curtailment hinders it from having a more significant impact since the effective delivered energy is reduced. With the aid of ESS, the delivered energy increases and solar could help in reducing CO_2 emissions by displacing coal. The results emphasized that ESS was also able to provide additional flexibility that enabled direct solar utilization. The flexibility of the grid is vital for solar energy since it is a variable source of energy. It is also essential that ESS can provide this since the charging and discharging cycle introduces energy loss, reducing the total delivered solar energy. Furthermore, it is essential to highlight that these additional CO_2 emissions were achieved with a lower annual generation cost.

5.4.3 Important of Investment's Timing

The results highlighted the importance of investment timing. As solar capacity grows, so does the expected curtailment, and with it, the need for additional ESS capacity. The analysis explored several logarithmic, linear and exponential growth strategies, and the results show that a gradual increase is still the cost-optimal approach rather than a sudden followed by a slow installation (logarithmic) or a slow followed by a sudden installation (exponential). Hypothetically, the logarithmic growth could be beneficial if the grid is severely lacking in ESS capacity. Nonetheless, it should grow until reaching optimal capacity, following the optimal growth trajectory, and continue a linear growth afterwards. On the other hand, exponential growth might be beneficial if a sudden price drop is anticipated in the future. However, as shown in this study, if the curtailment rate is not yet severe and the price decrease of ESS is gradual per year, then a gradual increase is the financially sound decision.

5.4.4 Deployment Responsibility

As shown in the optimal growth trajectory, the ESS capacity should be increased by around 30 GWh within the next 10 years to minimize the curtailment cost penalty. This study is limited by the assumption that the whole system will share the benefit of ensuring the competitiveness of solar energy. Further study is necessary to understand the responsibility of the government and existing market players in ensuring the viability of future solar and storage investments. The support given to initial solar investors should also be given to storage investors. The situation of new solar investors should also be considered since they will be more affected by the curtailment because they are entering the market at a point when curtailment is already expected. One potential solution would be to encourage new solar investors to include storage into their system by providing more subsidies or incentives to complementary solar storage plants.

5.4.5 Implications for Other Isolated Grids

Kyushu's 2 GW transmission line to the rest of Japan is insufficient for solving the curtailment problem in the region. Therefore, Kyushu could represent island nations with isolated electrical grids such as the Philippines, Indonesia, and Hawaii. The results in this study have shown that curtailment will drastically increase the cost of solar once the curtailment rate reaches 10%, and storage should be strongly considered to mitigate its financial impacts. This insight could serve as a precaution for energy planners since ESS represents an additional investment, which could be prevented by limiting the capacity of solar generation. This approach might be counter-intuitive in the effort to green the grid, but it is crucial to prevent wastage of solar energy, as it impacts its profitability.

However, it should be noted that the difference in solar irradiation and demand profiles have a huge impact on the cost of solar generation. For instance, the Philippines and Indonesia have minor variations in temperature, which could result in stable demand. Both countries also have higher solar irradiance that could offset some of the losses. The proposed cost-optimal storage capacity assessment methodology could be adapted for these territories since the storage cost and installed solar capacity are barely affected by changes in territory.

5.4.6 Importance and Limitation of the Proposed Approach

The proposed cost-optimal storage capacity assessment revealed the ESS growth trajectory that could minimize the cost of electricity generation from the combined PV and ESS system. Since there are a lot of potential growth paths, the computational requirements are enormous. A significant number of samples were used to find the optimal growth trajectory through the Monte Carlo random sampling approach. The proposed formulation for the LCOG was able to calculate the cost of generation as time progresses, as it is geared towards the actual generation per year. In contrast, the standard LCOE mainly focuses on the lifetime of the project. Through the LCOG, the growth trajectory was analyzed to find the set of cost-optimal growth trajectories.

Since the approach optimizes a certain planning horizon, it is only optimal within that period. It does not look further beyond this period. A longer planning horizon could be explored, but this will further increase the computational requirement. One way to handle this is to reduce the yearly intervals and assume minor changes within 2–3 years. By reducing the intervals, the analysis could also be used for 20–30 years. It might not be logical to increase this further since the difference in installed capacity beyond three years could significantly impact the results.

5.5 Conclusion

The proposed cost-optimal storage capacity assessment was able to identify the complementary ESS growth trajectory that could support rapid PV capacity growth. By separating the optimization process into a two-step process, the first step ensured that the optimization is technically viable, while the second step identified the ESS growth trajectory with the lowest generation cost. Levelized Cost of Generation (LCOG) was introduced as it could provide the ability to tackle the time-bound optimization of the installed storage capacity. The cost-optimal ESS growth trajectory has the lowest LCOG within the planning horizon. The incorporation of the Monte Carlo sampling significantly reduced the computational requirements of the analysis while ensuring the appropriate representation of the growth paths. In addition, the proposed LCOG calculation was able to incorporate the gradual growth of PV capacity and the changes in the cost, which enabled the optimization within the planning horizon. The results showed that there could be several paths to follow in installing ESS, but there is an optimum growth trajectory that could minimize the generation

cost. Regardless of the existing storage capacity, the results showed that the complementary capacity should rapidly increase until the optimal growth trajectory and then continuously follow the trajectory. Investing higher capacity reduces the utilization rate of the ESS, which leads to higher LCOG. The approach effectively identified the appropriate amount and timing for the storage capacity, thereby reducing early or delayed investment repercussions. These insights are essential considerations for energy planners and other stakeholders as it provides target values for each year.

As intended, following the optimal growth trajectory resulted in a decrease in curtailment; however, from a financial perspective, eliminating curtailment is infeasible. In Kyushu's case, the results show that the curtailment could be reduced to around 5–12% by following the optimal growth trajectory. The Levelized CO_2 emissions could decrease from 0.3238–0.3342 $kgCO_2$/kWh with only PV, to 0.2753–0.2825 $kgCO_2$/kWh with PV and ESS, by 2030. These results show that once curtailment reaches more than 10%, to maximize solar PV's potential in reducing CO_2 emissions, storage must be included in the energy transition plan. The proposed approach can help identify the optimal ESS growth trajectory, which could balance the acceptance of a certain percentage of solar energy wasted as curtailment and investment in ESS to absorb the curtailment.

Since the proposed approach mainly depends on the hourly simulation, it could be replicated in other territories, provided that the hourly data on demand and solar generation are available. Storage will be crucial in ensuring the competitiveness of solar, especially in isolated territories such as the Philippines, Indonesia, and Hawaii. The approach presented in this study could be used to evaluate the growth trajectories for these territories as well.

6 Impact Assessment of Electric Vehicles as Curtailment Mitigating Mobile Storage

The contents of this chapter is based on Dumlao, S. M. G., & Ishihara, K. N. (2021). Impact Assessment of Electric Vehicles as Curtailment Mitigating Mobile Storage in High PV Penetration Grid. Energy Reports, 8 (Special Issue: CPESE 2021), pg 736–744. doi: https://doi.org/10.1016/j.egyr.2021.11.223.

6.1 Introduction

6.1.1 Electric vehicles and the energy transition

Due to the CO2 emissions that cause global warming, several efforts are ongoing to reduce the world's dependence on fossil fuels. Reducing fossil fuel dependence will require the conversion of traditional technology to electricity-based technology that uses clean electricity. Electric vehicles (EVs) are seen as a potential solution in reducing the fossil fuel dependence of the transport sector and could also serve as secondary storage for renewable energy. In the US, it is estimated that vehicles are on the road only around 5% of the day on average and that at least 90% of personal vehicles are parked even during peak traffic hours [109]. At the same time, EVs are not considered as critical load, and the charging time could be deferred making it controllable from the perspective of system operators [110]. By discharging its stored energy during peak demand, EVs could also help in reducing peak demand [111], thereby reducing the need for additional thermal plants.

Kempton and Tomic [109] outlined that electricity in the grid generally falls under four categories, namely: baseload power, peak power, regulation, and spinning reserves. They focused on using EVs as spinning reserve because the batteries are paid for many hours as reserves but only utilized in short periods. Kempton and Kubo [111] utilized EV as peak power since the EVs' availability and Japan's peak demand matches. Initially, EVs could be tapped as regulation and spinning reserve, but as these markets become saturated, EVs can

transition to serve as storage for renewable energy generation [112]. EVs have the potential to support the electricity grid; however, there is a recent shift in demand for EVs as storage. In the previous decade, the focus is more on supporting the stability and reliability of the grid, but the recent increase in penetration of renewable energy merits using EV as storage. Transmission lines could also help by sending excess electricity to neighboring regions. However, since this will be difficult for grid-isolated islands like Ireland and fragmented grids like Australia, EVs as storage is a suitable alternative [112].

There are three strategies in utilizing EV as grid support or supplement, namely: (a) increase the available storage capacity of the vehicle, (b) schedule the connection time of the EV fleets, and (c) use intelligent controls [112]. The first option will incur additional cost and weight to the vehicle. The second entails consistent coordination with the fleet but will allow predictability. The last strategy will require additional communication infrastructure to control the fleet automatically. Although intelligent control might provide the most efficient use of the EV fleet, the added infrastructure will take further planning and additional cost. Nonetheless, EV has a clear potential in supporting the electricity grid of regions with high PV penetration.

6.1.2 Japan's situation

Kyushu has around 7.20 million passenger vehicles as of early 2021, divided into 1.95 million, 2.0 million, and 3.25 million standard, small, and mini cars, respectively [113]. On average, there were 250,000 newly registered cars in the past five years at a replacement rate of 3.5% per year [113]. Historical data shows that, although the number of cars is increasing, it is increasing at an average rate of less than 1% per year. These data show that the number of cars in Kyushu is stable. This large volume of cars presents itself as a potential solution to curtailment if a portion of these cars is converted to EVs. Furthermore, since Japan uses their cars less frequently than other industrialized countries, EVs have the potential to serve as additional storage [111].

According to the published data for 2020 by Japan Automobile Dealer Association [114], the local brands Mitsubishi and Nissan are the leading electric vehicle brands in Japan with a market share of 0.5% and 79.5%. Imports, which are generally assumed to be Tesla cars, command the remaining 20%. For this study, standard, and small, and mini cars will be treated as class A, B, and C, respectively. Table 6.1 summarizes the specification of the popular EVs in Japan [115] that fit into the identified classes and are also part of the list of subsidized EVs in the country [116]. The Tesla models represent class A with a capacity of 100 kWh. Nissan Leaf and Nissan e+ represent two possible class B EV alternatives, while Mitsubishi i-Miev represents class C.

Table 6.1: Popular electric vehicles in Japan

	Capacity (Adult)	Total energy storage (kWh)	Usable Energy (kWh)	Depth of discharge (%)	Vehicle range (km)	Consumption (wh/km)	Efficiency (km/kWh)	Normal Charge* (hours)	Quick Charge** (minutes)
Tesla Model S	5	100	95.0	0.95	525	181	5.25	15.0	65
Tesla Model X	7	100	95.0	0.95	507	187	5.35	15.0	65
Nissan Leaf	5	40	36.0	0.90	270	133	7.52	6.5	40
Nissan Leaf e+	5	62	56.0	0.90	385	145	6.90	10.0	62
Mitsubishi i-MiEV	7	16	14.5	0.90	85	171	5.86	5.0	21

Summarized specification from [115]; *using 7.4kW/hour; **75kW/hour DC for Tesla, and 50kW/hour DC for Nissan and Mitsubishi

6.1.3 Objective

Clearly, EVs can reduce curtailment by acting as mobile storage, and there are instances where cars are used seldomly. These EVs could be a solution to the increasing curtailment problem in electricity grids with high PV penetration. However, the required number of EVs necessary to significantly reduce curtailment and their corresponding impact is not yet fully explored. Therefore, this study aims to clarify the potential role of EVs in managing curtailment in electricity grids with high PV penetration. An energy balance analysis that focuses on the gradual growth of solar capacity and electric vehicle adoption will be conducted to assess the impact of utilizing electric vehicles as mobile storage to mitigate curtailment. Several target growth rates will be explored to estimate the volume of electric vehicles that could support the electricity grid and the corresponding impact on reducing curtailment. The Kyushu region in Japan was used as a case study since it continuously increases its solar capacity and is at the precipice of high PV curtailment scenario.

6.2 Methodology

6.2.1 Data

The energy data were collected from Kyushu Electric Company, where the hourly information about generation, transmission, and demand is published since April 2016 [36]. The data has hourly information regarding the supply and demand in the region. The information also includes curtailment for both solar and wind. Transmission and Pump Hydro Energy Storage (PHES) could be positive or negative. For transmission, negative values represent energy export while positive values indicate electricity import. For PHES, negative and positive values represent the charging and generation phases, respectively. For this study, the transmission is also considered as part of the total load. Pumped hydro storage is seen as both generator and load. Although the baseload generators (nuclear, geothermal, and biomass) could change within the year, the baseload was fixed to its maximum capacity. This study uses the 2018 energy balance data since curtailment began occurring in this particular year.

The statistical data about vehicles used in this study were gathered from Japanese websites. The overall passenger data came from Kyushu Transport Bureau under the Ministry of Land, Infrastructure, Transport, and Tourism. The number of vehicles owned and newly registered vehicles are updated every month since April 2013 [113]. Next Generation Vehicle Promotion Center (NeV) publishes the number of EV subsidy grants by prefecture from 2009 [117]. The number of grants per prefecture was used to calculate the EV penetration scenarios since it was assumed that all EVs currently get a subsidy. The center also published reports that outline trends and efforts for promoting "Next Generation" vehicles in Japan [116] and includes subsidy calculations and lists of subsidized vehicles in Japan.

Data regarding the market share of EV was gathered from the website of Japan Automobile Dealers Association (JADA) [114], where monthly purchases are outlined for each fuel type. The data is only available from January 2019. Using the list from JADA [114], the specifications of popular EVs in Japan were gathered from the EV Database [115]. The organization is entirely independent from the car industry and aims to published real-world data along with the laboratory test data from the car manufacturers.

6.2.2 Simulation tool and assumptions

The hourly energy balance simulation used the Python for Power System Analysis (PyPSA) Modelling Framework [53]. In the simulation, Kyushu was modeled with a single main bus (B0) with sub-buses (B1 and B2), as seen in 6.1. The energy demand of Kyushu, transmission to other regions, and coal generation are directly connected to the main bus B0. This configuration prevents coal from charging either the PHES or the additional EV storage. Sub-bus B1 connects the rest of the traditional generators, hydropower, and wind to the PHES, which allows the PHES to charge from these sources when necessary. This connection was necessary since historical data showed that there were instances when PHES charged from the traditional sources. Sub-bus B2 connects the solar generator to the PHES and the additional EV storage. B2 essentially isolates the EV storage from the other generators; thus, it can only charge from the excess energy. The discharge for both the PHES and EV goes directly to the main bus B0 to prevent loopback charging. The assigned capacity uses the latest generator data, which was explained in detail in Chapter 5.

The solar capacity is treated as a controlled variable, but the increments were based on the projected capacity growth in the region. In Chapter 5, it was discussed that as of 2021, the PV capacity in the region is 10 GW, which could increase by 600 MW, 800 MW, or 1000 MW depending on various issues in the region.

6.2.3 Logistics growth model

The logistics growth model is used to project the growth of EV. The formulation seen in 6.1 shows the exponential growth part and the dampening component that takes into consideration the ceiling of the growth. The logistic growth model is the solution to the

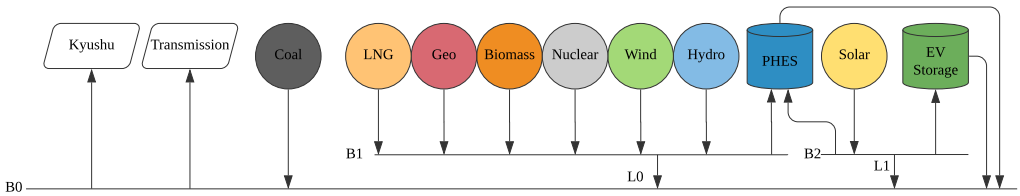

Figure 6.1: Configuration of the grid used in the simulation.

differential equation, and several variations are used in practice. In this study, 6.2 is mainly used to keep track of the values of N_0 and t_0. N_0 represents the initial number of the population at $t = 0$ while t_0 provides the absolute 0 for the time components, which are, in the case of this study, in years. These two values are essential in ensuring that the fitted coefficients are realistic. Exisitng EV data from 2008 until 2019 were fitted into the logistic growth model along with the target values for 2031. The maximum EV population was assumed to be 6 million cars.

$$\frac{dN\left(t\right)}{dt} = rN\left(t\right) \cdot \left(1 - \frac{N\left(t\right)}{M}\right) \tag{6.1}$$

$$N\left(t\right) = \frac{M}{1 + \left(\frac{M}{N_0} - 1\right) e^{-r(t-t_0)}} \tag{6.2}$$

$N(t)$ refers to the population at t; N_0refers to the population at $t = 0$; M is the maximum population; r is the rate of increase; t is the time period; t_0 is the time offset.

6.3 Results and Discussion

6.3.1 Energy balance by 2031

Figure 6.2 shows the impact of mobile storage capacity on the curtailment rate and penetration rate. Immediately, the impact of the approach on the solar capacity growth can be seen in Figure 6.2 (a) since higher PV capacity leads to a higher curtailment rate. Furthermore, the capacity of storage in reducing curtailment suffers. It could be seen that the curtailment reduction already plateaued near 10% for the 20 GW solar capacity scenario, whereas it could be reduced below 5% if the solar capacity by 2031 is reduced to 16 GW. However, as seen in Figure 6.2 (b), a higher PV capacity target will lead to higher solar penetration. Nonetheless, even for the penetration rate, it could be observed that the benefit of having more storage plateaus around 20 GWh storage capacity. Beyond this, there is a marginal increase in the benefit. Upon closer inspection, it could be seen that the lower the solar capacity, the impact of storage plateaus faster. For the 16 GW solar capacity, it already

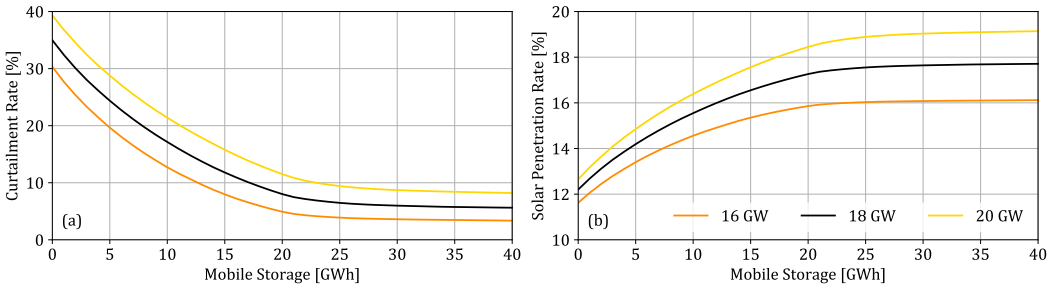

Figure 6.2: Impact of the mobile storage capacity on curtailment rate (a) and penetration rate (b) for various solar PV capacity scenario by 2031.

plateaued near 20 GWh while there is still some residual benefit for the 20 GW solar capacity until around 30 GWh storage capacity.

The plateaued impact of storage on the curtailment rate and solar penetration rate can be explained through Figure 6.3 and Figure 6.4. As seen in the energy balance, for the 16 GW solar + 20 GWh storage seen in Figure 6.3, most of the curtailment was already absorbed by the PHES and EV storage. It is noticeable that the additional storage is beneficial primarily during the spring and autumn season since the PHES is sufficient in absorbing the curtailment during winter and summer periods. However, if the region decided to increase the solar capacity target by 2031, Figure 6.4 shows that 20 GWh is still sufficient in handling most of the curtailment. Higher curtailment could be expected in the summer, and the additional EV storage will now be utilized. The residual curtailment increased in the spring, and the combined PHES and EV are insufficient in preventing curtailment during autumn. Nonetheless, this also shows that increasing the capacity beyond 20 GWh will only be beneficial during spring and autumn. Based on the decrease in curtailment shown in Figure 6.2 (a), additional capacity will have a minor impact on the overall curtailment. The capacity factor of the additional storage will be minimal to merit an increase in the target storage capacity.

6.3.2 Electric vehicles' potential mobile storage capacity and target growth rates

Based on the energy balance analysis, 20 GWh seems to be the ideal additional storage capacity by 2031. Table 6.2 estimates the required number of cars needed to achieve 20 GWh storage using various combinations of EV classes. The calculation assumed that only 70% of the rated storage could be used for grid storage to ensure that the cars are still usable for emergency situations. The data shows that around 300,000 cars would be needed if Scenario 1 is adopted. In this scenario, additional effort is needed to encourage more consumers to purchase class A. This scenario might be possible since the share of class A is increasing while class B is decreasing in Kyushu [113]. The required volume increases to around 420,000 cars for Scenario 2, which was adapted from the share of EV sales in 2020. In Scenario 3, the current passenger class combination is followed, where there

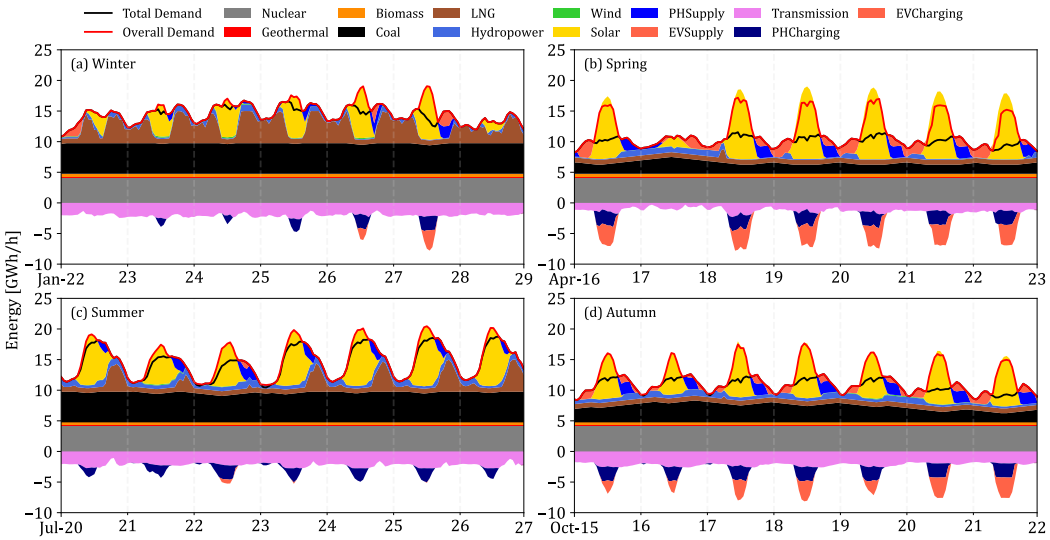

Figure 6.3: Energy balance for the 16 GW solar capacity with 20 GWh mobile storage capacity scenario. The area graph represents the cumulative energy generation in the region where the values above zero represent the power generation while values below zero represent the additional demand due to transmission and the charging of the PHES and EV. Curtailment occurs when the overall demand is lower than the generation.

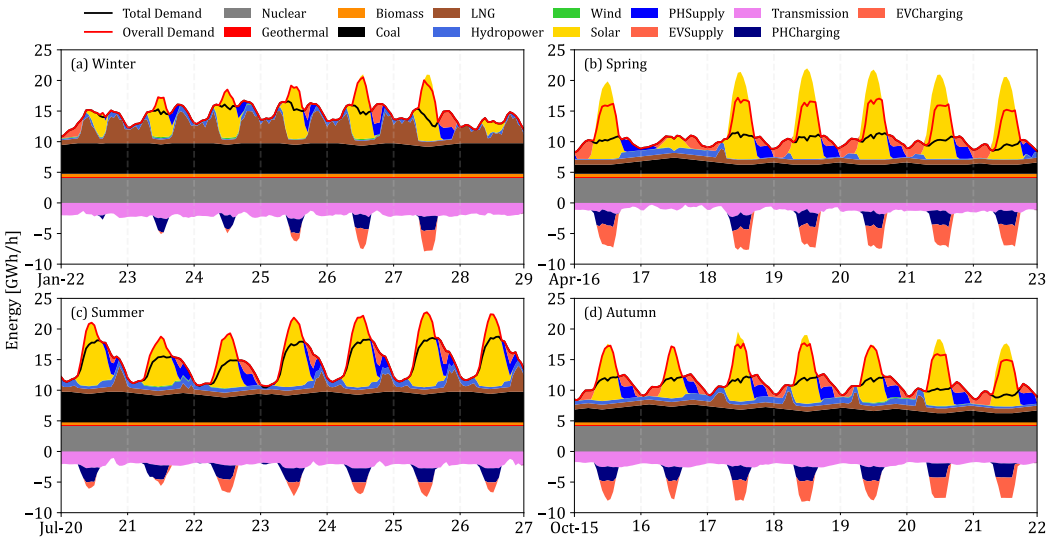

Figure 6.4: Energy balance for the 20 GW solar capacity with 20 GWh mobile storage capacity scenario. The area graph represents the cumulative energy generation in the region where the values above zero represent the power generation while values below zero represent the additional demand due to transmission and the charging of the PHES and EV. Curtailment occurs when the overall demand is lower than the generation.

is a significant number of class C cars. However, since class C EVs only have 16 kWh of storage, the required volume increased to around 570,000 cars. The target volumes in all scenarios are reasonable since it is less than 10% of the 7.2 million passenger cars in Kyushu, but achieving the value will depend on the capacity of the region to replace its passenger vehicles.

Table 6.2: Estimated Target EV fleet volume needed to achieve 20 GWh of Mobile Storage

Scenario	EV Class Combination [%]			Weighted Ave (kWh)	Target Vol (units)
	A (100 kWh)	B (60kWh)	C (16kWh)		
S1	90	10	-	67.20	297619
S2	20	80	-	47.60	420168
S3	25	30	45	35.14	569152

Based on the estimates in Table 6.2, the following are the initial target volume: (a) 300,000, (b) 420,000, and (c) 570,000. The logistics curve was fitted to reach these values by 2031. As seen in Figure 6.5 (a), higher targets resulted in steeper curves, but based on these values, it can be seen that most of the targets are within the Kyushu region's replacement capacity of 250,000 cars per year. These target values suggest that even with the usual replacement rate in the region, if people are encouraged to purchase electric vehicles rather than the conventional combustion engine, then the goal by 2031 is realistically achievable. However, based on the Business-as-Usual (BAU) growth, these targets are unachievable without external support. The closest target to BAU is 300,000 cars by 2031, which is only achievable if more people buy class A EVs. Therefore, this target requires more support to convince consumers. The most realistic target would be the 420,000 cars by 2031, where class B EVs are composed of 60 kWh EVs. Since the newer Nissan leaf e+ has a capacity of 60kWh, this target can be achieved realistically. Nonetheless, this would require around twice the replacement rate in contrast to BAU, as seen in Figure 6.5 (b). Utilizing class C EVs drastically increased the target growth per year. However, since these are smaller vehicles, it might be easier to support them financially since the cost of class C EVs, like the Mitsubishi i-Miev, is lower than the Tesla and Nissan alternatives.

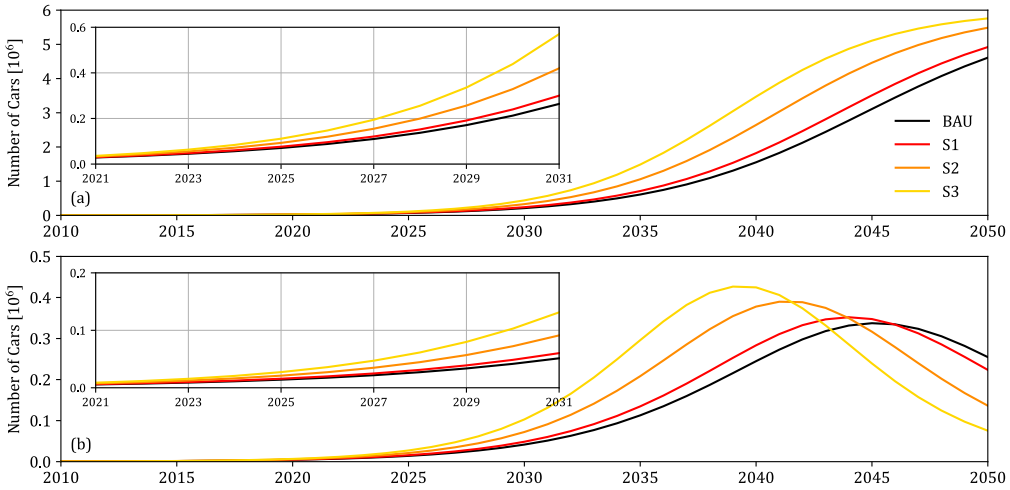

Figure 6.5: Total volume of electric vehicles (a) and annual increase (b) to reach several target volumes of electric vehicle by 2031. The insets for both subplots show the specific period under study from 2021 until 2031. S1, S2, and S3 refers to the scenarios listed in Table 6.2.

6.3.3 Electric vehicles' gradual impact on reducing curtailment

It can be seen in Figure 6.6 that using EV as mobile storage could keep the curtailment below 15%. In the "No EV Contract" scenario, the grid depends on the existing PHES to store excess solar energy, and the curtailment could already reach 20%–25% by 2025. By contracting the existing EV fleet in 2021, the curtailment could already be reduced to 10% from 15% in 2021. The curtailment in 2025 could be reduced to 10%–15%. As the PV capacity increases, the curtailment rate increases with it. Since the initial growth of EVs is slow, the curtailment still increased until 2027. At this point, EV's growth was able to catch up and reduce the curtailment to 8% and 12% by 2029 for the 600 MW/year and 1000 MW/year PV growth scenarios, respectively. Maximum benefit can be seen by 2031. Despite the increase in curtailment before 2027, the figure shows that the EV storage could still reduce the curtailment to under 15%, which is acceptable during the transition phase. This observation suggests that even with the gradual increase following the target EV volume growth rate, EV can help reduce curtailment prior to achieving the target volume.

As initially anticipated, the impact of the PV capacity growth rate has a significant impact on the curtailment rate. Even with the target values for 1000 MW/year PV growth scenario, the curtailment rate still reached 15%. Therefore, if EV mobile storage is explored, it might be best to stall the additional PV capacity until the EV volume can support higher PV capacity. For example, it might best to follow 600 MW/year PV growth scenario until 2027 and then increase it to 1000 MW/year. This proposition has the potential to maintain the curtailment rate below 10%.

The energy balance shown in Figure 6.3 and Figure 6.4 also highlight that the EVs are not necessarily connected all the time. EV as storage is primarily helpful during the spring and autumn season. This phenomenon should be taken into consideration when drafting the contract with the EV owners. It could provide additional flexibility to owners and grid operators. At the same time, the contract could be created to ensure that a certain portion of the fleet is connected when curtailment is anticipated. However, it is also possible that

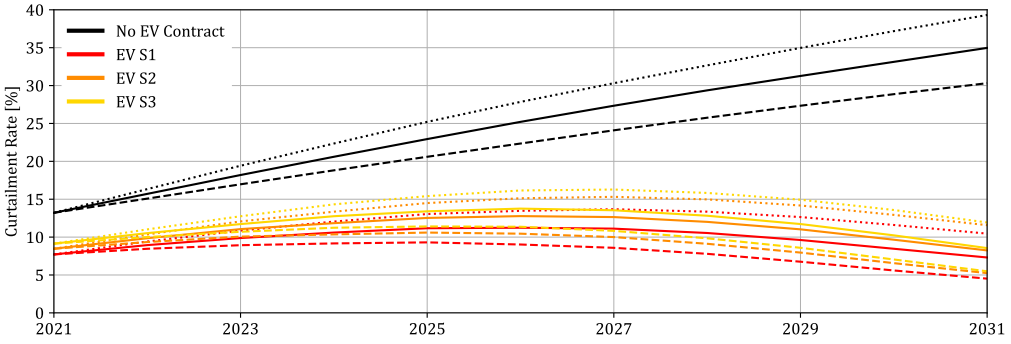

Figure 6.6: Progression of the curtailment reduction. The initial drop between the "No EV Contract" and the EV growth scenarios (EV S1, EV S2, and EV S3) was the result of contracting the existing EV fleet in 2021 as mobile storage. The dotted, solid, and dashed lines refer to 1000 MW, 800 MW, and 6000 MW PV capacity growth per year, respectively, which are the potential growth depending on various issues in the region.

only a fraction of the EV fleet is willing to be grid-connected; thus, the targets in this study should be interpreted as those willing to participate in the contract.

6.4 Conclusion

In this study, it was shown that EVs as mobile storage could significantly reduce curtailment. In the case of Kyushu, it will take 300,000 to 570,000 EVs to keep the curtailment to around 10%–15% in the next ten years. This volume represents less than 10% of Kyushu's 7.2 million passenger cars, but the current adoption rate of EVs is insufficient to reach these targets; thus, external support is necessary. Since the initial growth rate of EV is slow, it might be best to stall or reduce the PV installation rate until sufficient EV capacity is reached. For example, it was determined that it might be best to reduce the additional PV installation to 600 MW per year until 2027 to enable the EV storage capacity to catch up. After which, even with 1 GW per year, EV could keep the curtailment rate below 10%. EV mobile storage, or energy storage in general, cannot completely eliminate curtailment since it will suffer from low capacity factor, which will make it less economical. For the remaining curtailment, seasonal alternatives must be explored. This study clarified the impact of EVs as mobile storage. EV as storage is ideal for regions experiencing curtailment due to mismatch of supply and demand, and car owners seldomly use their cars. The latter condition occurs when there are alternatives sufficient for typical daily tasks and cars become necessary only for particular activities.

7 Pareto-Optimal Genetic Algorithm for Hydrogen Technology Adoption

7.1 Introduction

7.1.1 Hydrogen as a Long-term Chemical Storage

Chemical energy storage covers technologies where electrical energy produces chemical compounds that could later generate electricity [88]. Electricity can be stored through the production of gas or liquid that could later be used for energy generation or direct utilization [90]. Since chemical storage such as hydrogen, ammonia, and methane are highly dense storage options [90], these have been considered as Power-to-Fuel options that could support the electricity grid decarbonization efforts [118]. Chemical storage is also seen as a necessary support infrastructure that will enable more renewable energy into the grid [119]. The production plant for chemical energy storage is often separate from the generation plant and the chemical could be store in facilities that could be in a completely separate location. Such characteristics show that infrastructure surrounding chemical storage could easily be separated, leading to both positive and negative results.

As a chemical storage, hydrogen has the potential to replace fossil fuel energy sources since it has high energy density and could be used in power plants, transportation, and industrial feedstock. It could also be generated using electricity and, by extension, through renewable energy. Therefore, it could also serve as additional energy demand for excess RE. However, hydrogen production through electricity is still expensive. Producing hydrogen using only excess RE further increases its production cost as it reduces the capacity factor of the electrolyzer. Nonetheless, the continuous increase of renewable energy in the energy grid has lead to some changes in the energy market. Prices tend to go down during peak production of wind and solar, especially in instances where the demand is misaligned with the supply.

Electrolysis is the process of spitting H_20 into H_2 and O_2 molecules with the use of electricity [120]. Hydrogen produced through electrolysis solely from renewable energy such as wind, solar PV, and sometimes geothermal and nuclear energy is called green hydrogen. However, the production cost of green hydrogen remains to be high. The major drawback of green hydrogen production is the low capacity factor of the electrolyzer [121]. To improve

the capacity factor, it has been suggested that electricity from the grid should be used to augment the electricity produced by renewable energy [122]. However, home-grown hydrogen production might not be sufficient for major economies like Europe and Japan, and these economies will simply import green hydrogen from regions with abundant renewables, and this might cause new dependencies between states [123]. Japan has already started to make procurement deals with Australia, Brunei, Norway, and Saudi Arabia [124].

Fonseca et al. [125] summarized the characteristics and challenges of hydrogen production in their systematic literature review about hydrogen design trends. They concluded that there is a focus on using hydrogen as a storage medium to mitigate the risk in renewable energy. There are also efforts to push hydrogen for other use, such as fuel in cars, broilers, and power plants, which could help induce the hydrogen economy. A case study in Germany showed that establishing the hydrogen infrastructure might be demanding but reasonable if the transportation and chemical industry are included in the discussion [126].

Although hydrogen might replace LNG in the power plants in the future, Al-Kuwari and Schönfisch argues that the demand for LNG will remain the same as it will be used to generate low-carbon hydrogen through [127]. This might not be far from the reality since today's hydrogen production is still dominated by fossil fuels, and most companies are hedging on CCUS technology [123].

7.1.2 Multi-objective Optimization

Multi-objective problems that consider several factors might not have a single best solution, but rather, a set of potential solutions [128]. A solution good for one function may be inappropriate for another function, which makes it difficult to search for a solution that satisfies or optimizes all the objective functions [129]. Furthermore, it could also be possible that several unknowns surrounding the analysis. This situation merits the exploration of several combinations for the solution.

To arrive at a working solution for a real world multi-objective problem, trade-off methods such as priori methods, interactive methods, Pareto-dominated methods are utilized [129]. Priori methods typically involve an iterative process of assigning weights to each objective function in accordance with its importance or preference to the designer [130]. This approach is sensitive to the assigned weights and requires the user to have a reasonable insight into the problem. In the interactive method, the solution process is also iterative, but within each iteration, there are steps where some information is shown to the decision-maker to ask for preference [131]. The information provided during the "interactive" parts provides the optimal solutions. In Pareto-dominated methods, a set of solutions called the pareto optimal front is calculated by identifying the nondominated solutions. A solution x_1 dominates another solution x_2 if x_1 is better than x_2 in at least one objective while not worse than x_2 in any other objectives [132]. A solution X is said to be a nondominated solution if there are no other solutions that dominate X [132]. In this study, the concept of Pareto optimal front was preferred over the prior and interactive methods since this method

provides a set of solutions that could provide additional insights into the energy transition for hydrogen adaption.

Genetic algorithm is a well-known algorithm, which mimics the Darwinian theory of survival of the fittest in nature [133]. It uses chromosomes to represent potential solutions, a biologically inspired operator to change parts some of the characteristics of the previous generation, and a fitness selection to identify parts of the population (parent and offspring) that will proceed to the next generation [134]. Crossover and mutation are usually used to produce new solutions within the search space by making variations from the existing ones. Crossover recombines the chromosomes of the parents to produced a varies offspring while mutation modifies the parents of a parent to generate new offspring for the next generation [135]. In each iteration, a selection algorithm has to be implemented to identify the parts of the population that will proceed to the next generation. In [136], Chen and Lee presented a framework for ranking and selecting problems when the simulations are evaluated with more than one performance measure. The approach uses the concept of Pareto optimality in the ranking and selection scheme. Combined with the concept of the Pareto-optimal front, a rank and select genetic algorithm will be used in this study.

7.1.3 Objective

Hydrogen could serve as the final step in decarbonizing the electricity grid, but its adaption will significantly alter the composition of the infrastructure in the grid. Such change will require the analysis of various combinations of both the additional hydrogen infrastructure and the changes, whether an increase or a decrease, to the other technology that could support it. Since the typical charging, storage, and discharging components of storage is separate for chemical storage like hydrogen, this presents additional complexity in the optimization. Hydrogen fuel could also be imported rather than produced locally. These factors contribute to the multi-objective nature of the optimization. Moreover, since hydrogen is a maturing technology, many unknowns must be considered that will lead to various potential priority rankings.

Therefore, given the requirements of the analysis, this study aims to conduct a Pareto optimal genetic algorithm-based optimization to identify and assess the various hydrogen adaption pathways to understand the technical limitations of additional infrastructure in the grid. The proposed rank and select Pareto optimal genetic algorithm will be used to systematically explore the viable technology configurations that could reduce the fossil fuel in the grid while maintaining the energy balance. The optimization's primary goal is to minimize the changes in the grid to reduce the resistance to changes in the grid. By minimizing the additional infrastructure, the approach aims to provide the close to least cost investment for the adaption. The Pareto optimal approach will also provide a balance between the parameters involved in the change, thereby providing alternatives. Since there are various priorities, this study aims to reveal the various solutions and provide insights on the advantages and disadvantages of these solutions.

7.2 Methodology

7.2.1 Overview

Figure 7.1 shows the overview of the proposed Rank and Select Pareto Optimal Genetic Algorithm Approach, where three process clusters are highlighted. First, a selective grid sampling, which used preliminary simulation results to set the boundary conditions, was used for the initial calculation. The second process revolves around the Pareto Optimal Genetic Algorithm approach, which started with evaluating the initial solution through the Rank and Select Pareto Front selector. The identified Pareto fronts go through the Genetic Algorithm mutations to generate mutated parameters. These parameters go through another hourly energy balance simulation, and its results go back to the Pareto front selector to complete the loop. Q1 serves as the logical terminator for the Genetic Algorithm loop. The final Pareto Fronts were then analyzed to select the scenarios for further evaluation. The processes are further discussed in the subsections below.

7.2.2 Scenario Generation

Aside from the necessary hydrogen infrastructure, this study also looks into hydrogen technology's logical or chronological adaption. From this process, three potential adaption scenarios were identified. First, it is possible to adapt a purely local hydrogen adaption track, which is represented in green arrows in Figure 7.2. This adaption track does not incorporate importation, which could be beneficial for the self-sustainability of the grid. This track is similar to adding more diurnal storage, but for long-term storage. However, since hydrogen provides the ability to import the fuel, the study also explored this track by adding seasonal and yearlong importation scheme represented by blue and red arrows, respectively. Another potential possibility is the complete dependence on imported hydrogen. In this track, represented by black arrows, the installation of electrolyzers was skipped. Instead, it proceeds directly to the importation of hydrogen and then the installation of tanks and

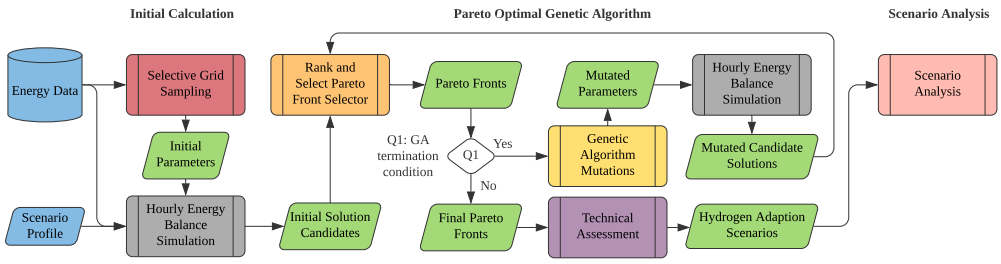

Figure 7.1: Proposed Rank and Select Pareto Optimal Genetic Algorithm Approach. The blue parallelograms represent the input of the system while the green parallelograms represent the intermediate output of the processes. Q1 serves as the logical terminator for the Genetic Algorithm loop.

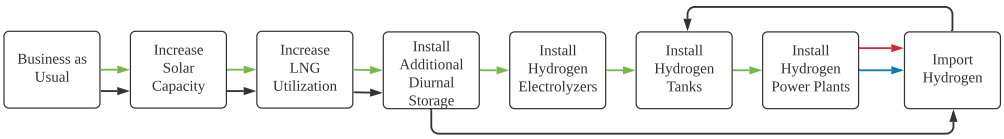

Figure 7.2: Hydrogen Technology Adaption Scenarios. The green line represents the purely local hydrogen adaption track which ends prior to the importation of hydrogen. The blue line then represents the seasonal imports while the red line represents the yearlong imports. The black line represents the pure import scenario which skips the installation of the local electrolyzer.

power plants. It might also skip the installation of additional diurnal storage, but this was no longer represented in the figure for simplicity.

For the simulation, these four scenarios could be represented by only the first three scenarios namely, no import, seasonal imports, and yearly imports, since the pure import scenario could be presented as a subset of the yearly import scenario in the proposed approach.

7.2.3 Hourly Simulation

The hourly simulation used Python for the Power System Analysis (PyPSA) Modeling Framework (v0.18.1) [53]. The PyPSA environment provides a framework for the buses, lines, loads, generators, storage, and units, among many other parameters. In this simulation, Kyushu was modeled as a single point, but additional sub-buses were added to monitor the changes in the energy balance due to various combinations of the system infrastructure, as seen in Figure 7.3. The coal generator was connected directly to the main bus B0 to prevent it from charging the diurnal storage or providing power to the electrolyzer. Since there are still instances when the existing diurnal capacity is charged by the other generators, albeit minimal, sub-bus B4 was provisioned to monitor this power flow.

For this study, the synthetic load and solar generation profile for the average year (2018) generated in Chapter 4 was used for the optimization. Similarly, the generator parameters seen in Table 7.1 that were used in the previous chapters were also used in this study. These generator properties were consolidated based on various sources [42]–[44]. The solar capacity growth in Kyushu from 2012 to 2020, which was detailed in [5], was used as a reference for the potential growth of solar PV in the region. For the business as usual scenario, the scenario used the latest published capacity of around 10 GW in 2021 [36].

This study assumed a total roundtrip efficiency of 42%. The electrolyzer was modeled through L7 with an efficiency of 60% while the hydrogen power plant was modeled through L8 with an efficiency of 70%. The simulation further assumes minimal leakage for the hydrogen storage, which is represented by the seasonal storage in the figure. Similar to the output of diurnal storage, the output of the hydrogen plant was directly connected to the main bus to prevent loopback charging. The capacity of the hydrogen plant was calculated as the peak power generation after the 70% efficiency is applied. The hydrogen import in bulk at the start of each week following the import scenario constraints (e.g. only during winter for seasonal import scenario).

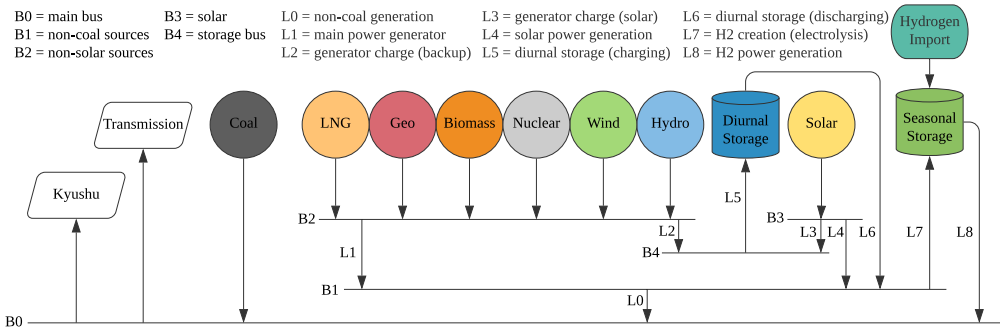

Figure 7.3: Configuration of the grid used in the simulation.

Table 7.1: Generators in Kyushu as of FY 2019

Generator	Power [MW]	Carrier	$\text{Output}_{\min}$ [%]	Ramp Limit [%]
Coal	7037	Coal	30	1
LNG	5250	Gas	15	40
Geothermal	160	Renewable	100	0
Biomass	450	Renewable	100	0
Solar	10000	Renewable	0	100
Nuclear	4140	Non-GHG	100	0
Wind	355	Renewable	15	40
Hydro	4000	Renewable	15	40

7.2.4 Selective Grid Sampling

The capacity range of the infrastructure seen in Table 7.2 is based on preliminary simulation to check the edge cases. A selective grid sampling was used to select the extreme cases and various conditions in between to generate the initial population of candidates. Five samples per capacity range was selected except for Diurnal Capacity, where there were only 2. In total, 6250 initial combinations were tested for each scenario profile. These initial combination went through the hourly energy balance simulation. The scenarios that were able to satisfy the energy balance (survivors) then represented the initial solution.

Table 7.2: Capacity Range of the Infrastructure

Parameter	Variable	Unit	Min	Max	Inc	n	$gridn$
LNG Budget	LF	TWh	0.0	28.0	2.00	15	5
PV Capacity	PV	GW	20.0	40.0	2.00	11	5
Diurnal Capacity	DS	GWh	13.5	33.5	20.00	2	2
H2 Electrolyzer Capacity	EL	GW	0.0	20.0	0.50	41	5
H2 Tank Capacity	TN	GWh	0.0	2000.0	50.00	41	5
H2 Power Plant Capacity	HP	GW	0.0	11.2	0.28	41	5

7.2.5 Rank and Select Pareto Front

Identifying the Pareto Front in two axes is straightforward, but the challenge for multi-objective optimization with more than 2 variables is identifying a way to represent the variables in 2 variables. In this study, the concept of rank and select was utilized. The variables were clustered into two rankers where one is focused on the hydrogen technology and the other one focused on the other technology that complements it. Figure 7.4 shows one of the ranking clusters used in this study. Since one of the goals is the reduction of LNG, it is the priority in the ranking. PV capacity and storage are already saturated in the region; thus, these two variables were the second and third priority. These three clusters together represent the technology that complements hydrogen adaption. The electrolyzer capacity, tank capacity, hydrogen power plant, and hydrogen fuel imports (HF) represents the second cluster of rankers. Through several iterations, it was discovered that the hydrogen fuel import should be ranked first among the variables associated with hydrogen. This change also made the ranking consistent, where the fuel-related variables were ranked first, followed by the infrastructure-related variables.

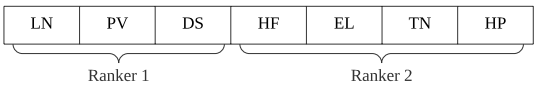

Figure 7.4: Ranker Cluster used for the Seasonal and Yearly Import Scenario for the Rank and Select Approach. HF refers to Hydrogen Fuel Imports, which was always 0 in the No Import Scenario; thus, it was removed for that scenario. The other variables are defined in Table 7.2.

Using this ranker, the Rank and Select Approach goes through two steps. First, the candidate population was clustered together based on ranker 1. In each cluster, all the values for each of the variables in the ranker 1 is the same and the values for the variables in ranker 2 provides the variation. Then, in each cluster, the values are further ranked using ranker 2, and the top combination was selected to represent that cluster. At the end of step 1, the surviving population represents the combinations with the least infrastructure following the ranking order of both ranker 1 and ranker 2. Since ranker 1 was used for the clustering, this surviving population leans more towards the variation in ranker 1.

In step 2, the surviving population is assigned a rank based on ranker 1 and ranker 2. The ranks are then used in the selection of the pareto fronts by identifying the non-dominated solution, which is defined as the solution which could improve in one axis without degrading the other axis. Figure 7.5 shows an example of the approach where the orange dots are the non-dominated solution. As seen in the axis annotation, for each orange dot, there is no blue dot, which improves on one axis without degrading the other axis.

7.2.6 Genetic Algorithm

The study utilizes the genetic algorithm's idea of mutation to improve the corresponding values in the surviving population. For each of the surviving population, the approach

mutates each one of the variables in ranker 1 by reducing the values by 1 step following the increments in Table 7.2. Since such mutation might require additional infrastructure to compensate, the corresponding values in rank 2 were incrementally increased until a valid combination (energy balance is satisfied) is identified. This mutated solution is then added to the surviving population. The mutation is done for all the surviving specimens. Afterwhich, the combined parent and offspring solutions go through the rank and select approach to generate the next Pareto front.

In each iteration, the previous and current Pareto fronts are compared to assess if there are still changes. The genetic algorithm iteration ends when no more changes are seen between generations. However, since there is a possibility that the iteration might run indefinitely, a max number of iteration is assigned based on the number of the initial population. More generation is given to scenarios where the initial surviving population is low to give it more time to mutate. In comparison, less generation is provided to the scenario with an already diverse initial population. The variation detector and max generation are the logical terminator for the genetic algorithm.

7.2.7 Technical Assessment

At the end of the genetic algorithm iteration, the approach will provide several candidates for analysis. The technical assessment mainly analyzes the solutions' variations and identifies solutions for further analysis. In the case of the study, the extreme cases (leaning towards ranker 1 or ranker 2) and the mixed cases (those that represents the balance between the two) were selected for further analysis.

The selected solutions were visualized into a radar chart to provide an intuitive or tangible way to compare the combinations. Other parameters, such as the energy balance, local

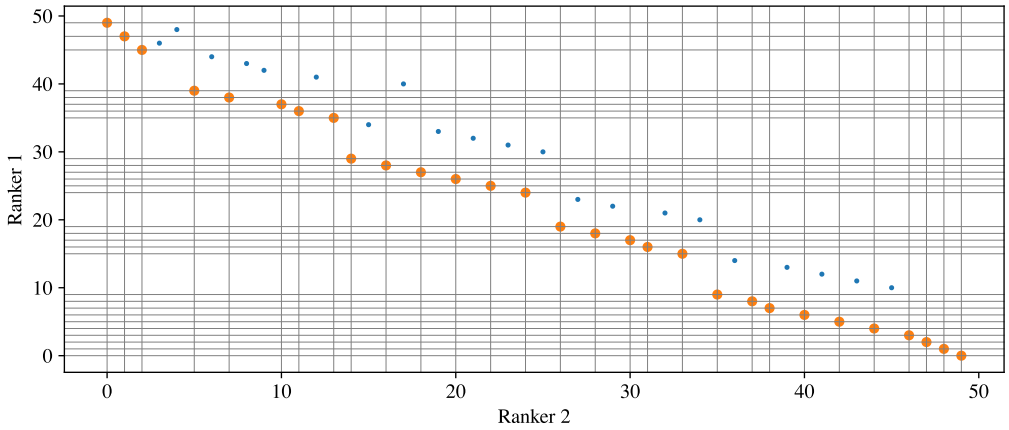

Figure 7.5: A sample visualization of the Rank and Sort Pareto Optimal Front. The blue dots and orange dots represents the surviving population after step 1. The orange dots were selected as the Pareto optimal front. The axis annotation was added to provide an easier comparison between the dominant and non-dominant solutions. Note: since the goal is to minimize the additional infrastructure, lower rank is better, which is why the Pareto optimal front is on the bottom-left side of the figure.

hydrogen production, optimized LNG capacity, and solar curtailment, were also extracted and then tabulated or visualized.

7.3 Results

Table 7.3 summarizes the relevant variable for the scenario analysis. Scenarios A, B, C, and D are the reference scenarios that were previously explored. These scenarios were added to serve as a comparison to the scenarios with hydrogen technology. The other results are clustered further based on the hydrogen import limitations such as local production only (L1-L3), seasonal imports (S1-S6), and yearly imports (Y1-Y12). Since the yearly import presents various combinations, the no-LNG import scenarios (Y7-Y12) were further clustered. As anticipated, the infrastructure necessary to maintain the balance in the grid is dependent on the import availability of hydrogen. Figure 7.6 highlights various scenarios that represents each cluster.

From Scenario A in Figure 7.6, which represents the business as usual in 2020, an equivalent of around 46% of fossil fuel-based energy generation must be replaced with a carbon-neutral energy source to decarbonize the grid. This share roughly translates to 46 TWh since Kyushu consumes around 100 TWh per year.

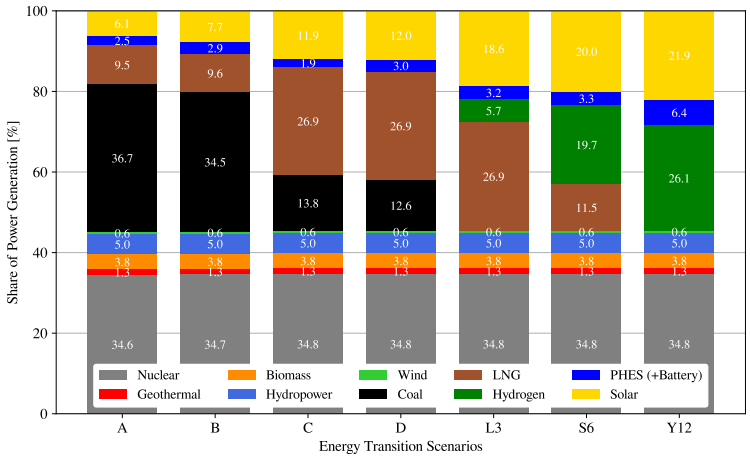

Figure 7.6: Overview of the Energy Balance for the Scenario Analysis

No Import

Based on the optimization results, the variations in local hydrogen production scenarios were limited and could be represented by three Pareto optimal solutions. The variations among these parameters is visualized in Figure 7.7 and the corresponding energy balance is shown in Figure 7.8. From these figures, L1 shows that a larger amount of PV capacity is necessary to provide enough energy for the electrolyzers to produce enough hydrogen

Table 7.3: Hydrogen Technology Adaption Scenarios

Name units	LF TWh	PV GW	DS GWh	EL GW	TN GWh	HP GW	HL TWh	HF TWh	LC GW	CR %
A	10	10	13.5	0.0	0.0	0	0.0	0.0	5.25	14
B	10	16	13.5	0.0	0.0	0	0.0	0.0	5.25	31
C	28	16	13.5	0.0	0.0	0	0.0	0.0	5.25	12
D	28	16	33.0	0.0	0.0	0	0.0	0.0	5.25	2
L1	28	40	33.0	2.5	2.0	2.8	1.8	0.0	5.21	20
L2	28	36	33.0	5.0	2.0	2.8	2.9	0.0	5.21	8
L3	28	40	13.5	9.0	2.0	5.6	6.0	0.0	5.24	11
S1	28	40	33.0	2.5	1.5	2.8	1.2	1.4	4.77	21
S2	24	40	33.0	3.5	1.5	2.8	1.9	2.8	4.77	17
S3	20	40	33.0	10.0	0.5	5.6	4.3	4.2	4.19	4
S4	18	40	33.0	7.0	0.5	5.6	3.5	7.0	4.19	9
S5	12	40	33.0	8.0	1.0	5.6	4.0	12.6	3.09	6
S6	12	40	13.5	13.0	1.5	6.2	6.5	14.0	3.32	3
Y1	28	40	33.0	2.5	1.5	2.8	1.2	1.4	4.77	21
Y2	22	40	33.0	4.5	1.5	2.8	2.5	4.2	4.77	15
Y3	18	40	33.0	7.0	0.5	5.6	3.5	7.0	4.19	9
Y4	12	40	33.0	9.0	0.5	3.4	4.0	12.6	4.25	5
Y5	10	40	13.5	13.0	1.0	5.6	6.6	15.4	3.37	4
Y6	4	40	13.5	13.5	1.1	8.4	6.5	21.0	1.88	3
Y7	0	20	13.5	0.0	2.0	10.1	0.0	37.8	0	10
Y8	0	22	13.5	1.0	2.0	11.2	0.3	36.4	0	10
Y9	0	24	33.0	2.0	2.0	8.4	0.3	33.6	0	3
Y10	0	30	33.0	5.0	2.0	8.4	1.3	29.4	0	3
Y11	0	34	33.0	8.0	1.6	8.4	2.4	26.6	0	2
Y12	0	40	33.0	7.5	1.5	8.4	3.4	23.8	0	7

LF: LNG Budget; PV: PV Capacity; DS: Diurnal Capacity; EL: H2 Electrolyzer Capacity; TN: H2 Tank Capacity; HP: H2 Power Plant Capacity; HL: H2 Fuel Local Production; HF: H2 Fuel Imports; LC: LNG Capacity; CR: Curtailment Rate

fuel to support the Hydrogen Power Plant. L2 shows that higher EL capacity would require less solar capacity. L3 shows the dynamics between the hydrogen infrastructure and diurnal storage. In all cases, a significant storage capacity is needed. Although these scenarios were able to decommission coal capacity totally, a substantial amount of LNG is still necessary to maintain the energy balance. However, this shows that with the help of LNG, a combination of PV and hydrogen technology could already decommission coal capacity. Since H2 is also a flexible energy source, it provided additional flexibility in the grid that allowed more solar penetration, as seen in the increase in the solar penetration rate between scenario D and L1.

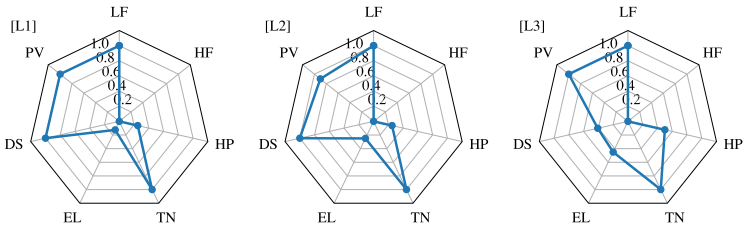

Figure 7.7: Normalized Radar Chart of the No Import Scenario

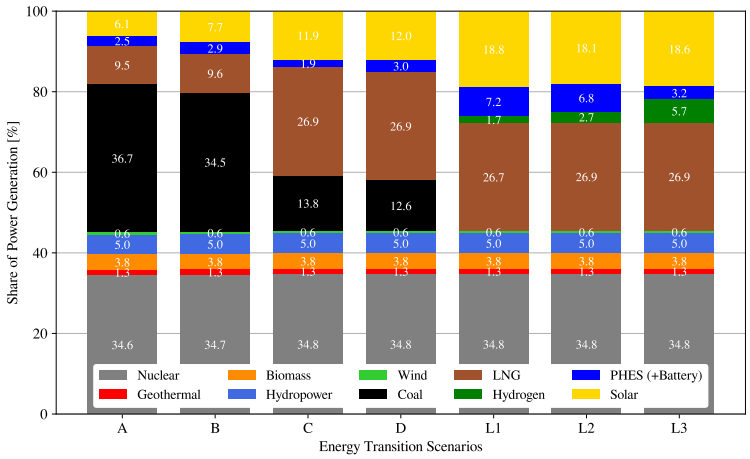

Figure 7.8: Energy Balance of the selected No Hydrogen Import Scenario

The energy balances for the (A) business-as-usual, (B) increased solar, (C) minimized coal, and (D) increased diurnal storage were added as references. These were ordered based on the theoretical progression towards the local hydrogen production scenario. The figure also shows the composition of the grid for the three scenarios identified in Figure 7.8.

Seasonal Import

Providing the option to import hydrogen during the winter season provided more options. Compared to the L2, it can be seen in Figure 7.10 that there is an increase in direct solar utilization despite having the same solar capacity since the system can now start reducing the generation capacity of LNG. The seasonal import managed to supply enough hydrogen during the winter, reducing the necessary LNG capacity. As the available hydrogen imports increase, the system gradually decreases LNG capacity since hydrogen plants could already handle the winter peak. As a result, the total annual LNG fuel demand also decreased. The electrolyzers were also able to absorb much of the excess solar curtailment, as shown in the progressively decreasing curtailment rate shown in Table 7.3.

In the best-case scenario, the LNG fuel budget goes down to 12 TWh in S5 and S6. In terms of import fuel, these two scenarios are the same. They are compromises between diurnal storage and electrolyzer capacity. Higher electrolyzer leads to less curtailment, but this could be attributed to the lower efficiency of electrolyzers relative to the diurnal storage.

Yearlong Import

The configuration of Y1 is identical to S1 since there is an abundant LNG budget. Y2-Y6 shows the gradual increase in electrolyzer and H2 import due to the decreasing LNG budget. The LNG capacity also decreases. As previously observed, the curtailment decreases as EL capacity increases since the electrolyzer essentially absorbs that excess energy. The shift in

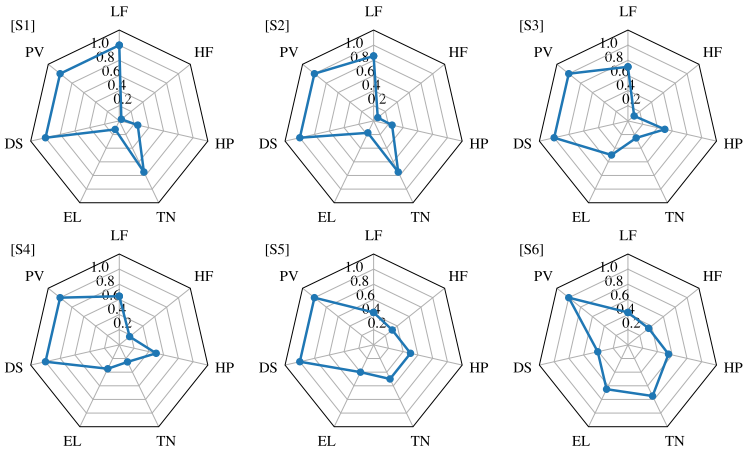

Figure 7.9: Normalized Radar Chart of the Seasonal Import Scenario

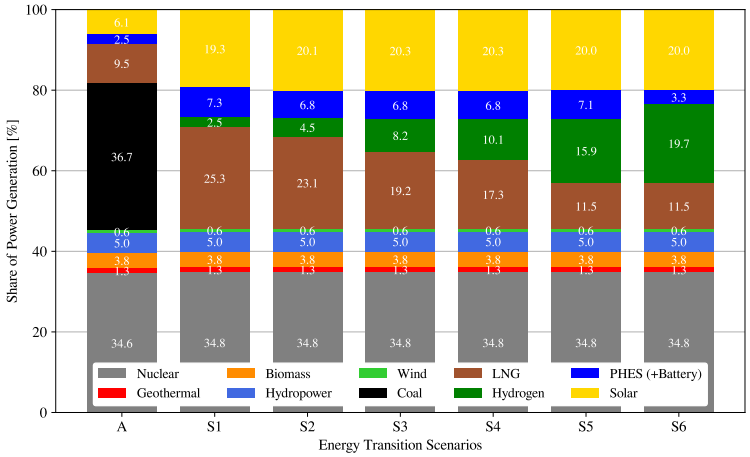

Figure 7.10: Energy Balance of the selected Seasonal Import Scenario

the transition can be seen in the exchange of the position in Figure 7.11 for LF and HF. In all cases, maximum solar capacity should be allocated. Similar to previous scenarios, the curtailment rate reduces as EL increases. Y6 represents the combination of technology that almost removed LNG as seen in Figure 7.12. However, this was achieved by maximizing the hydrogen technology and PV capacity.

Y7-Y12 was grouped differently since it shows various combinations that could eliminate both LNG and coal capacity in the grid. This group, which is compared in Figure 7.13, already begins with a relatively low curtailment compared to the other scenarios because it also begins with lower solar PV capacity. However, this is only achievable if around 38 TWh of equivalent H2 energy generation is imported. It essentially replaced the share of coal in the grid when compared with Scenario A. This scenario heavily depends on import infrastructure, hydrogen tanks, and H2 power plants, which might be considered as extremely on the side of the hydrogen technology as depicted in Figure 7.13. The rest of the

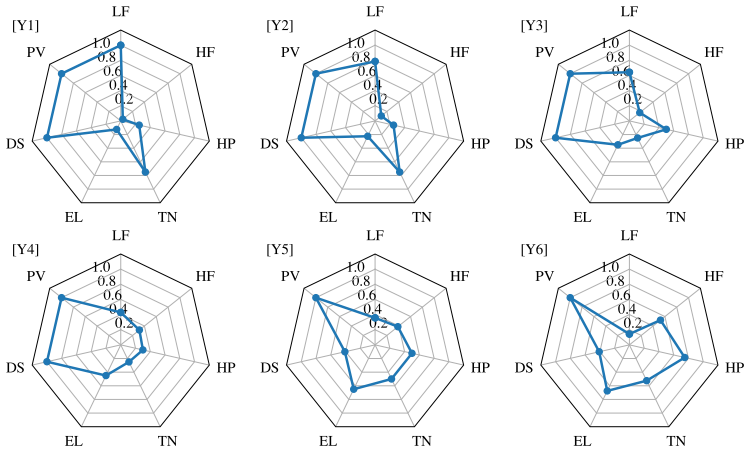

Figure 7.11: Normalized Radar Chart of the Yearly Import Scenario (with LNG)

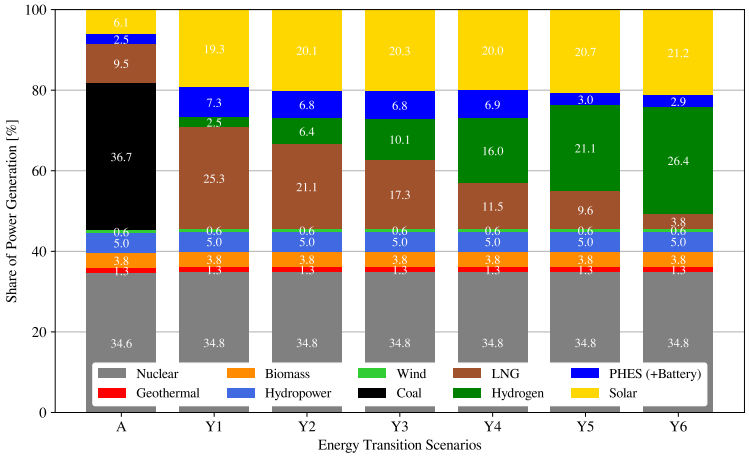

Figure 7.12: Energy Balance of the selected Yearly Import Scenario (with LNG)

scenario in this cluster represents the gradual decrease in the hydrogen dependence towards more direct solar consumption, diurnal storage, and local hydrogen fuel production.

In Y9, both PV and DS were introduced, producing enough excess energy to merit the installation of electrolyzers. Y10-Y12 progressively increased PV capacity which reduced the necesssary H2 power plant capacity since PV could hanlde more peak demand. The resulting capacity is equivalent to the current power generation of both LNG and coal under a high PV penetration scenario. Although Y12 seems to be the best scenario, Y10 or Y11 provides more balance between the available technology.

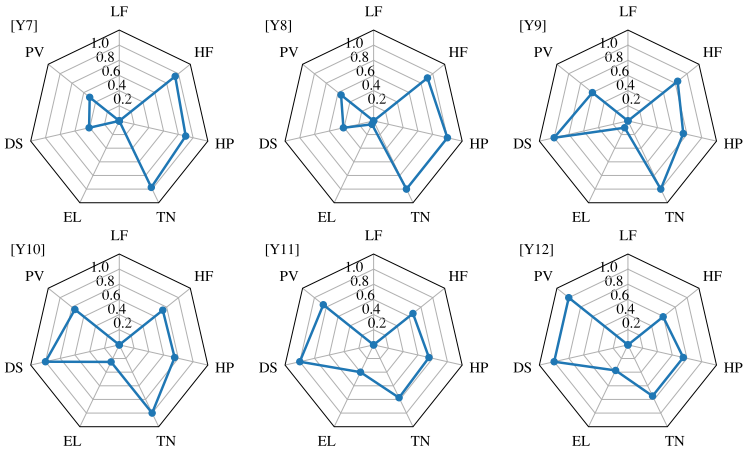

Figure 7.13: Normalized Radar Chart of the Yearly Import Scenario (without LNG)

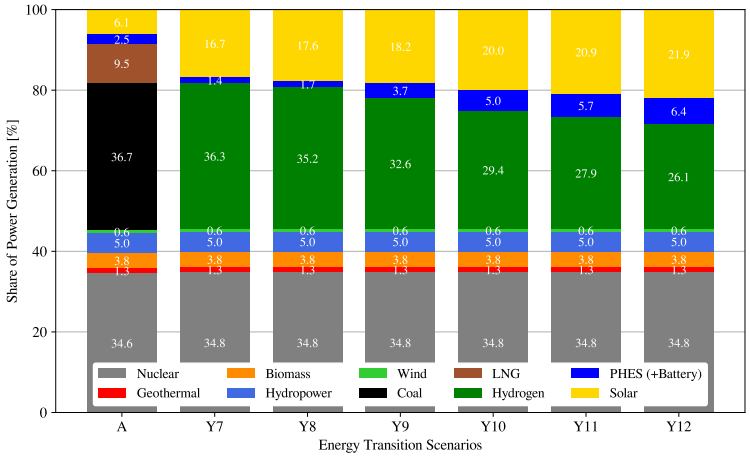

Figure 7.14: Energy Balance of the selected Yearly Import Scenario (without LNG)

7.4 Discussion

7.4.1 Hydrogen Import Scenarios

The results showed that producing local hydrogen could help eliminate the coal capacity, but this will come at the cost of investing more solar energy. Since the results shows that the solar PV capacity in the region must be quadrupled to support the local hydrogen production, this might not be a viable solution due to the speed at which solar PV could be deployed (maximum of 2 GW per year) and the current saturation rate of the PV market in Kyushu. However, it might be feasible if the new installations are directly connected to electrolyzers. Nonetheless, further calculations regarding the business model of individual electrolyzers must be done to assess this viability. Despite the financial cost, the results shows that with the additional flexibility of hydrogen, more solar PV capacity could directly penetrate

the grid, which could be seen as another potential benefit of investing in local hydrogen electrolyzers.

As shown in Chapter 4, the difficulty in eliminating coal is due to the relatively higher demand in winter and the lower solar PV production during this period. However, by focusing mainly on importing hydrogen fuel during this season, the results show that dependence on LNG could already be reduced. Again, this assumes the same condition in the no import scenario where more solar capacity will be necessary to produce the necessary hydrogen capacity for the rest of the year.

The yearly import scenario showed the dynamics between LNG and hydrogen mainly since these energy sources are both flexible sources. With the proper infrastructure, LNG could be directly replaced by hydrogen. However, the results showed that there could be a balance between these two. Therefore, during the transition period, where the hydrogen infrastructure is not yet entirely dependable, it might be best to aim for a balance between these two.

Although it was not the direct objective, the proposed approach also revealed that LNG could be eliminated. However, this could also be seen as merely shifting the dependence on LNG towards hydrogen. This scenario might benefit the decarbonization efforts if the imported hydrogen is produced under a carbon neutral scenario. In the near future, most of the production are centered around blue hydrogen, which still produces carbon emissions.

7.4.2 Investment on Hydrogen Technology

The study primarily aimed at understanding the combination of hydrogen technology that could reduce the carbon dioxide emission in the grid. The results showed that the approach could achieve this, but it also shows that significant investment will be necessary to realize this green future. With the difficulty in even reducing the power generation from coal, if hydrogen remains expensive, both the fuel and the necessary infrastructure, this will be the major roadblock in this transition. At this point, it will now depend on the government's commitment to this energy transition. Based on the capacity requirements seen in this study, this might not be achievable in the next decade. However, hopefully, this could be the target by 2050.

7.4.3 Complexity of the Problem

The problem of hydrogen technology adaption has numerous parameters that must be considered. The priority in these parameters could even influence the analysis. The proposed rank and select Pareto optimal approach provided a systematic exploration that considers the balance between the hydrogen technology and other technology that could support its adaption. The concept of mutation through the genetic algorithm was useful in modifying the initial solutions from the selective grid sampling. By going through several generations

of mutations, the Pareto optimal solutions were improved to identify the Pareto optimal solutions.

However, after the whole process, it is still necessary to manually evaluate the variations among the proposed solutions to maximize the variations between them. Therefore, the approach could be improved by adding an algorithm that would maximize the variations between the provided solution.

7.5 Conclusion

Believing on the potential of chemical storage to complete the process of the energy transition towards zero carbon, this study sought to understand the infrastructure demands of the hydrogen-dependent transition pathways. The import scenarios highlighted the limitation of the local production of hydrogen even at higher PV penetration. It also highlighted the importance of more grid flexibility to increase PV penetration further. This might be the main argument in the total decommissioning of coal power plants – it is not flexible enough and thus is not compatible with high PV penetration. Despite the limitation, the study showed that coal could be decommissioned completely with the combined effort of LNG, PV, and hydrogen, but it will come at a huge financial cost.

The results showed that the rank and select Pareto optimal approach coupled with genetic algorithm's mutation could be used to systematically explore the combination of technology that could minimize the use of fossil-fuel-based energy generation while maintaining the energy balance. Although this study mainly focused on seven variables, which were further clustered into two rankers, it could also be used for a higher number of variables, but the two clusters must be counter to each other. The current approach works as long as the two ranking clusters result in a reversed ranking (e.g., lower LNG fuel leads to a higher rank in ranker 1, but it will also require higher hydrogen fuel, leading to a lower rank in ranker 2 and vice versa). For instance, this approach will be challenging to evaluate the infrastructure between hydrogen and ammonia. In such a case, another fitness function will most likely be needed to provide a more precise answer.

8 Conclusion

8.1 Summary

This dissertation investigated scenarios such as decommissioning coal capacity, adding complementary diurnal storage, utilizing electric vehicles as mobile storage, and incorporating hydrogen technology to understand the potential, limitations, and implications of these scenarios to support solar PV in leading the energy transition towards zero carbon. Using the model built for Kyushu's case, these scenarios' viability was scrutinized using mathematical, machine learning, and heuristic tools. In all scenarios, the simulation ensured that the hourly balance was satisfied.

As a summary, the primary outcomes from the conducted research in this dissertation include:

1. Solar curtailment is unavoidable once the PV penetration rate reaches around 8% due to the flexibility of other energy sources and the mismatch between supply and demand.
    a) As a baseload generator, coal is incapable of supporting the variability of solar PV. On the other hand, since LNG is flexible, it could support solar PV. However, dependence on LNG must be minimized since additional demand for LNG will lead to higher global prices.
    b) The mismatch of supply and demand is observed during spring and autumn. Within the week, curtailment will most likely happen on the weekends and within the day, between 9:00 to 15:00.
2. Solar PV could reduce the existing coal capacity with LNG support, but it is insufficient to decommission coal due to its variability. Winter is a vital issue in considering solar PV as an energy transition driver due to the significant mismatch between PV supply and energy demand during this season. PV is still insufficient during extreme summer temperatures despite the relatively larger PV power generation.
3. Diurnal storage can help reduce solar curtailment, but the storage's capacity factor must also be considered. For stationary storage, proper assessment is necessary since these infrastructures will only serve this single purpose. On the other hand, additional incentives must be provided for temporary storage like electric vehicles. People generally purchase this equipment for transportation, and grid storage is only a secondary consideration or even a mere afterthought.

4. The dissertation clarified the impact of weather in reducing the capacity of coal power plants due to the dispatchable generation capacity of these plants, which solar could not consistently replace. Stand-by power plants are necessary to ensure the reliability of the electricity grid. These plants must be operated when significant solar generation reduction or demand increase is predicted.

5. The dissertation shed some light on the time component of the energy transition, where the proper timing of additional infrastructure influences the operational cost of the system. The changes in the installed capacity and cost of the infrastructure must be considered during the planning stage to maximize the synergy of the additional infrastructure.

6. The dissertation demonstrated the complexity of planning multiple infrastructures, which makes the energy transition a multi-objective problem given the various factors that influence the final design. As a result, there might not be a single best solution, but a set of potential solutions since the objective function might contradict each other.

7. Finally, the dissertation raised the issue of merely shifting the dependence on one technology to another to decarbonize the grid. It is necessary to ensure that new technology like hydrogen is produced under the concept of carbon neutrality. Otherwise, the net carbon emission will remain a problem.

8.2 Prospects and Future Outlook

From the viewpoint of the global discussion on energy transition, this dissertation used the case of Kyushu as a representative case of Japan's future energy scenario. Kyushu encapsulates Japan's characteristics: an isolated electricity grid, temperate climate, and highly industrialized sectors. Although each region in Japan currently has different energy mixes, the diversity of the energy sources in Kyushu could be achieved by other regions in the country. Most of these regions also have nuclear power plants (currently under retrofitting) and have the potential to increase the penetration rate of solar PV. Therefore, the results in this study could apply to other regions in Japan and represent the country in global discourse.

Kyushu's isolated electricity grid case could be comparable to South Korea, Taiwan, the Philippines, and Hawaii since the connection to other electricity grids is limited. Therefore, the insights gained in this study could be used in these electricity grids, especially in regions with similar climates. For instance, the difficulty in decommissioning coal power plants should serve as a warning for islanded grids that hopes to pursue high PV penetration. Locally, the results could be a model for the Chugoku and Shikoku region since they might soon face the same issues based on the PV penetration in FY 2020. Likewise, the rest of the country will most likely follow soon except for highly dense regions like the Kanto and Kansai region, where the land area for PV installation is expensive and scarce.

From the modeling perspective, the mathematical, machine learning, and heuristic tools used in this dissertation could easily be adapted to countries with hourly data. For instance, although the demand pattern will most likely be different, the weather-driven demand synthesis could be used to generate demand profiles based on historical weather and energy data, and these synthetic data could be used to explore various weather conditions. In addition, the heuristics used in this dissertation is crucial in discussing various changes in the grid if different priorities must be explored prior to the final decision.

Overall, the dissertation aimed at understanding the potential, limitations, and implications of various energy transition paths that are compatible with solar PV. The dissertation showed that PV could be a driver for the energy transition, but it will need the support of other technology to accomplish the decarbonization goals that will meet the Paris Agreement and UN Sustainable Development Goals.

8.3 Future Work

This study treated the Kyushu region as one geographical unit and, in effect, disregarded the variations within the region. For future work, the transmission lines and location of the power plants must be explored to understand the internal dynamics in the region. The distribution of the additional solar PV might cause an additional burden to the transmission lines and land availability in the region. At the same time, the weather also varies within the region, and as shown in Chapter 4, the weather influences the actual generation of solar PV. This was considered in the study's initial design but was omitted due to the lack of accessible data to model the region's demand-side. The demand-side information is necessary to perform the hourly energy balance simulation. With the proper data, performing an intra-region analysis could provide additional insights into the internal dynamics of the power plants in the region.

Aside from the electric vehicles discussed in this study, fuel cell vehicles (FCVs) are also emerging as another decarbonization effort for the transport sector. Although the future of small-scale grid-connected electrolyzer-equipped refilling stations is still contested, since the grid might tap into hydrogen as a fuel source for electricity, FCVs might become a double-edged sword. On the one hand, it could support the growth of the hydrogen market, reducing the cost of hydrogen when bought in bulk. However, on the other hand, it might also cause an increase in demand and compete with the grid in terms of fuel supply, increasing the cost of hydrogen fuel. This macroeconomics is beyond the scope of this research.

This research heavily focused on the supply side of the energy balance, and with efforts such as virtual power plants and time-of-use services, the demand side could also help in reducing the necessary infrastructure in the grid. As highlighted in the scenarios involving coal decommissioning (Chapter 4) and Hydrogen Adaption (Chapter 7), peak demand is one problem. Suppose these peak demands could be rescheduled or prevented, then more coal capacity could be decommissioned already in the short-term, and less hydrogen power plant capacity would be necessary for the long term. Such research work would require

insights into the behavioral information regarding the users, which is beyond the scope of the available data in this study.

Bibliography

[1] S. M. G. Dumlao and K. N. Ishihara, "Reproducing solar curtailment with fourier analysis using japan dataset," *Energy Reports*, vol. 6, pp. 199–205, 2020. DOI: 10.1016/j.egyr.2019.11.063.

[2] S. M. G. Dumlao and K. N. Ishihara, "Weather-driven scenario analysis for decommissioning coal power plants in high PV penetration grids," *Energies*, vol. 14, no. 9, p. 2389, 2021. DOI: 10.3390/en14092389.

[3] S. M. G. Dumlao and K. N. Ishihara, "Dynamic cost-optimal assessment of complementary diurnal electricity storage capacity in high PV penetration grid," vol. 14, no. 15, p. 4496, 2021. DOI: 10.3390/en14154496.

[4] S. M. G. Dumlao and K. N. Ishihara, "Impact assessment of electric vehicles as curtailment mitigating mobile storage in high PV penetration grid," *Energy Reports*, vol. 8, pp. 736–744, 2022. DOI: 10.1016/j.egyr.2021.11.223.

[5] K. Knüpfer, S. M. G. Dumlao, M. Esteban, T. Shibayama, and K. N. Ishihara, "Analysis of PV subsidy schemes, installed capacity and their electricity generation in japan," *Energies*, vol. 14, no. 8, p. 2128, 2021. DOI: 10.3390/en14082128.

[6] E. Martinot, "Grid Integration of Renewable Energy," *Annual Review of Environment and Resources*, pp. 223–254, 2016. DOI: 10.1146/annurev-environ-110615-085725.

[7] REN21, *Renewables 2020 Global Status Report*, Available: https://www.ren21.net/wp-content/uploads/2019/05/gsr_2020_full_report_en.pdf, 2020.

[8] B. K. Sovacool, "How long will it take? conceptualizing the temporal dynamics of energy transitions," *Energy Research & Social Science*, vol. 13, pp. 202–215, 2016. DOI: 10.1016/j.erss.2015.12.020.

[9] A. Grubler, "Energy transitions research: Insights and cautionary tales," *Energy Policy*, vol. 50, pp. 8–16, 2012. DOI: 10.1016/j.enpol.2012.02.070.

[10] R. York and S. E. Bell, "Energy transitions or additions?" *Energy Research & Social Science*, vol. 51, pp. 40–43, 2019. DOI: 10.1016/j.erss.2019.01.008.

[11] M. Sarrica, S. Brondi, P. Cottone, and B. M. Mazzara, "One, no one, one hundred thousand energy transitions in europe: The quest for a cultural approach," *Energy Research & Social Science*, vol. 13, pp. 1–14, 2016. DOI: 10.1016/j.erss.2015.12.019.

[12] J. Stephenson, B. Barton, G. Carrington, D. Gnoth, R. Lawson, and P. Thorsnes, "Energy cultures: A framework for understanding energy behaviours," *Energy Policy*, vol. 38, no. 10, pp. 6120–6129, 2010. DOI: 10.1016/j.enpol.2010.05.069.

[13] REN21, *Renewables 2021 Global Status Report*, Available: https://www.ren21.net/wp-content/uploads/2019/05/GSR2021_Full_Report.pdf, 2021.

[14] International Energy Agency, *Status of power system transformation 2019*, Available: https://www.iea.org/reports/status-of-power-system-transformation-2019 Accessed: 2021-03-06.

[15] M. Perez, R. Perez, K. R. Rábago, and M. Putnam, "Overbuilding & curtailment: The cost-effective enablers of firm PV generation," *Solar Energy*, vol. 180, pp. 412–422, 2019. DOI: 10.1016/j.solener.2018.12.074.

[16] P. Denholm, R. Margolis, and J. Milford, "Production Cost Modeling for High Levels of Photovoltaics Penetration," *Renewable Energy Laboratory Technical Report*, no. February, pp. 87–118, 2008, Available: https://www.nrel.gov/docs/fy08osti/42305.pdf.

[17] California Independent System Operator, "Energy and environmental goals drive change," *Technical Report*, p. 4, 2016, Available: https://www.caiso.com/Documents/FlexibleResourcesHelpRenewables_FastFacts.pdf.

[18] P. Denholm and R. M. Margolis, "Evaluating the limits of solar photovoltaics (PV) in electric power systems utilizing energy storage and other enabling technologies," *Energy Policy*, vol. 35, no. 9, pp. 4424–4433, 2007, ISSN: 3014215. DOI: 10.1016/j.enpol.2007.03.004.

[19] P. Denholm and R. M. Margolis, "Evaluating the limits of solar photovoltaics (PV) in traditional electric power systems," *Energy Policy*, vol. 35, no. 5, pp. 2852–2861, 2007. DOI: 10.1016/j.enpol.2006.10.014.

[20] E. K. Hart, E. D. Stoutenburg, and M. Z. Jacobson, "The Potential of Intermittent Renewables to Meet Electric Power Demand: Current Methods and Emerging Analytical Techniques," *Proceedings of the IEEE*, vol. 100, no. 2, pp. 322–334, 2012, ISSN: 0018-9219. DOI: 10.1109/JPROC.2011.2144951.

[21] D. B. Richardson and L. Harvey, "Strategies for correlating solar PV array production with electricity demand," *Renewable Energy*, vol. 76, pp. 432–440, 2015, ISSN: 9601481. DOI: 10.1016/j.renene.2014.11.053.

[22] P. D. Lund, J. Lindgren, J. Mikkola, and J. Salpakari, "Review of energy system flexibility measures to enable high levels of variable renewable electricity," *Renewable and Sustainable Energy Reviews*, vol. 45, pp. 785–807, 2015, ISSN: 13640321. DOI: 10.1016/j.rser.2015.01.057.

[23] S. A. Janko, M. R. Arnold, and N. G. Johnson, "Implications of high-penetration renewables for ratepayers and utilities in the residential solar photovoltaic (PV) market," *Applied Energy*, vol. 180, pp. 37–51, 2016, ISSN: 3062619. DOI: 10.1016/j.apenergy.2016.07.041.

[24] S. Impram, S. V. Nese, and B. Oral, "Challenges of renewable energy penetration on power system flexibility: A survey," *Energy Strategy Reviews*, vol. 31, p. 100 539, 2020. DOI: 10.1016/j.esr.2020.100539.

[25] N. Y. Mansouri, R. J. Crookes, and T. Korakianitis, "A projection of energy consumption and carbon dioxide emissions in the electricity sector for Saudi Arabia: The case for carbon capture and storage and solar photovoltaics," *Energy Policy*, vol. 63, pp. 681–695, 2013, ISSN: 3014215. DOI: 10.1016/j.enpol.2013.06.087.

[26] P. Denholm and T. Mai, "Timescales of energy storage needed for reducing renewable energy curtailment," *Renewable Energy*, vol. 130, pp. 388–399, 2019. DOI: 10.1016/j.renene.2018.06.079.

[27] Lazard, *Lazard's Levelized Cost of Storage Analaysis - version 6.0*, Available: https://www.lazard.com/perspective/levelized-cost-of-energy-and-levelized-cost-of-storage-2020/ Accessed on 8 May 2021, 2020.

[28] E. O'Shaughnessy, J. R. Cruce, and K. Xu, "Too much of a good thing? global trends in the curtailment of solar PV," *Solar Energy*, vol. 208, pp. 1068–1077, 2020. DOI: 10.1016/j.solener.2020.08.075.

[29] Kevin Eber and David Corbus, *Hawaii solar integration study: Executive summary*, Available: https://www.nrel.gov/docs/fy13osti/57215.pdf, 2013.

[30] Japan Ministry of Economy, Trade, and Industry, *Japan's Fifth Strategic Energy Plan (provisional translation)*, Available: https://www.enecho.meti.go.jp/en/category/others/basic_plan/5th/pdf/strategic_energy_plan.pdf, 2018.

[31] Japanese Law Translation, *Act on special measures concerning procurement of electricity from renewable energy sources by electricity utilities (act no. 108 of august 30, 2011)*, Available: http://www.japaneselawtranslation.go.jp/law/detail/?id=2573&vm=&re=02 (accessed 2021-12-20).

[32] Ito, Yoko, "A Brief History of Measures to Support Renewable Energy: Implications for Japan's FIT review obtained from domestic and foreign cases of support measures.," *Institute of Energy Economics of Japan*, 2015, Available: https://eneken.ieej.or.jp/data/6330.pdf.

[33] Data of Japan, *Japan administrative division*, Available: https://github.com/dataofjapan/land Accessed: 2021-10-28.

[34] Organization for Cross-regional Coordination of Transmission Operators, JAPAN, *System information about the major electric power companies in japan*, Available: https://www.occto.or.jp/keitoujouhou/index.html (accessed 2020-10-01).

[35] Kyushu Electric Company, *Kyushu Electric Company Renewable Energy Application (Japanese)*, Available: https://www.kyuden.co.jp/td_renewable-energy_application_index.html Accessed: 2021-12-08, 2021.

[36] Kyushu Electric Company, *Supply and Demand Information (Japanese)*, Available: https://www.kyuden.co.jp/td_service_wheeling_rule-document_disclosure Accessed: 2021-10-28, 2021.

[37] Kyushu Electric Company, *Kyushu Electric Company Group Annual Report 2018*, Available: http://www.kyuden.co.jp/var/rev0/0149/3830/c7ujptmy_all.pdf Accessed: 2021-04-28, 2018.

[38] Statistics Bureau, Ministry of Internal Affairs and Communications, Japan, *Statistical Handbook of Japan 2021*, Available: https://www.kyushu.meti.go.jp/keizai-db/db_top.html Accessed: 2021-12-20, 2021.

[39] Kyushu Bureau of Economy, Trade, and Industry, *Kyushu Economic and Industrial Data (in Japanese)*, Available: https://www.stat.go.jp/english/data/handbook/pdf/2021all.pdf, 2019.

[40] Kyushu Electric Company, *Transmission Line Configuration in Kyushu (Japanese)*, Available: https://www.kyuden.co.jp/var/rev0/0240/3791/hgajn6ar.pdf Accessed: 2021-04-28, 2019.

[41] Federation of Electric Power Companies of Japan, *Electricity Review Japan 2019*, Available: https://www.fepc.or.jp/library/pamphlet/pdf/04_electricity.pdf Accessed: 2021-10-08, 2019.

[42] Agency for Natural Resources and Energy, *Electric power survey statistical data*, Available: https://www.enecho.meti.go.jp/statistics/electric_power/ep002/results_archive.html Accessed: 2021-01-08.

[43] Ministry of Land, Infrastructure, Transport and Tourism, *Japan power plant gis data*, Available: https://nlftp.mlit.go.jp/ksj/jpgis/datalist/KsjTmplt-P03.html Accessed: 2020-06-08, 2007.

[44] Japan Beyond Coal, *Japan coal plant database*, Available: https://beyond-coal.jp/map-and-data/ Accessed: 2020-09-29, 2020.

[45] Kyushu Electric Power Company, *Kyuden group environmental data book 2020*, Available: http://www.kyuden.co.jp/var/rev0/0270/6338/env_data_2020.pdf Accessed: 2021-03-18, 2020.

[46] S. Pfenninger, A. Hawkes, and J. Keirstead, "Energy systems modeling for twenty-first century energy challenges," *Renewable and Sustainable Energy Reviews*, vol. 33, pp. 74–86, 2014, ISSN: 13640321. DOI: 10.1016/j.rser.2014.02.003.

[47] H.-K. Ringkjøb, P. M. Haugan, and I. M. Solbrekke, "A review of modelling tools for energy and electricity systems with large shares of variable renewables," *Renewable and Sustainable Energy Reviews*, vol. 96, pp. 440–459, 2018. DOI: 10.1016/j.rser.2018.08.002.

[48] R. Morrison, "Energy system modeling: Public transparency, scientific reproducibility, and open development," *Energy Strategy Reviews*, vol. 20, pp. 49–63, 2018. DOI: 10.1016/j.esr.2017.12.010.

[49] F. Wiese, R. Bramstoft, H. Koduvere, *et al.*, "Balmorel open source energy system model," *Energy Strategy Reviews*, vol. 20, pp. 26–34, 2018. DOI: 10.1016/j.esr.2018.01.003.

[50] S. Pfenninger and B. Pickering, "Calliope: A multi-scale energy systems modelling framework," *Journal of Open Source Software*, vol. 3, no. 29, p. 825, 2018. DOI: 10.21105/joss.00825.

[51] M. Howells, H. Rogner, N. Strachan, *et al.*, "OSeMOSYS: The open source energy modeling system," *Energy Policy*, vol. 39, no. 10, pp. 5850–5870, 2011. DOI: 10.1016/j.enpol.2011.06.033.

[52] L. Thurner, A. Scheidler, F. Schafer, *et al.*, "Pandapower—an open-source python tool for convenient modeling, analysis, and optimization of electric power systems," *IEEE Transactions on Power Systems*, vol. 33, no. 6, pp. 6510–6521, 2018. DOI: 10.1109/tpwrs.2018.2829021.

[53] T. Brown, J. Hörsch, and D. Schlachtberger, "PyPSA: Python for power system analysis," *Journal of Open Research Software*, vol. 6, 2018. DOI: 10.5334/jors.188.

[54] Open Energy Modelling Initiative, *Open energy modelling initiative website and wiki*, Available: https://openmod-initiative.org/ (accessed 2021-12-28).

[55] B. Heard, B. Brook, T. Wigley, and C. Bradshaw, "Burden of proof: A comprehensive review of the feasibility of 100% renewable-electricity systems," *Renewable and Sustainable Energy Reviews*, vol. 76, pp. 1122–1133, 2017. DOI: 10.1016/j.rser.2017.03.114.

[56] Tom Brown and Jonas Hörsch and David Schlachtberger and Fabian Hofmann and Fabian Neumann, *Python for power system analysis (pypsa) v0.18.1 documentation*, Available: https://github.com/PyPSA/PyPSA/tree/v0.18.1/doc Accessed: 2021-12-18.

[57] Andrew Makhorin, *Glpk (gnu linear programming kit)*, Available: https://www.gnu.org/software/glpk/glpk.html Accessed: 2021-12-18.

[58] John Forrest, Ted Ralphs, and Haroldo Gambini Santos, *Cbc (coin-or branch and cut)*, Available: https://github.com/coin-or/Cbc/tree/releases/2.10.5 Accessed: 2021-12-18.

[59] Gregory Glockner, *Parallel and distributed optimization with gurobi*, Available: https://www.gurobi.com/resource/parallel-and-distributed-optimization/ Accessed: 2021-12-18.

[60] Gurobi Optimization, *Academic program and licenses*, Available: https://www.gurobi.com/academia/academic-program-and-licenses/ Accessed: 2021-12-18.

[61] Deutscher Bundestag, *Bundestag passes the coal phase-out law*, Available: https://www.bundestag.de/dokumente/textarchiv/2020/kw27-de-kohleausstieg-701804 Accessed: 2021-03-14, 2020.

[62] Europe Beyond Coal, *Overview: National coal phase-out announcements in Europe*, Available: https://beyond-coal.eu/wp-content/uploads/2021/01/Overview-of-national-coal-phase-out-announcements-Europe-Beyond-Coal-January-2021.pdf Accessed: 2021-03-14, 2021.

[63] Government of Canada, *Coal phase-out: The powering past coal alliance*, Available: https://www.canada.ca/en/services/environment/weather/climatechange/canada-international-action/coal-phase-out.html Accessed: 2021-03-14, 2018.

[64] S. Kumar, H.-T. Kwon, K.-H. Choi, J. H. Cho, W. Lim, and I. Moon, "Current status and future projections of LNG demand and supplies: A global prospective," *Energy Policy*, vol. 39, no. 7, pp. 4097–4104, 2011. DOI: 10.1016/j.enpol.2011.03.067.

[65] Shell Corporation, *Lng outlook 2020*, Available: https://www.shell.com/energy-and-innovation/natural-gas/liquefied-natural-gas-lng/lng-outlook-2020.html Accessed: 2021-03-16, 2020.

[66] Nikkei Asia, *Severe winter forecast sparks recovery in asia's lng prices*, Available: https://asia.nikkei.com/Business/Markets/Commodities/Severe-winter-forecast-sparks-recovery-in-Asia-s-LNG-prices Accessed: 2021-03-16, 2020.

[67] A. Bunodiere and H. S. Lee, "Renewable energy curtailment: Prediction using a logic-based forecasting method and mitigation measures in kyushu, japan," *Energies*, vol. 13, no. 18, p. 4703, 2020. DOI: 10.3390/en13184703.

[68] M. Guittet, M. Capezzali, L. Gaudard, F. Romerio, F. Vuille, and F. Avellan, "Study of the drivers and asset management of pumped-storage power plants historical and geographical perspective," *Energy*, vol. 111, pp. 560–579, 2016. DOI: 10.1016/j.energy.2016.04.052.

[69] Y. Li, W. Gao, Y. Ruan, and Y. Ushifusa, "The performance investigation of increasing share of photovoltaic generation in the public grid with pump hydro storage dispatch system, a case study in japan," *Energy*, vol. 164, pp. 811–821, 2018. DOI: 10.1016/j.energy.2018.09.029.

[70] N. E. Koltsaklis and A. S. Dagoumas, "State-of-the-art generation expansion planning: A review," *Applied Energy*, vol. 230, pp. 563–589, 2018. DOI: 10.1016/j.apenergy.2018.08.087.

[71] A. Ioannou, A. Angus, and F. Brennan, "Risk-based methods for sustainable energy system planning: A review," *Renewable and Sustainable Energy Reviews*, vol. 74, pp. 602–615, 2017. DOI: 10.1016/j.rser.2017.02.082.

[72] M. J. Santos, P. Ferreira, and M. Araújo, "A methodology to incorporate risk and uncertainty in electricity power planning," *Energy*, vol. 115, pp. 1400–1411, 2016. DOI: 10.1016/j.energy.2016.03.080.

[73] R. Schaeffer, A. S. Szklo, A. F. P. de Lucena, *et al.*, "Energy sector vulnerability to climate change: A review," *Energy*, vol. 38, no. 1, pp. 1–12, 2012. DOI: 10.1016/j.energy.2011.11.056.

[74] B. Bartók, "Changes in solar energy availability for south-eastern europe with respect to global warming," *Physics and Chemistry of the Earth, Parts A/B/C*, vol. 35, no. 1-2, pp. 63–69, 2010. DOI: 10.1016/j.pce.2010.03.008.

[75] H. Cutforth and D. Judiesch, "Long-term changes to incoming solar energy on the canadian prairie," *Agricultural and Forest Meteorology*, vol. 145, no. 3-4, pp. 167–175, 2007. DOI: 10.1016/j.agrformet.2007.04.011.

[76] Japan Meteorological Agency, *Past regional weather data*, Available: http://www.data.jma.go.jp/risk/obsdl/index.php Accessed: 2021-01-08.

[77] W. F. Holmgren, C. W. Hansen, and M. A. Mikofski, "Pvlib python: A python package for modeling solar energy systems," *Journal of Open Source Software*, vol. 3, no. 29, p. 884, 2018. DOI: 10.21105/joss.00884.

[78] W. Holmgren and R. Andrews, *Pvlib: Tmy to power tutorial*, Available: https://nbviewer.jupyter.org/github/pvlib/pvlib-python/blob/master/docs/tutorials/tmy_to_power.ipynb Accessed: 2021-01-08.

[79] D. Erbs, S. Klein, and J. Duffie, "Estimation of the diffuse radiation fraction for hourly, daily and monthly-average global radiation," *Solar Energy*, vol. 28, no. 4, pp. 293–302, 1982. DOI: 10.1016/0038-092x(82)90302-4.

[80] Ministry of Economy, Trade and Industry of Japan, *Recent situation of thermal power generation*, Available: https://www.meti.go.jp/shingikai/enecho/shoene_shinene/sho_energy/karyoku_hatsuden/pdf/h29_01_04_00.pdf Accessed: 2021-03-18, 2017.

[81] Ministry of Economy, Trade and Industry of Japan, *Report on power generation costs*, Available: https://www.enecho.meti.go.jp/committee/council/basic_policy_subcommittee/mitoshi/cost_wg/006/pdf/006_05.pdf Accessed: 2021-03-10, 2015.

[82] Advisory Panel to the Foreign Minister on Climate Change, *Promote new diplomacy on energy through leading global efforts against climate change*, Available: https://www.mofa.go.jp/files/000337158.pdf Accessed: 2021-03-10, 2018.

[83] Ministry of Environment of Japan, *Evaluation of co2 emissions of thermal power generation*, Available: https://www.env.go.jp/council/06earth/y0613-16/ref06-16.pdf Accessed: 2020-03-10, 2016.

[84] F. Díaz-González, A. Sumper, O. Gomis-Bellmunt, and R. Villafáfila-Robles, "A review of energy storage technologies for wind power applications," *Renewable and Sustainable Energy Reviews*, vol. 16, no. 4, pp. 2154–2171, 2012. DOI: 10.1016/j.rser.2012.01.029.

[85] T. Kousksou, P. Bruel, A. Jamil, T. E. Rhafiki, and Y. Zeraouli, "Energy storage: Applications and challenges," *Solar Energy Materials and Solar Cells*, vol. 120, pp. 59–80, 2014. DOI: 10.1016/j.solmat.2013.08.015.

[86] C. K. Das, O. Bass, G. Kothapalli, T. S. Mahmoud, and D. Habibi, "Overview of energy storage systems in distribution networks: Placement, sizing, operation, and power quality," *Renewable and Sustainable Energy Reviews*, vol. 91, pp. 1205–1230, 2018. DOI: 10.1016/j.rser.2018.03.068.

[87] M. Mahmoud, M. Ramadan, A.-G. Olabi, K. Pullen, and S. Naher, "A review of mechanical energy storage systems combined with wind and solar applications," *Energy Conversion and Management*, vol. 210, p. 112 670, 2020. DOI: 10.1016/j.enconman.2020.112670.

[88] M. Aneke and M. Wang, "Energy storage technologies and real life applications – a state of the art review," *Applied Energy*, vol. 179, pp. 350–377, 2016. DOI: 10.1016/j.apenergy.2016.06.097.

[89] T. M. Gür, "Review of electrical energy storage technologies, materials and systems: Challenges and prospects for large-scale grid storage," *Energy & Environmental Science*, vol. 11, no. 10, pp. 2696–2767, 2018. DOI: 10.1039/c8ee01419a.

[90] V. Dias, M. Pochet, F. Contino, and H. Jeanmart, "Energy and economic costs of chemical storage," *Frontiers in Mechanical Engineering*, vol. 6, 2020. DOI: 10.3389/fmech.2020.00021.

[91] S. Kuravi, J. Trahan, D. Y. Goswami, M. M. Rahman, and E. K. Stefanakos, "Thermal energy storage technologies and systems for concentrating solar power plants," *Progress in Energy and Combustion Science*, vol. 39, no. 4, pp. 285–319, 2013. DOI: 10.1016/j.pecs.2013.02.001.

[92] E. Borri, A. Tafone, A. Romagnoli, and G. Comodi, "A review on liquid air energy storage: History, state of the art and recent developments," *Renewable and Sustainable Energy Reviews*, vol. 137, p. 110 572, 2021. DOI: 10.1016/j.rser.2020.110572.

[93] H. Vikström, S. Davidsson, and M. Höök, "Lithium availability and future production outlooks," *Applied Energy*, vol. 110, pp. 252–266, 2013. DOI: 10.1016/j.apenergy.2013.04.005.

[94] C. Doetsch and J. Burfeind, "Vanadium redox flow batteries," in *Storing Energy*, Elsevier, 2016, pp. 227–246. DOI: 10.1016/b978-0-12-803440-8.00012-9.

[95] B. Zakeri and S. Syri, "Electrical energy storage systems: A comparative life cycle cost analysis," *Renewable and Sustainable Energy Reviews*, vol. 42, pp. 569–596, 2015. DOI: 10.1016/j.rser.2014.10.011.

[96] V. Jülch, "Comparison of electricity storage options using levelized cost of storage (LCOS) method," *Applied Energy*, vol. 183, pp. 1594–1606, 2016. DOI: 10.1016/j.apenergy.2016.08.165.

[97] O. Schmidt, S. Melchior, A. Hawkes, and I. Staffell, "Projecting the future levelized cost of electricity storage technologies," *Joule*, vol. 3, no. 1, pp. 81–100, 2019. DOI: 10.1016/j.joule.2018.12.008.

[98] O. Schmidt, A. Hawkes, A. Gambhir, and I. Staffell, "The future cost of electrical energy storage based on experience rates," *Nature Energy*, vol. 2, no. 8, 2017. DOI: 10.1038/nenergy.2017.110.

[99] W. J. Cole and A. Frazier, "Cost projections for utility-scale battery storage," Tech. Rep., 2019. DOI: 10.2172/1529218.

[100] C. S. Lai and M. D. McCulloch, "Levelized cost of electricity for solar photovoltaic and electrical energy storage," *Applied Energy*, vol. 190, pp. 191–203, 2017. DOI: 10.1016/j.apenergy.2016.12.153.

[101] W. Short, D. Packey, and T. Holt, "A manual for the economic evaluation of energy efficiency and renewable energy technologies," Tech. Rep., 1995. DOI: 10.2172/35391.

[102] C. S. Lai, G. Locatelli, A. Pimm, Y. Tao, X. Li, and L. L. Lai, "A financial model for lithium-ion storage in a photovoltaic and biogas energy system," *Applied Energy*, vol. 251, p. 113 179, 2019. DOI: 10.1016/j.apenergy.2019.04.175.

[103] M. Das, M. A. K. Singh, and A. Biswas, "Techno-economic optimization of an off-grid hybrid renewable energy system using metaheuristic optimization approaches – case of a radio transmitter station in india," *Energy Conversion and Management*, vol. 185, pp. 339–352, 2019. DOI: 10.1016/j.enconman.2019.01.107.

[104] R. Gupta, M. C. Soini, M. K. Patel, and D. Parra, "Levelized cost of solar photovoltaics and wind supported by storage technologies to supply firm electricity," *Journal of Energy Storage*, vol. 27, p. 101 027, 2020. DOI: 10.1016/j.est.2019.101027.

[105] V. Jülch, T. Telsnig, M. Schulz, *et al.*, "A holistic comparative analysis of different storage systems using levelized cost of storage and life cycle indicators," *Energy Procedia*, vol. 73, pp. 18–28, 2015. DOI: 10.1016/j.egypro.2015.07.553.

[106] J. S. Anagnostopoulos and D. E. Papantonis, "Study of pumped storage schemes to support high RES penetration in the electric power system of Greece," *Energy*, vol. 45, no. 1, pp. 416–423, 2012, ISSN: 3605442. DOI: 10.1016/j.energy.2012.02.031.

[107] J. Liu, C. Hu, A. Kimber, and Z. Wang, "Uses, Cost-Benefit Analysis, and Markets of Energy Storage Systems for Electric Grid Applications," *Journal of Energy Storage*, vol. 32, 2020, ISSN: 2352152X. DOI: 10.1016/j.est.2020.101731.

[108] Ministry of Economy, Trade, and Indisty (Japan), *Solar PV Domestic trends: Changes in capital costs and their composition by year of installation (translated; pg 29)*, Available: https://www.meti.go.jp/shingikai/santeii/pdf/063_01_00.pdf Accessed on 8 May 2021, 2020.

[109] J. Tomić and W. Kempton, "Using fleets of electric-drive vehicles for grid support," *Journal of Power Sources*, vol. 168, no. 2, pp. 459–468, 2007, ISSN: 3787753. DOI: 10.1016/j.jpowsour.2007.03.010.

[110] P. Denholm, M. Kuss, and R. M. Margolis, "Co-benefits of large scale plug-in hybrid electric vehicle and solar PV deployment," *Journal of Power Sources*, vol. 236, pp. 350–356, 2013, ISSN: 3787753. DOI: 10.1016/j.jpowsour.2012.10.007.

[111] W. Kempton and T. Kubo, "Electric-drive vehicles for peak power in Japan," *Energy Policy*, vol. 28, no. 1, pp. 9–18, 2000, ISSN: 3014215. DOI: 10.1016/S0301-4215(99)00078-6.

[112] W. Kempton and J. Tomić, "Vehicle-to-grid power implementation: From stabilizing the grid to supporting large-scale renewable energy," *Journal of Power Sources*, vol. 144, no. 1, pp. 280–294, 2005, ISSN: 3787753. DOI: 10.1016/j.jpowsour.2004.12.022.

[113] Kyushu Transport Bureau, *Passenger vehicles in kyushu*, Available: http://wwwtb.mlit.go.jp/kyushu/toukei/syaryousuu.htm Accessed: 2020-04-12, 2020.

[114] Japan Automobile Dealears Association, *Sales by fuel type (passenger cars)*, Available: http://www.jada.or.jp/data/month/m-fuel-hanbai/ Accessed: 2020-04-12, 2020.

[115] Electric Vehicle Database, *Electric vehicle specifications*, Available: https://ev-database.org/ Accessed: 2020-04-12.

[116] Japan Next Generation Vehicle Promotion Center, *Strategy for diffusing the next generation vehicles in japan*, Available: http://www.cev-pc.or.jp/event/pdf/xev_in_japan_eng.pdf Accessed: 2020-04-12, 2020.

[117] Next Generation Vehicle Promotion Center (NeV), *Subsidy grants by prefecture*, Available: http://www.cev-pc.or.jp/tokei/koufu.html Accessed: 2020-06-08, 2020.

[118] A. Sternberg and A. Bardow, "Power-to-what? – environmental assessment of energy storage systems," *Energy & Environmental Science*, vol. 8, no. 2, pp. 389–400, 2015. DOI: 10.1039/c4ee03051f.

[119] R. Schlögl, "Chemical energy storage enables the transformation of fossil energy systems to sustainability," *Green Chemistry*, vol. 23, no. 4, pp. 1584–1593, 2021. DOI: 10.1039/d0gc03171b.

[120] P. Nikolaidis and A. Poullikkas, "A comparative overview of hydrogen production processes," vol. 67, pp. 597–611, 2017. DOI: 10.1016/j.rser.2016.09.044.

[121] Y. Shibata, "Is power to gas feasible in japan?," 2016, Available: https://eneken.ieej.or.jp/data/6549.pdf (accessed 2021-06-02). [Online]. Available: https://eneken.ieej.or.jp/data/6549.pdf.

[122] L. Janke, S. McDonagh, S. Weinrich, *et al.*, "Optimizing power-to-h2 participation in the nord pool electricity market: Effects of different bidding strategies on plant operation," vol. 156, pp. 820–836, 2020. DOI: 10.1016/j.renene.2020.04.080.

[123] T. V. de Graaf, I. Overland, D. Scholten, and K. Westphal, "The new oil? the geopolitics and international governance of hydrogen," *Energy Research & Social Science*, vol. 70, p. 101 667, 2020. DOI: 10.1016/j.erss.2020.101667.

[124] Monica Nagashima, *Japan's Hydrogen Strategy and Its Economic and Geopolitical Implications*, Available: https://www.ifri.org/sites/default/files/atoms/files/nagashima_japan_hydrogen_2018_.pdf, Oct. 2018.

[125] J. D. Fonseca, M. Camargo, J.-M. Commenge, L. Falk, and I. D. Gil, "Trends in design of distributed energy systems using hydrogen as energy vector: A systematic literature review," *International Journal of Hydrogen Energy*, vol. 44, no. 19, pp. 9486–9504, 2019. DOI: 10.1016/j.ijhydene.2018.09.177.

[126] S. Schiebahn, T. Grube, M. Robinius, V. Tietze, B. Kumar, and D. Stolten, "Power to gas: Technological overview, systems analysis and economic assessment for a case study in germany," *International Journal of Hydrogen Energy*, vol. 40, no. 12, pp. 4285–4294, 2015. DOI: 10.1016/j.ijhydene.2015.01.123.

[127] O. Al-Kuwari and M. Schönfisch, "The emerging hydrogen economy and its impact on LNG," *International Journal of Hydrogen Energy*, 2021. DOI: 10.1016/j.ijhydene.2021.10.206.

[128] L. H. Lee, E. P. Chew, S. Teng, and D. Goldsman, "Optimal computing budget allocation for multi-objective simulation models," in *Proceedings of the 2004 Winter Simulation Conference, 2004.*, IEEE. DOI: 10.1109/wsc.2004.1371365.

[129] Y. Cui, Z. Geng, Q. Zhu, and Y. Han, "Review: Multi-objective optimization methods and application in energy saving," *Energy*, vol. 125, pp. 681–704, 2017. DOI: 10.1016/j.energy.2017.02.174.

[130] R. H. Stewart, T. S. Palmer, and B. DuPont, "A survey of multi-objective optimization methods and their applications for nuclear scientists and engineers," *Progress in Nuclear Energy*, vol. 138, p. 103 830, 2021. DOI: 10.1016/j.pnucene.2021.103830.

[131] V. Ojalehto, K. Miettinen, and T. Laukkanen, "Implementation aspects of interactive multiobjective optimization for modeling environments: The case of GAMS-NIMBUS," *Computational Optimization and Applications*, vol. 58, no. 3, pp. 757–779, 2014. DOI: 10.1007/s10589-014-9639-y.

[132] E. Zitzler, K. Deb, and L. Thiele, "Comparison of multiobjective evolutionary algorithms: Empirical results," *Evolutionary Computation*, vol. 8, no. 2, pp. 173–195, 2000. DOI: 10.1162/106365600568202.

[133] Z. Michalewicz and M. Schoenauer, "Evolutionary algorithms for constrained parameter optimization problems," *Evolutionary Computation*, vol. 4, no. 1, pp. 1–32, 1996. DOI: 10.1162/evco.1996.4.1.1.

[134] S. Katoch, S. S. Chauhan, and V. Kumar, "A review on genetic algorithm: Past, present, and future," *Multimedia Tools and Applications*, vol. 80, no. 5, pp. 8091–8126, 2020. DOI: 10.1007/s11042-020-10139-6.

[135] P. Poulos, G. Rigatos, S. Tzafestas, and A. Koukos, "A pareto-optimal genetic algorithm for warehouse multi-objective optimization," *Engineering Applications of Artificial Intelligence*, vol. 14, no. 6, pp. 737–749, 2001. DOI: 10.1016/s0952-1976(01)00036-7.

[136] E. J. Chen and L. H. Lee, "A multi-objective selection procedure of determining a pareto set," *Computers & Operations Research*, vol. 36, no. 6, pp. 1872–1879, 2009. DOI: 10.1016/j.cor.2008.06.003.

Funding

The doctoral studies of Samuel Matthew G. Dumlao at Kyoto University was funded by the Ministry of Education, Culture, Sports, Science, and Technology of Japan. Additional funding was also acquired through the Ambitious Intelligence Dynamic Acceleration (AIDA) Program of Kyoto University.

Colophon

This thesis was typeset with LaTeX 2_ε. It uses the *Clean Thesis* style developed by Ricardo Langner. The design of the *Clean Thesis* style is inspired by user guide documents from Apple Inc.

Download the *Clean Thesis* style at `http://cleanthesis.der-ric.de/`.